

**EFFECTS OF MOISTURE-INDUCED THICKNESS SWELLING  
ON THE MICROSTRUCTURE OF ORIENTED STRAND  
BOARD**

by

Vinicius Munaldi Lube

B.Sc., Universidade Federal do Espírito Santo, 2013

A THESIS SUBMITTED IN PARTIAL FULFILLMENT OF  
THE REQUIREMENTS FOR THE DEGREE OF

MASTER OF SCIENCE

in

The Faculty of Graduate and Postdoctoral Studies

(Forestry)

THE UNIVERSITY OF BRITISH COLUMBIA

(Vancouver)

November 2016

© Vinicius Munaldi Lube, 2016

## **Abstract**

When wood becomes wet and then dries, restraint of shrinkage at the surface of wood by wetter surface and also sub-surface layers causes tensile stresses to develop resulting in micro-checking. Wood elements in composites such as oriented strand board (OSB) also swell and shrink when they become wet and dry. Furthermore, some wood elements are large enough to develop unbalanced surface and sub-surface tensile stresses. Hence, moisture changes and swelling and shrinkage of OSB might result in micro-checking. I test this hypothesis in this thesis. I also examine whether micro-checking contributes to thickness swelling of OSB. I used macro-photography, X-ray micro-computed tomography, and field emission scanning electron microscopy to probe the microstructure of OSB exposed to wetting and drying. These techniques were used to visualize and quantify the thickness swelling of OSB and the dimensions of micro-checks and other voids in OSB during and after wetting and drying. The spatial micro-distribution of a zinc borate biocide in OSB was also examined before and after samples were exposed to wetting and drying. Numerous surface and internal micro-checks developed in OSB exposed to wetting and drying as I hypothesized. Micro-checks developed during wetting, unlike the pattern of checking found in solid wood. Enlargement of voids was also observed during wetting and drying. Micro-checks occurred at the interface between latewood and earlywood and in the rays of softwood flakes and, less commonly, in the rays of aspen flakes. My results indicate that the pattern of micro-checking of OSB is different in some respects to that of solid wood, and suggest that micro-checking contributes to the irreversible thickness swelling of OSB. I briefly discuss the implications of my findings for the development of treatments designed to reduce the irreversible thickness swelling of OSB.

## **Preface**

The research presented in this thesis is the original work of Vinicius Munaldi Lube. The experimental design, data analyses and writing were done under the supervision of Professor Dr. Philip D. Evans with the occasional assistance from my committee members, Dr. Simon C. Ellis and Dr. Scott Renneckar.

Portions of Chapter 3 have been published in conference proceedings with restricted distribution (see below). I carried out all the experimental work and wrote the papers under the supervision of Professor Dr. Philip D. Evans. The publications in question are:

Lube, V., Evans, P.D. (2015). An inexpensive method to simultaneously measure the swelling, shrinkage and checking of treated wood. Proceedings of American Wood Protection Association Conference, Asheville, North Carolina, USA (12<sup>th</sup> to 14<sup>th</sup> April 2015), 39-42.

Lube, V., Evans, P.D. (2016). Surface micro-checking of oriented strand board exposed to wetting and drying. Proceedings of American Wood Protection Association Conference, San Juan, Puerto Rico, USA (1<sup>st</sup> to 3<sup>rd</sup> May 2016), 11 pp.

## Table of Contents

<b>Abstract</b> .....	<b>ii</b>
<b>Preface</b> .....	<b>iii</b>
<b>Table of Contents</b> .....	<b>iv</b>
<b>List of Tables</b> .....	<b>vii</b>
<b>List of Figures</b> .....	<b>viii</b>
<b>Acknowledgements</b> .....	<b>xv</b>
<b>Dedication</b> .....	<b>xvii</b>
<b>Chapter 1: Introduction</b> .....	<b>1</b>
<b>1.1 Oriented strand board</b> .....	<b>1</b>
<i>1.1.1 Structure and thickness swelling of OSB</i> .....	<b>3</b>
<b>1.2 Micro-checking</b> .....	<b>4</b>
<b>1.3 General hypothesis</b> .....	<b>5</b>
<b>1.4 Outline of thesis</b> .....	<b>7</b>
<b>Chapter 2: Review of the Literature</b> .....	<b>8</b>
<b>2.1 Manufacture of oriented strand board</b> .....	<b>8</b>
<i>2.1.1 Wood species</i> .....	<b>9</b>
2.1.1.1 Softwood and hardwood .....	<b>11</b>
2.1.1.2 Mixed species .....	<b>15</b>
<i>2.1.2 Production of OSB strands</i> .....	<b>16</b>
<i>2.1.3 Drying of strands</i> .....	<b>17</b>
<i>2.1.4 Blending</i> .....	<b>18</b>
2.1.4.1 Resins (adhesive) .....	<b>18</b>
2.1.4.2 Wax sizing .....	<b>19</b>
<i>2.1.5 Mat forming</i> .....	<b>20</b>
<i>2.1.6 Pressing</i> .....	<b>20</b>
<b>2.2 Properties of OSB</b> .....	<b>21</b>
<i>2.2.1 Physical properties</i> .....	<b>21</b>
2.2.1.1 Density .....	<b>21</b>
<i>2.2.2 Thickness swelling of OSB and other particulate wood composites</i> .....	<b>22</b>
<b>2.3 Micro-checking of wood and wood composites</b> .....	<b>24</b>



2.3.1 Definitions.....	24
2.3.2 Location of micro-checks and variation of micro-checking in different species .....	26
2.3.3 Development of micro-checks during wetting and drying .....	26
2.3.4 Internal checking .....	27
<b>2.4 Imaging of OSB and micro-checking .....</b>	<b>27</b>
2.4.1 X-ray CT imaging .....	28
2.4.2 Field emission scanning electron microscopy (FE-SEM) .....	30
<b>2.5 Methods of reducing thickness swelling and micro-checking of wood and wood composites .....</b>	<b>31</b>
2.5.1 Improving dimensional stability of wood and wood composites .....	31
2.5.2 Reducing micro-checking of wood and wood composites.....	33
<b>2.6 Concluding summary.....</b>	<b>33</b>
<b>Chapter 3: Surface Micro-Checking of Treated Wood and OSB Exposed to Wetting and Drying.....</b>	<b>34</b>
<b>3.1 Introduction .....</b>	<b>34</b>
<b>3.2 Materials and methods .....</b>	<b>35</b>
3.2.1 Experimental design.....	35
3.2.2 Preparation of specimens.....	36
3.2.3 Moisture-induced degradation measurements .....	38
3.2.3.1 Apparatus to quantify thickness swelling and micro-checking of OSB	38
3.2.3.2 Measurements of thickness swelling and moisture content of OSB ....	39
3.2.3.3 Measurements of surface micro-checking and voids in OSB .....	40
3.2.3.4 Measurements of swelling/shrinkage, micro-checking and moisture content of aspen and pine wood treated with a water-repellent preservative ..	41
3.2.4 Statistical analysis of data .....	42
<b>3.3 Results .....</b>	<b>42</b>
3.3.1 Thickness swelling and moisture content of OSB .....	42
3.3.2 Surface checking and formation of voids in OSB .....	44
3.3.3 Dimensional stability, checking and moisture content of treated wood .....	50
<b>3.4 Discussion .....</b>	<b>52</b>

3.5 Conclusions .....	54
<b>Chapter 4: Internal Changes to the Microstructure of OSB Exposed to Wetting and Drying .....</b>	<b>56</b>
4.1 Introduction .....	56
4.2 Materials and methods .....	57
4.2.1 Materials .....	57
4.2.2 X-ray micro-CT .....	57
4.2.2.1 Conventional CT system .....	60
4.2.2.2 Helical scanning CT system .....	62
4.2.2.3 Visualization and segmentation of different phases in OSB .....	66
4.2.3 FE-SEM .....	68
4.3 Results .....	74
4.3.1 X-ray micro-CT .....	74
4.3.1.1 Conventional X-ray micro-CT system .....	74
4.3.1.2 Helical X-ray micro-CT system .....	77
4.3.2 Field emission scanning electron microscopy .....	89
4.4 Discussion .....	95
4.5 Conclusions .....	98
<b>Chapter 5: General Discussion, Suggestions for Further Research and Conclusions .....</b>	<b>99</b>
5.1 General discussion .....	99
5.2 Further research .....	100
5.3 Conclusions .....	102
<b>Bibliography .....</b>	<b>103</b>
<b>Appendices .....</b>	<b>116</b>
Appendix 1 - Surface checking and voids of OSB specimens before and after wetting and drying cycle used in Chapter 3 .....	116
Appendix 2 - Internal microstructure of OSB data sets. Helical X-ray micro-CT images of all 2D frames that were subject to image analysis .....	121
Appendix 3 - FE-SEM images of OSB samples embedded with a low-viscosity epoxy resin .....	132

## List of Tables

Table 2.1 - Species used to manufacture OSB commercially and experimentally .....	10
Table 2.2 - Comparison of the physical and mechanical properties of aspen and lodgepole pine .....	14
Table 2.3 - Wood density, panel density and compaction ratio of OSB .....	22
Table 3.1 - Frames used for the analysis of thickness swelling and moisture content during wetting and drying of each specimen .....	40
Table 3.2 - Moisture content (MC) of untreated and water-repellent treated aspen and southern pine samples after wetting and drying .....	42
Table 4.1 - Concentration of ingredients used to make up a low-viscosity epoxy resin embedding medium .....	69

## List of Figures

Figure 1.1 - Computer-generated images showing the different layers and orientations of strands within OSB panels; core layer cross-oriented (a- arrowed white); core layer oriented randomly (b- arrowed white). Scale bars are 5 mm (redrawn from: Structural Board Association 2005) .....	1
Figure 1.2 - Computer-generated image showing the main uses of OSB in housing; wall sheathing (arrowed left), roof (arrowed centre) and sub-floor (arrowed right).....	2
Figure 1.3 - In-plane photograph of OSB showing irreversible thickness swelling caused by moisture-induced swelling (b- arrowed centre). Note the permanent thickness swelling (b- area above the dashed line) relative to the original board (a). Scale bars are 4 mm .....	4
Figure 1.4 - Micro-check in pine wood. Scale bar is 100 $\mu\text{m}$ .....	4
Figure 1.5 - Messmate stringybark ( <i>Eucalyptus oblique</i> L'Her.) sample after intense microwave modification; left-hand side of the sample is unmodified natural wood (ovendry density of 778 $\text{kg/m}^3$ ); the right-hand side (arrowed) of the sample is microwave modified wood (ovendry density of 686 $\text{kg/m}^3$ ). (photograph c/o Torgovnikov and Vinden 2009) .....	5
Figure 1.6 - Light microscopy image of a transverse section of parallel-strand lumber made from spruce. Note fractured and delaminated zones indicated by arrowheads. (image c/o Konnerth and Gindl 2006) .....	6
Figure 2.1 - Typical sequence during the manufacture of OSB. The logs are debarked and furnish is produced by the strander, followed by screening, drying, blending, forming, hot pressing, and finally sawing and cooling (redrawn from: Thoemen et al. 2010) .....	8
Figure 2.2 - Diagrams showing the 3D structure of a softwood (top) and hardwood (bottom); the wood species are: lodgepole pine (top - 75x) and aspen (bottom - 90x), respectively (redrawn from: Panshin and De Zeeuw 1980) .....	12
Figure 2.3 - Diagram of cell wall delamination in both radial and tangential planes, showing transwall and intrawall fracture types. (redrawn from: Donaldson 2010) .	25
Figure 2.4 - FE-SEM back-scattered electron image of tracheids in plywood coated with a stain. Note coating penetration into micro-checks in the wood cell wall. Scale bar is 10 $\mu\text{m}$ . (redrawn from: Singh et al. 2007) .....	25
Figure 3.1 - Transverse section of aspen (left) and southern pine (right). Note the vessel elements (V) in aspen and the resin canals (R) and earlywood (EW) and latewood (LW) in pine. Scale bars are 150 $\mu\text{m}$ .....	36
Figure 3.2 - Parent OSB sample (left) measuring 50.8 x 50.8 mm (length x width) and 10.5 mm in thickness and specimen (right) measuring 20.0 x 2.5 mm (length x width) and 10.5 mm in thickness .....	36
Figure 3.3 - Sample (middle) measuring 100 x 40 x 25 mm (longitudinal x radial x tangential) and matched samples (left and right) measuring 6 x 40 x 25 mm	

(longitudinal x radial x tangential). The edges of the sample were sealed with white silicone .....	37
Figure 3.4 - Matched specimens (5 x 5 x 5 mm) used for swelling/shrinkage, checking and MC measurements. Top view on the left, and side view on the right .....	38
Figure 3.5 - Diagram showing all the steps involved in treating solid wood samples with a water-repellent preservative. The first step was to seal the edges of the samples using a silicone sealant (a), followed by impregnation (b), conditioning (c), sanding (d) and finally excising specimens (e) from treated samples using a razor blade ..	38
Figure 3.6 - Imaging system (arrowed a and b) used to visualize effects of wetting and drying on the surface microstructure of OSB and solid wood: hot plate (a- arrowed left) heats up water or air in a vented Erlenmeyer flask (a- arrowed left); saturated air is directed via a transparent hose (b- arrowed right-centre) onto a specimen (b- arrowed centre) held firmly using a metal clamp (b- arrowed bottom) .....	39
Figure 3.7 - Wood specimen mounted on a concertina-type stage and exposed to wetting and drying .....	41
Figure 3.8 - Average percentage thickness swelling (TS) and moisture content (MC) of OSB specimens during wetting and drying .....	43
Figure 3.9 - Thickness swelling, moisture content, and associated images of an OSB specimen during wetting and drying. The start and end points of the cycle were (A*) and (Q*), respectively. Vertical scale on frames (y axes) in millimeters.....	44
Figure 3.10 - Springback of part of a softwood flake in an OSB specimen after moisture-cycling: (a) Specimen before wetting and drying showing compressed and buckled tracheids; (b) Specimen after wetting and drying. Note the recovery of buckled tracheids (arrowed left), as well as delamination (arrowed bottom left) causing adjacent flakes to separate by approximately 20 $\mu\text{m}$ . Scale bars are 200 $\mu\text{m}$ .....	45
Figure 3.11 - Formation of micro-checks and delamination taking place during wetting (Frame H) near the core of an OSB specimen (as in Figure 14), and subsequent propagation and enlargement of micro-checks during drying (Frames I to P). Scale bars (Frames A and Q) are 200 $\mu\text{m}$ .....	46
Figure 3.12 - Micro-checking of rays (Frame F) taking place during wetting near the surface layers of an OSB specimen (as in Figures 3.10 and 3.13), and subsequent propagation and enlargement of micro-checks during drying (Frames I to P). Scale bars (Frames A and Q) are 200 $\mu\text{m}$ .....	46
Figure 3.13 - Micro-checking of part of a softwood flake in OSB before (a) and after wetting and drying (b): (a) Tangential micro-check (bottom left) at the latewood-earlywood interface and a radial micro-check (top right); (b) Propagation and enlargement of micro-checks that formed during wetting (arrowed). Scale bars are 200 $\mu\text{m}$ .....	47

Figure 3.14 - Delamination (arrowed top) and micro-checking (arrowed bottom) of softwood flake in OSB before (a) and after (b) wetting and drying. Large void between softwood flakes (arrowed left of centre). Scale bars are 200 $\mu\text{m}$ .....	47
Figure 3.15 - Bark inclusion between two wood flakes in OSB before (a) and after (b) wetting and drying. Note the development of a large check within the body of the bark inclusion. Scale bars are 200 $\mu\text{m}$ .....	48
Figure 3.16 - Area of OSB specimens before (Dry) and after moisture cycling (Wet/Dry) that can be attributed to surface micro-checks (triangles) occurring within wood flakes (bottom) or voids (circles) occurring between flakes,. Non-overlap of error bars indicates that individual means are significantly different ( $p < 0.05$ ) .....	48
Figure 3.17 - Surface checking (black) and voids (white) in part of an OSB (greyscale) specimen (as in Figure 3.9) before (left) and after (right) wetting and drying. The area occupied by checks is 0.56 and 2.02% of the specimen's area before and after swelling, respectively. The area occupied by voids is 0.77 and 3.60% of the specimen's area before and after swelling, respectively. The irreversible swelling of the specimen was 19.4%. Vertical scale in mm .....	49
Figure 3.18 - Swelling/shrinkage and area of checks in treated and untreated southern pine samples during wetting and drying .....	50
Figure 3.19 - Swelling and shrinkage of treated and untreated aspen samples during wetting and drying .....	51
Figure 3.20 - Check in a southern pine sample (frames top left to bottom right) that developed during wetting (blue arrows) and drying (red arrows). Check initiated at the beginning of drying (arrowed left), at the interface between latewood and earlywood, and partially closed-up at the end of drying (arrowed right). Most frames during wetting were omitted because no changes were visualized. Scale bar is 0.5 mm .....	51
Figure 4.1 - Plug (right) extracted from an OSB board using a 10 mm diameter steel plug cutter (top left - not to scale).....	58
Figure 4.2 - Steps involved in soaking the OSB plug in water for 48 hours. Two beakers (30 mL and 50 mL) were used to soak the plug in water; the larger beaker was filled with 40 mL of tap water (a); the plug was placed on the water in the larger beaker (b- arrowed centre); and finally the smaller beaker was placed into the larger beaker (c- arrowed right) to force the plug under the water in the larger beaker ...	58
Figure 4.3 - Diagram showing a 3D image (bottom) of part of an OSB plug and the 2D slices (width x thickness - highlighted blue) at 0, 10, 20, 30, 40, 50, 60, 70, 80, 90, and 100 % of plug's length, which were subject to image analysis. A total of 22 slices (frames) were selected from data sets for the analysis (11 frames from both <i>dry</i> (top left) and <i>wet/dry</i> (top right) data sets) .....	59
Figure 4.4 - Conventional X-ray micro-CT system initially used to probe the effects of moisture on the microstructure of OSB. (photograph c/o McKay 2015).....	61

Figure 4.5 - State-of-the-art high-cone-angle helical micro-CT system (HELISCAN) developed in the Department of Applied Mathematics at The Australian National University. Photo source: Professor Tim J. Senden.....	63
Figure 4.6 - Acquisition geometry of a conventional micro-CT device (a) compared to higher resolution helical scanning micro-CT device (b). $L$ is the sample-distance, and $R$ is the camera-length. Higher signal-to-noise ratio is achieved with high-cone-angle helical scanning (b) (redrawn from: Evans et al. 2015b) .....	63
Figure 4.7 - In-plane greyscale image (1524 x 1344 pixels or 15.4 x 13.1 mm, 10.5 $\mu\text{m}$ voxel size) of an unleached OSB specimen obtained using a conventional X-ray micro-CT device. Denser material (zinc) is white; wood is grey and voids/air space are black. (Source: Evans et al. 2015a) .....	64
Figure 4.8 - Orthogonal greyscale image (2520 x 2520 pixels, 4.4 $\mu\text{m}$ voxel size) of an OSB plug (10 mm diameter) obtained using a high-cone-angle helical micro-CT device. Denser material (zinc) is white; wood is grey and voids/air space are black .....	64
Figure 4.9 - In-plane rendered greyscale image of a dry OSB plug obtained using a high-cone-angle helical micro-CT device imaged at 4.4 $\mu\text{m}$ voxel size. Denser material (zinc) is white; wood is grey and voids/air space are black. Scale bar is 1.25 mm .....	65
Figure 4.10 - Histograms of <i>dry</i> (left) and <i>wet/dry</i> (right) OSB plug; the phases automatically detected are: air space/voids (black); wood (brown) and zinc (green) .....	67
Figure 4.11 - Manual segmentation of checks and voids carried out with the help of a drawing tablet and a laptop computer (MacBook Pro 2.5 GHz Intel Core i5 with 8 GB of RAM; Apple; Cupertino, CA, USA) running Photoshop.....	68
Figure 4.12 - OSB sample exposed to the wetting & drying cycle which was identical to that used in Chapter 3 (Section 3.2.3.2).....	70
Figure 4.13 - Samples soaked in distilled water for 72 hours: (a) glass flasks were placed into 30 mL beakers to submerge samples in water. Note the silicon bumps at the bottom of the glass flask (b- arrowed right) to ensure that samples were fully submerged in water.....	70
Figure 4.14 - Cutting pattern for OSB specimens: (a) the sample measuring 20.0 x 2.5 x 10.5 mm (length x width x thickness) was subjected to one of the three treatments (control, water soaking or wetting and drying), and it was then cut into three parts using a hand-held, single-edged, carbon steel razor blade; (b) two specimens, each measuring approximately 3.0 x 3.0 x 2.5 mm (thickness x length x width), were cut from the core and surface layers with the same razor blade.....	71
Figure 4.15 - Oven drying of specimens for 3 days at $70 \pm 2^\circ\text{C}$ prior to embedding them with a low-viscosity epoxy resin .....	71
Figure 4.16 - Specimen embedding capsules (5 x 10 mm) (left) placed on a plastic holder (right); a low-viscosity epoxy resin was transferred into the capsules using a	

pipette until the capsules containing OSB specimens were completely filled with resin.....	72
Figure 4.17 - Capsules containing a fully saturated OSB specimen (arrowed left). Hardened epoxy resin-embedded-specimens after curing in an oven at $70^{\circ}\text{C} \pm 2^{\circ}\text{C}$ for two days (right).....	72
Figure 4.18 - Preparation of FE-SEM specimens in a fume hood (a); hardened resin-impregnated specimens were sanded and polished (b) until the surface was smooth and free of scratches. Inspection of specimens was carried out using a binocular microscope while specimens were clamped at the base of the microscope (c) .....	73
Figure 4.19 - Finished epoxy resin-embedded-specimens (3 treatments x 2 locations x 5 blocks) mounted on aluminum stubs using double-sided tape. A set of resin-free non-embedded specimens was also prepared (arrowed right) .....	73
Figure 4.20 - Zeiss UltraPlus field emission scanning electron microscope (FE-SEM) (Carl Zeiss International. <a href="http://www.zeiss.com/microscopy">http://www.zeiss.com/microscopy</a> ) .....	74
Figure 4.21 - 3D rendered X-ray micro-CT image of a leached OSB specimen obtained using a conventional micro-CT system. Wood is rendered brown; voids are black; and zinc is green. Note checks arrowed red; aspen vessel element arrowed white; and latewood band in pine arrowed cyan .....	75
Figure 4.22 - Orthogonal rendered X-ray micro-CT image of a leached OSB specimen obtained using a conventional CT system. Note the presence of micro-checks arrowed red in the wood flake. Wood is rendered brown; voids are black; and zinc is green.....	76
Figure 4.23 - 3D rendered X-ray micro-CT image of an unleached OSB specimen obtained using a conventional CT system. Red axis (z) represents the thickness of the board, and zinc is rendered green. Note that zinc forms a fine network in the composite, oriented in the x-y plane. Scale bar is 4 mm.....	77
Figure 4.24 - <i>Dry</i> OSB plug (left) and the same plug after wetting and drying (right) - the thickness of the plug increased from 10.5 mm ( <i>dry</i> ) to 12.8 mm as a result of wetting and drying. The irreversible thickness swelling was 21.98% .....	78
Figure 4.25 - Perspective view of OSB plug before (left) and after wetting and drying (right) .....	78
Figure 4.26 - Matched in-plane rendered helical X-ray micro-CT images of part of an OSB plug before (a) and after wetting and drying (b). Red arrows indicate existing internal checking in <i>dry</i> OSB (a), and green arrows represent internal checking formation in <i>wet/dry</i> OSB (b). Note the formation of several new internal micro-checks (arrows in b), as well as the enlargement of existing ones. Scale bars are 1 mm .....	79
Figure 4.27 - In-plane rendered helical X-ray CT images showing part of an OSB sample. Note individual aspen and pine flakes delineated by adhesive bond lines containing zinc (rendered green). Aspen flakes highlighted red in <i>dry</i> (a) and	



<i>wet/dry</i> (b) data sets. Note larger checks (blue) in pine flakes (brown), compared to aspen flakes (red) in both <i>dry</i> and <i>wet/dry</i> data sets. Partial recovery of vessel elements in aspen's upper flake after wetting and drying is clear in (b). Scale bars are 0.5 mm .....	80
Figure 4.28 - In-plane rendered helical X-ray micro-CT image of the centre (slice at 50%) of a <i>wet/dry</i> OSB data set. Wood is rendered brown; lumens are black; voids magenta; cracks cyan; and zinc is white. Scale bar is 1 mm .....	81
Figure 4.29 - Matched in-plane rendered helical X-ray micro-CT images of part of the OSB plug before (a) and after wetting and drying (b). The phases shown are: wood (brown), zinc (green), voids (magenta) and cracks (cyan). Scale bars are 1 mm..	82
Figure 4.30 - Matched in-plane rendered helical X-ray micro-CT images of part of the OSB plug before (a) and after wetting and drying (b). The phases shown are: cell-lumen (black), voids (magenta) and cracks (cyan). Scale bars are 1 mm .....	82
Figure 4.31 - Matched in-plane rendered helical X-ray micro-CT images of part of the OSB plug before (a) and after wetting and drying (b). The phases shown are: voids (magenta) and cracks (cyan). Scale bars are 1 mm .....	83
Figure 4.32 - Area occupied by the phases representing strands (square) and cell-lumens (triangle) in the <i>dry</i> v. <i>wet/dry</i> OSB data sets (slices from 0-100 %) across the specimen's length.....	84
Figure 4.33 - Area occupied by phases representing voids (circle) and checks (dash) in the <i>dry</i> v. <i>wet/dry</i> OSB data sets (slices from 0-100 %) across the specimen's length. Changes in voids or checks appeared to be proportional in frames.....	85
Figure 4.34 - Area occupied by the zinc phase in the <i>dry</i> v. <i>wet/dry</i> OSB data sets (slices from 0-100 %) across the specimen's length. Note the decrease in area occupied by zinc associated with wetting and drying .....	85
Figure 4.35 - Graph showing the average area of phases from all slices from the <i>dry</i> and <i>wet/dry</i> data sets. Note that voids and cracks occupy a greater proportion of the overall area in the <i>wet/dry</i> data set .....	86
Figure 4.36 - Area of phases from replicate slices from the <i>dry</i> (red) v. <i>wet/dry</i> (blue) data sets. Non-overlap of error bars indicates that individual means are significantly different ( $p < 0.05$ ) .....	86
Figure 4.37 - Matched out-of-plane rendered X-ray micro-CT images of part of an OSB plug before (a) and after wetting and drying (b). Wood is rendered brown; voids are black; and zinc is white. Note that less zinc is present in the image after wetting and drying. Scale bar is 0.5 mm .....	87
Figure 4.38 - Matched orthogonal rendered X-ray micro-CT images of part of an OSB plug before (a) and after wetting and drying (b). Wood is rendered brown; voids are black; and zinc is white. Green arrows point to the same aspen vessel element. Scale bars are 0.5 mm .....	87
Figure 4.39 - Out-of-plane images showing the 3D distribution of zinc in both <i>dry</i> (a & c) and <i>wet/dry</i> (b & d) data sets. Images on the bottom (c & d) only show the	

presence of zinc. Note that the <i>wet/dry</i> data set (d) suggests that wetting and drying reduced the level of zinc in the OSB specimen .....	88
Figure 4.40 - FE-SEM image from an OSB specimen exposed to 72 h of water soaking and subsequent drying. Note the within wall (arrowed left) and inter-wall (arrowed right) fractures (highlighted cyan) in pine latewood .....	90
Figure 4.41 - FE-SEM image obtained from an OSB specimen exposed to the wetting & drying cycle used in Chapter 3. Note the within wall micro-check in the earlywood of a cross-section of a pine flake (arrowed centre) .....	90
Figure 4.42 - FE-SEM image of an OSB specimen exposed to 72 h of water soaking and subsequent drying; effective infiltration of embedding medium in voids (arrowed right) and in earlywood has clearly occurred (arrowed left), but infiltration does seem to be as complete in latewood (arrowed centre) .....	91
Figure 4.43 - FE-SEM image of an unsoaked OSB specimen that acted as control. Note a long micro-check (arrowed centre) at a radial surface between a pine flake and an adjacent aspen flake (vessel element arrowed left) .....	91
Figure 4.44 - FE-SEM image of an unsoaked OSB specimen that acted as control. Note a long micro-check (arrowed centre) at a cross-section of a pine flake; a resin canal is arrowed right .....	92
Figure 4.45 - FE-SEM image of an unsoaked OSB specimen that acted as control. Note micro-checks (arrowed left) within a cross-section of an aspen flake; an inter-strand void is arrowed right .....	92
Figure 4.46 - FE-SEM image of an OSB specimen that was not embedded with resin and was exposed to the wetting & drying cycle used in Chapter 3. Note that the surface of the specimen is fuzzy and the interface of the micro-check (arrowed left) in latewood of a softwood flake is not clearly visible. Intervessel pits in part of an aspen flake are arrowed right .....	93
Figure 4.47 - FE-SEM image of an OSB specimen that was not embedded with resin and was exposed to 72 h water soaking and subsequent drying. Note the indistinct checks (arrowed black) in between earlywood and latewood bands of softwood. Higher magnification inset (square box) is shown below in Figure 4.48 .....	93
Figure 4.48 - Magnified FE-SEM image of the same OSB specimen shown above in Figure 4.47. Note that the fuzzy torn surface obscures micro-checks .....	94
Figure 4.49 - FE-SEM image of an OSB specimen that was not embedded with resin and was exposed to the wetting & drying cycle in Chapter 3. Note aspen vessel element (arrowed) .....	94

## Acknowledgements

I would like to express my sincere thanks to Professor Dr. Philip D. Evans for supervising and giving me valuable assistance throughout the course of my Master's study. His mentoring also provided me with valuable lessons about academia and life in general. Furthermore, his scientific knowledge and experience have certainly been key factors that contributed to the quality of the research in this thesis. The funding obtained by Professor Evans was essential for the completion of this research. I'm very honoured to have received the opportunity to be a part of 'the Evans Group'.

I would like to extend my thanks to my supervisory committee members Dr. Simon C. Ellis and Dr. Scott Renneckar, and also Mr. Dan Price and Mr. Kevin Blau from Tolko, for your support and helpful suggestions.

I thank all of the people at The Australian National University (ANU) who helped me with X-ray micro-CT and FE-SEM: Dr. Andrew Kingston, Dr. Michael Turner, Dr. Holger Averdunk, Dr. Tim Senden (Department of Applied Mathematics, RSPE); Dr. Ajay Limaye (Visualization Lab, ANU Supercomputing Facility); Dr. Hua Chen and Dr. Frank Brink (ANU's Centre for Advanced Microscopy).

My warmest thanks go to Dr. Ciprian Lazarescu and Professor Dr. Stavros Avramidis for their mentoring, advice and friendship. I'm greatly indebted to my family and many friends at UBC, especially those in my research group: Barend Lötter, George Chan, Joseph Kim, Kenny Cheng, Sina Heshmati, Siti Hazneza, Will He and Yuner Zhu. Thanks for all of your suggestions, time, friendship and support.

I thank the support of the Faculty of Graduate and Postdoctoral Studies and the Faculty of Forestry at UBC, for providing me with a grant to travel to the United States of America (USA) to present my work at the 111<sup>th</sup> American Wood Protection Association

(AWPA) Annual Meeting in 2015. I thank the AWPA for granting me a Travel Award to travel to Puerto Rico in the USA to present my work a second time at the 112<sup>th</sup> AWPA Annual Meeting in 2016.

My sincere gratitude to the donors of the Donald S. McPhee Fellowship and VanDusen Graduate Fellowship in Forestry for their financial support, and Gayle Kosh and Robin Poirier-Vasic for their help. Cindy Prescott and Dan Naidu, also from the Faculty of Forestry, helped me a lot during tough times. Thank you very much.

## Dedication

*To science.*

# Chapter 1: Introduction

## 1.1 Oriented strand board

Oriented strand board (OSB) is a wood composite panel manufactured from thin wood strands bonded together under heat and pressure with a thermosetting water-resistant adhesive. The panel is usually composed of three layers, in which strands in the upper and lower (face) layers are oriented parallel to the long axis of the panel, whereas smaller strands in the centre of the panel are cross-oriented (Figure 1.1a) or randomly-oriented (Figure 1.1b) relative to those in the surface layers (Tsoumis 1991). According to Kline (2005), OSB is composed (w/w) of approximately 95% wood, 4% adhesive and 1% wax sizing.

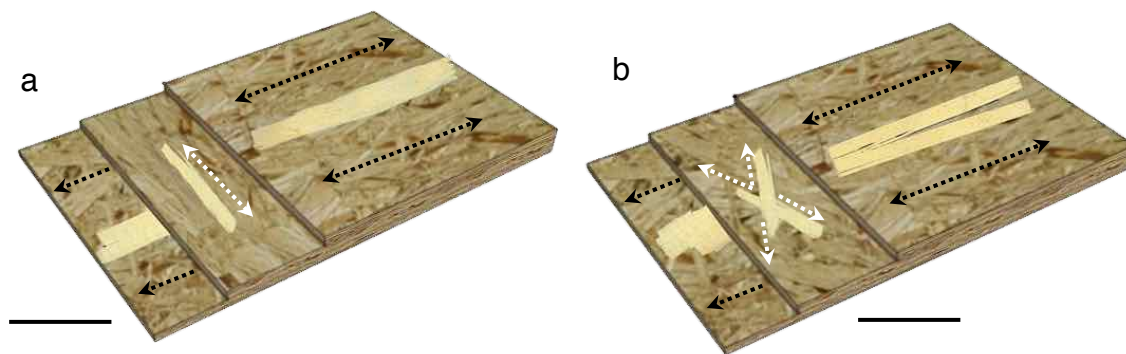


Figure 1.1 - Computer-generated images showing the different layers and orientations of strands within OSB panels; core layer cross-oriented (a- arrowed white); core layer oriented randomly (b- arrowed white). Scale bars are 5 mm (redrawn from: Structural Board Association 2005)

OSB is used as an engineered structural panel in a wide range of construction and industrial applications (Structural Board Association 2005). It is the most common structural wood-based panel used for housing in North America, in applications such as roof and wall sheathing and sub-floors (Figure 1.2) (Grossman 1992, Moya et al. 2008). Other common end uses for OSB are: web material for I-joists, structural insulated panels, pallets, stands, furniture frames, decks, platforms, shelves, packaging (Janssens 1998), and more recently engineered wood flooring (Barbuta et al. 2012).

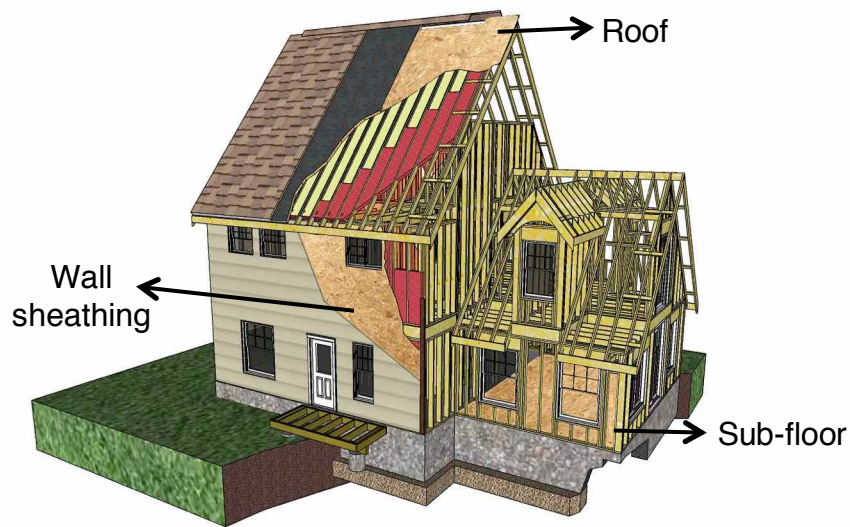


Figure 1.2 - Computer-generated image showing the main uses of OSB in housing; wall sheathing (arrowed left), roof (arrowed centre) and sub-floor (arrowed right)

According to the Structural Board Association (2005) OSB became available commercially in North America in 1981, and gradually displaced its predecessor, waferboard. Since then there has been rapid growth in the production of OSB, mainly at the expense of plywood. Some of the reasons for this growth in production of OSB compared to plywood according to Cloutier (1998) are: (i) reduction in the availability of good quality logs for peeling plywood veneer; (ii) OSB can be made with lower quality logs and cheaper woods; (iii) OSB unlike plywood does not contain large defects such as knots and holes; and (iv) the size of OSB panels is less constrained by equipment and technology. One of the most significant advantages of OSB compared to plywood is the conversion efficiency of the raw material (Kelly 1977); strand yields for OSB are 85-90 percent according to Shmulsky and Jones (2011), whereas the comparable figure for plywood is 40 percent (Plinke et al. 2010).

The production of OSB in North America in 2015 was 20.4 billion ft<sup>2</sup> (3/8-inch basis) (1.9 billion m<sup>2</sup> - 9.5 mm basis) and will increase in the coming years, according to The Engineered Wood Association (APA, 2016). Hence, North America is by far the largest producer of OSB, with 85% of the world's production (UNECE/FAO 2015).

OSB used in buildings can become wet during the early stages of construction, when panels are unprotected and exposed to rainwater or high levels of relative humidity (Winterowd et al. 2003). Water easily penetrates OSB through the void network between overlapping strands and is absorbed by wood strands (Suchsland 1959, Wu and Piao 1999). These strands swell due to the hygroscopic nature of wood, and cause thickness increases in the panel (Winterowd et al. 2003). Thickness swelling of OSB (Figure 1.3) is a limiting factor in many applications, because it leads to unacceptable variation in thickness between and within boards (Suchsland 1962, Carll and Wiedenhoef 2009, Akrami et al. 2014). Such variation in thickness creates a non-planar surface, which may then need to be levelled by sanding (Taylor et al. 2008), at considerable expense (Carll and Wiedenhoef 2009, Shmulsky and Jones 2011).

#### *1.1.1 Structure and thickness swelling of OSB*

Thickness swelling of OSB is associated with permanent losses in strength (Wu and Piao 1999), and misalignment of boards when they are used as an underlay for flooring, as mentioned above (Shmulsky and Jones 2011). Thickness swelling of OSB is the net product of two components (Halligan 1970): (1) reversible thickness swelling caused by hygroscopic swelling of wood strands; and (2) irreversible thickness swelling (springback - Figure 1.3b) resulting from recovery of compression strains imparted to the composite during hot pressing (Neusser et al. 1965). In addition to springback, straightening of strands (Lloyd 1984, Irle 2001), the failure of adhesive bonds and the development of voids within particulate composites also contribute to irreversible thickness swelling (Hsu et al. 1988, Wu and Piao 1999). According to Shaler (1986), an aspen flakeboard with a density of  $700 \text{ kg/m}^3$  contains approximately 7.3% of inter-strand voids. If these voids increase in size, the density of the flakeboard will become lower and mechanical properties will decrease (Kelly 1977). In-plane density variation in OSB contributes to the formation of delamination and voids according to Bucur (2011).



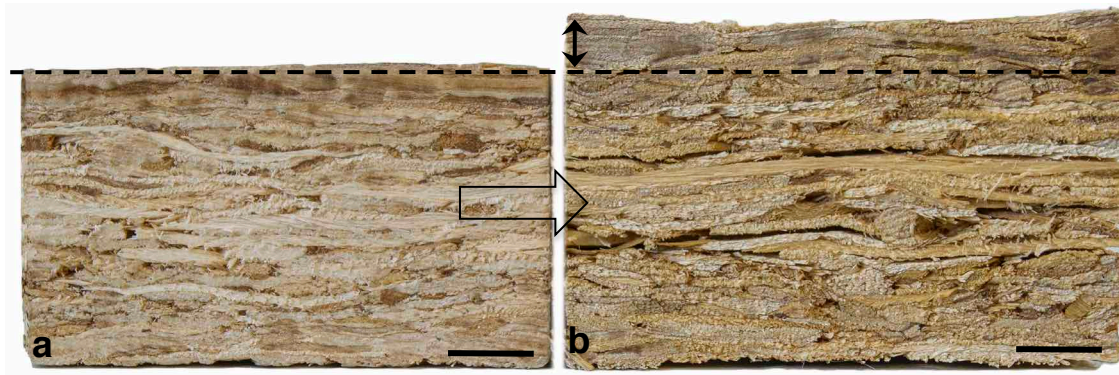


Figure 1.3 - In-plane photograph of OSB showing irreversible thickness swelling caused by moisture-induced swelling (b- arrowed centre). Note the permanent thickness swelling (b- area above the dashed line) relative to the original board (a). Scale bars are 4 mm

## 1.2 Micro-checking

Micro-checks are voids in wood resulting from the separation of wood cell under moisture-induced or mechanical stresses (Donaldson 2010). Large checks visible to the naked eye in solid wood are termed macro-checks. Checks that are smaller are termed micro-checks (Figure 1.4). Such checks can be observed under a microscope or using other visualization techniques (Bucur 2011). Checks in solid wood are defined as “cracks, if they penetrate through solid wood or deeper than 75 % of the board’s thickness” (Flæte et al. 2000). The latter is not relevant to wood composites such as OSB, as checks do not penetrate through panels. In this thesis I define a micro-check in OSB as a longitudinal separation of wood tissue occurring within strands, as opposed to voids created by delamination of adhesive bond-lines.

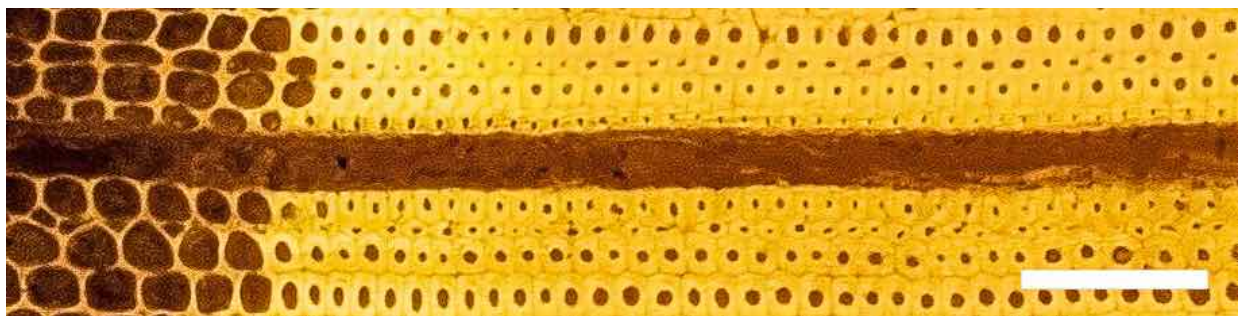


Figure 1.4 - Micro-check in pine wood. Scale bar is 100 µm

### 1.3 General hypothesis

Evans et al. (2015b) briefly mentioned the micro-checking of OSB, but in comparison to the micro-checking of solid wood, micro-checking of OSB has received little attention. However, the micro-checking of OSB is likely to be complicated by the presence of numerous glue-lines that are more dimensionally stable than wood, and also by voids in the composite that do not restrain the dimensional movement of individual flakes. Glue-line failure and the formation of voids in wood composites when they swell contributes to the irreversible thickness swelling of composites, as mentioned above (Wu and Piao 1999, Konnerth and Gindl 2006). Voids created by internal checks can lead to increases in the dimensions of solid wood. For example, when wood is subjected to intense microwave radiation the formation of numerous internal checks in the wood substantially increases the dimensions of the wood leading to a 13% reduction in the oven dry density of the wood (Figure 1.5) (Torgovnikov and Vinden 2009). The formation of micro-checks is also associated with volume changes in other materials for example silicic volcanic rocks, sulfate-rich clay and Vertisol (a type of soil in which there is a high content of expansive clay known as montmorillonite that forms deep cracks in drier seasons) (Cox and Etheridge 1989, Amann et al. 2014, Gargiulo et al. 2015). The drying and shrinkage of solid wood is often associated with the development of micro-checks due to restraint of shrinkage at the surface of wood by wetter surface and also sub-surface layers causing unbalanced tensile stresses (Schniewind 1963). When these stresses exceed the tensile strength of wood, checks develop.

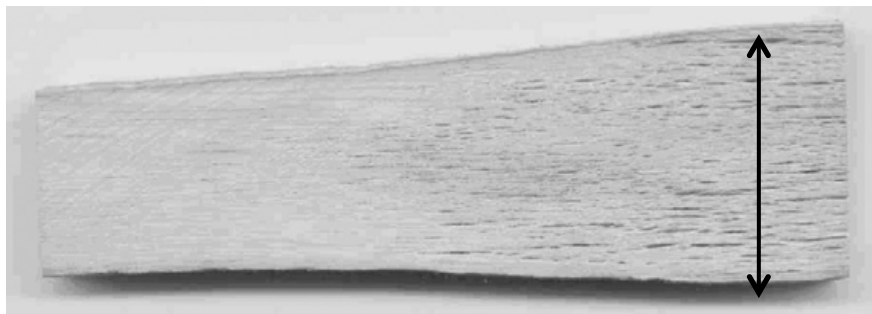


Figure 1.5 - Messmate stringybark (*Eucalyptus oblique* L'Her.) sample after intense microwave modification; left-hand side of the sample is unmodified natural wood (ovendry density of 778 kg/m<sup>3</sup>); the right-hand side (arrowed) of the sample is microwave modified wood (ovendry density of 686 kg/m<sup>3</sup>). (photograph c/o Torgovnikov and Vinden 2009)

In the case of wood composites such as OSB, flaking or stranding of logs creates checks in flakes (Geimer et al. 1985, Bucur 2011), which may enlarge when OSB swells and shrinks as a result of wetting and drying. Furthermore, some flakes are large enough to develop unbalanced surface and sub-surface tensile stresses. Hence, moisture changes at the surface and internally in OSB might result in intra-strand checking, in addition to delamination of adhesive bond lines (Figure 1.6).

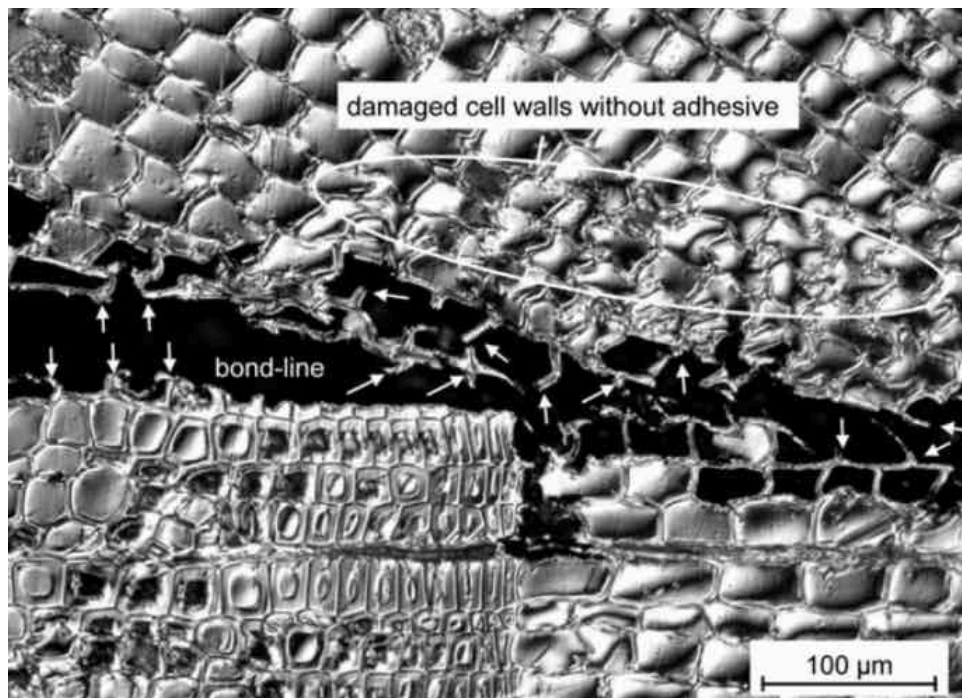


Figure 1.6 - Light microscopy image of a transverse section of parallel-strand lumber made from spruce. Note fractured and delaminated zones indicated by arrowheads. (image c/o Konnerth and Gindl 2006)

In this thesis I hypothesize that micro-checking will develop when OSB is exposed to wetting and drying. I further hypothesize that surface and internal micro-checking of OSB in addition to inter-strand delamination will contribute to the irreversible thickness swelling of OSB.

## **1.4 Outline of thesis**

Chapter 1 of this thesis provides background information on OSB and provides a general hypothesis for the thesis. Chapter 2 provides background information on manufacture of OSB; micro-checking of wood; physical properties including thickness swelling of OSB; imaging of OSB and micro-checking; and the methods used to reduce thickness swelling of OSB. Chapter 3 describes an inexpensive high-resolution macro-photography system that was used to visualize the swelling and shrinkage of wood and OSB specimens in real-time. The same system was used to quantify the surface micro-checking of solid wood and OSB, and to explore whether surface micro-checking contributed to the irreversible swelling of OSB. In Chapter 4 the microstructure of OSB is probed at higher resolution using X-ray micro-computed tomography (X-ray micro-CT). X-ray micro-CT is used to examine the internal microstructure of OSB and the changes in microstructure (including micro-checking) that occur when OSB is subjected to wetting and drying. Field emission scanning electron microscopy (FE-SEM) is used to examine the fracture surfaces of micro-checks. Chapter 4 also explores the extent to which micro-checking contributes to the irreversible thickness swelling of OSB. Finally, Chapter 5 discusses the results of Chapters 3 & 4 and how they support my general hypothesis, makes recommendations for future research, and draws overall conclusions.

## Chapter 2: Review of the Literature

### 2.1 Manufacture of oriented strand board

OSB is a structural panel made from oriented wood strands bonded together with a thermosetting adhesive, as mentioned in Chapter 1. The manufacture of OSB (Figure 2.1) begins with debarking of logs, which are then stored in water or transferred to a stranding machine. After stranding, flakes (or furnish) are then dried and blended with resin(s) and wax. Blending of face and core flakes typically occur in separate blenders and may use different resin formulations. Face resins are usually liquid or powdered phenolics, whereas core resins are phenolics or, increasingly, isocyanates (Winandy and Kamke 2003). During blending, other additives can be incorporated into the furnishes, for example wax or biocides, such as zinc borate. Oriented layers of strands within the mattress (face, core, face, for example) are laid sequentially, each by a different forming head, onto a moving belt until the desired number of layers are present (generally three). A hot press consolidates the mattress of oriented and layered strands and, heats it up to cure the resins and achieve a target density (Moslemi, 1974b).

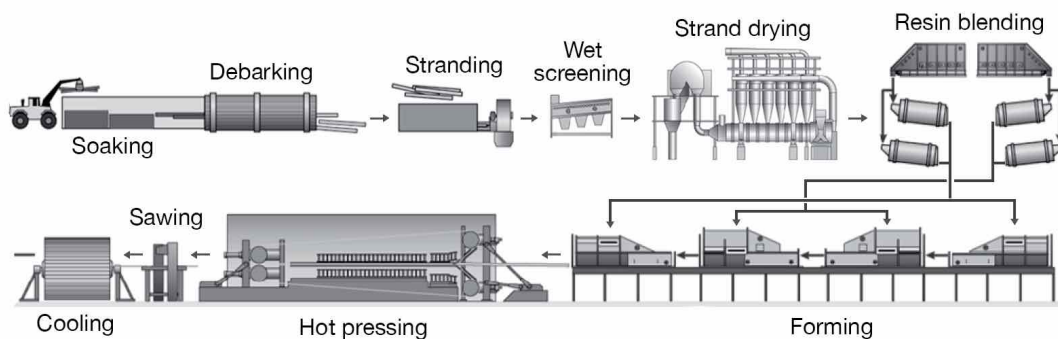


Figure 2.1 - Typical sequence during the manufacture of OSB. The logs are debarked and furnish is produced by the strander, followed by screening, drying, blending, forming, hot pressing, and finally sawing and cooling (redrawn from: Thoemen et al. 2010)

According to Maloney (1993), the manufacture, properties and microstructure of OSB are affected by several factors including: (i) raw material, such as wood species, and their anatomical structure; wood density; moisture content; extractives present in the wood; and (ii) process parameters, such as target board density; compaction ratio; composition of boards; type and amount of resin and wax; flake moisture content; flake geometry; time and temperature and pressure applied during hot pressing.

### 2.1.1 Wood species

The use of single or mixed wood species for the manufacture of OSB is described in several studies (Turner 1954, Akrami et al. 2014). The wood species used to manufacture OSB has a significant effect on board properties according to Kelly (1977), and it interacts with almost every other variable involved in the manufacturing process (Febrianto et al. 2010). The effect of 'species' on panel properties is mainly related to the strong effect of wood density on the microstructure of panels. Woods with a density up to 550 kg/m<sup>3</sup> are recommended for the manufacture of OSB because they permit high compaction ratios and larger contact between surfaces of strands during hot pressing—the opposite occurs with high-density woods (Maloney 1993). Hence, OSB made from low-density wood is uniform and has good capacity to distribute compression forces between and within strands. As a result it has better flexural properties and internal bond strength than OSB made from denser species (Cloutier 1998). However, variability in wood density within species is important and large within-species variation can negatively affect processing operations, such as stranding, drying, application of adhesive and pressing of OSB (Maloney 1993). OSB manufactured in western Canada mainly uses trembling aspen (*Populus tremuloides* Michx.) (Smook 2011). Trembling aspen was first used in waferboard, a panel that resembles OSB (Stark et al. 2010). OSB displaced waferboard and became the predominant structural panel used in North America, surpassing plywood production in the year 2000 (Structural Board Association 2005). Now other wood species such as southern pine (*Pinus spp.*), paper birch (*Betula papyrifera* Marsh.), red maple (*Acer rubrum* L.), sweetgun (*Liquidambar styraciflua* L.), and yellow-poplar (*Liriodendron tulipifera* L.) are

commonly used to manufacture OSB (Stark et al. 2010). In addition, a large number of medium-density softwood and hardwoods have been tested in the laboratory to determine their suitability for the manufacture of OSB (Winandy and Kamke 2003).

Table 2.1 lists the species used to manufacture OSB in the laboratory and in commercial plants.

Table 2.1 - Species used to manufacture OSB commercially and experimentally

Scientific name	Popular name	Production type	Reference
<i>Pinus contorta</i> Dougl.	Lodgepole pine	Commercial*	Morrison-Knudsen Forest Products (1987)
<i>Populus tremuloides</i> Michx.	Aspen	Commercial*	Cloutier (1998)
<i>Betula papyrifera</i> Marsh.	Paper birch	Commercial*	Cloutier (1998)
<i>Populus spp.</i>	Aspen	Commercial*	Wu (1999)
<i>Pinus spp.</i>	Southern pine	Commercial*	Wu (1999)
<i>Pinus massoiana</i> Lamb.	Massion pine	Commercial**	Wolcott et al. (1997)
<i>Populus deltoides</i> Bartr.	Poplar	Commercial**	Wolcott et al. (1997)
<i>Abies grandis</i> Lindl.	Grand fir	Experimental	Sobral Filho (1981)
<i>Quercus rubra</i> L.	Red oak	Experimental	Geimer (1982)
<i>Populus x euramericana</i> cv. <i>San Martine</i>	Hybrid poplar	Experimental	Zhou (1989)
<i>Tsuga canadensis</i> (L.) Carr.	E. Hemlock	Experimental	Avramidis and Smith (1989)
<i>Pinus strobus</i> L.	White pine	Experimental	Avramidis and Smith (1989)
<i>Shorea spp.</i>	Meranti Bukit	Experimental	Sasaki et al. (1989)
<i>Pinus echinata</i> Mill.	Shortleaf pine	Experimental	Biblis (1989)
<i>Liquidambar styraciflua</i> L.	Sweetgum	Experimental	Biblis (1985)
<i>Pinus densiflora</i> Sieb. et Zucc.	Japanese red pine	Experimental	Sasaki et al. (1989)
<i>Pseudotsuga menziesii</i> D. Don	Douglas-fir	Experimental	Canadido et al. (1990)
<i>Carya illinoensis</i> K. Koch	Pecan hickory	Experimental	Brunette (1991)
<i>B. papyrifera</i> Marsh.	Paper birch	Experimental	Au et al. (1992)
<i>P. tremuloides</i> Michx.	Aspen	Experimental	Macnatt et al. (1992)
<i>Populus balsamifera</i> L.	Balsam poplar	Experimental	Aston (1993)
<i>Liriodendron tulipifera</i> L.	Tulip poplar	Experimental	Grigoriou and Biblis (1995)
<i>Hevea brasiliensis</i> (Müll. Arg.)	Rubberwood	Experimental	Yusoff and Horie (1997)
<i>Cryptomeria japonica</i> D. Don	Sugi	Experimental	Zhang et al. (1998)
<i>Chamaecyparis obtusa</i> Endl.	Hinoki	Experimental	Zhang et al. (1998)
<i>Populus grandidentata</i> Michx.	Bigtooth	Experimental	Wu (1999)
<i>Eucalyptus grandis</i> (Hill ex Maiden)	Eucalyptus	Experimental	Iwakiri et al. (2002)

\* US and Canadian OSB industry; \*\* Chinese OSB industry

Because 'wood species' has a significant effect on the properties of OSB including those examined in this thesis, the following paragraphs review research on the effects of wood species on the properties of OSB.

The wood properties that influence the properties of OSB include the proportion of earlywood and latewood, nature of the transition from earlywood to latewood (texture), width of growth rings, heartwood-sapwood ratio, porosity, dimensions of fibers and tracheids (cell wall thickness, lumen diameter, length and width), and wood's extractive content (Beer 1982, Pugel et al. 1990). Few studies have examined the effects of wood microstructure on the properties of OSB, but one study by Pecho et al. (2005) suggested that it had an effect on the mechanical properties and thickness swelling of OSB. Pecho et al. (2005) examined the effect of juvenile and mature wood of radiata pine (*Pinus radiata* D. Don) on the physical-mechanical properties of OSB. They observed a decrease in internal bond strength and an increase in the thickness swelling of boards with increasing proportions of juvenile wood in the OSB. They attributed this to the presence of a wider earlywood band and a thinner cell wall, which had greater capacity to adsorb water.

#### 2.1.1.1 Softwood and hardwood

The anatomy of hardwoods is much more variable than that of softwoods for a number of reasons. Firstly hardwoods are composed of several cell types including fibers, vessel elements of different sizes and arrangements, and axial parenchyma of varying abundance (Wiemann 2010). Secondly, the rays which make up the radial cellular system show great diversity in cell sizes and shapes (Panshin et al. 1964). In contrast, softwoods are mainly composed of one cell type, longitudinal tracheid and there is far less diversity in cellular microstructure than that observed in hardwoods (Figure 2.2).



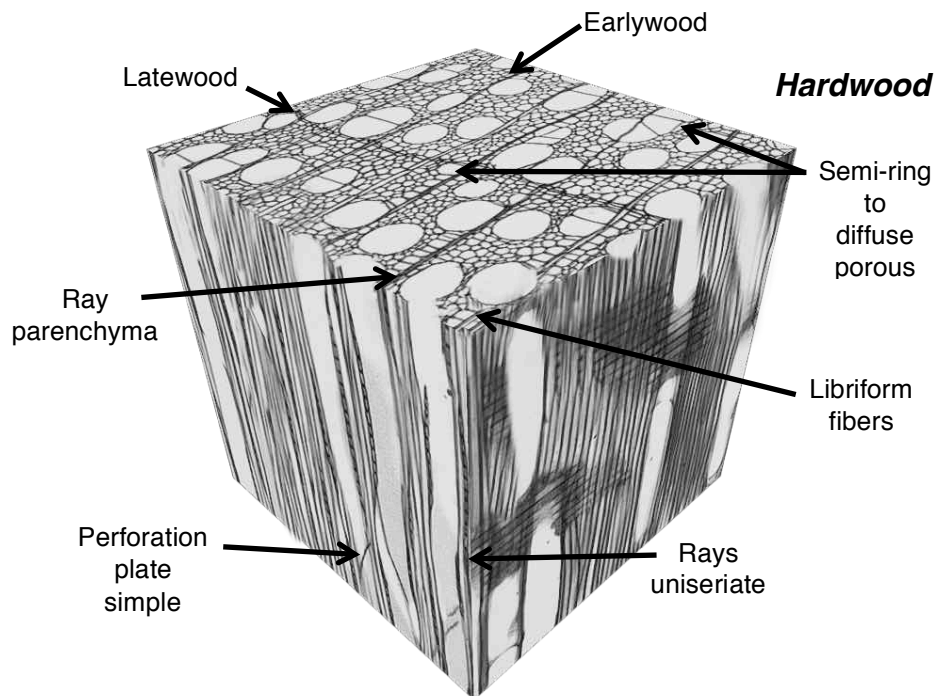
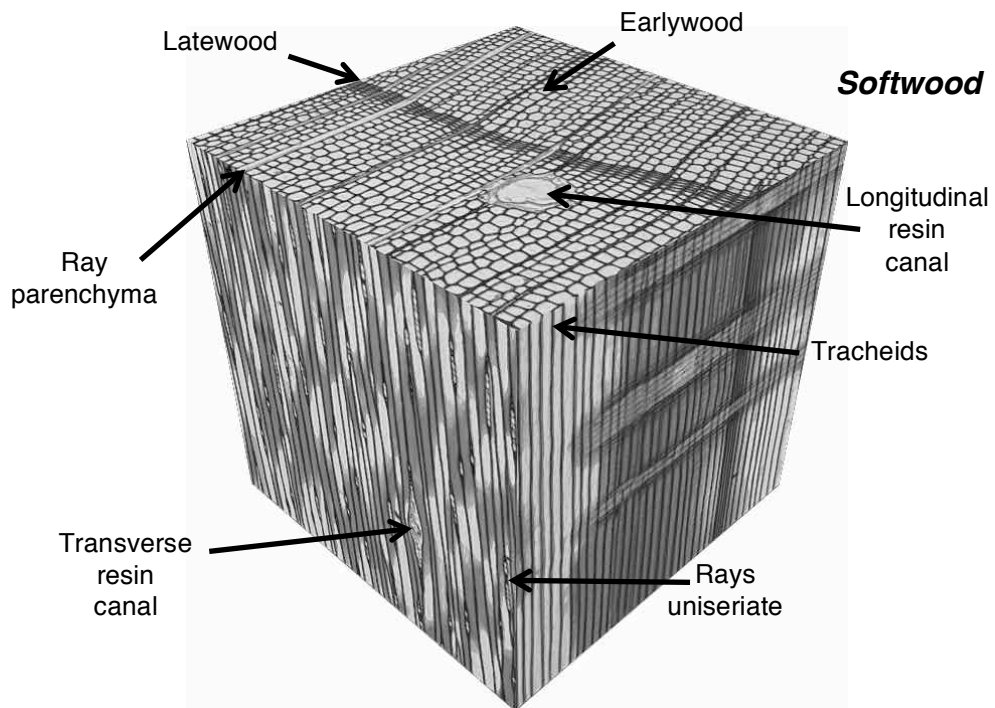


Figure 2.2 - Diagrams showing the 3D structure of a softwood (top) and hardwood (bottom); the wood species are: lodgepole pine (top - 75x) and aspen (bottom - 90x), respectively (redrawn from: Panshin and De Zeeuw 1980)

The OSB I examine experimentally in this thesis is made from a mix of trembling aspen and lodgepole pine. Therefore, a description of their anatomical, physical and mechanical properties follows (Table 2.2).

Trembling aspen is Canada's most abundant aspen species (Zsuffa 1996). It is found across Canada and is one of the few commercially important hardwood species in western Canada (Einspahr and Wyckoff 1990). Aspen is a semi-ring- to diffuse-porous hardwood characterized by relatively short fibers (1.32 mm average) and high wood moisture content (Panshin and De Zeeuw 1980). The pores are small, mostly evenly distributed throughout annual growth rings, and contain simple perforation plates. The sapwood of aspen is white, and the heartwood is light brown. The wood is uniform in texture; straight-grained; light and soft; has good dimensional stability and low to moderate shrinkage (Wiemann 2010). The rays are uniseriate and essentially homocellular. Aspen is primarily used for the manufacture of OSB and bleached Kraft pulp (Ondro 1989).

Lodgepole pine is native to western North America. It occurs from New Mexico to north of the Arctic Circle and from the eastern foothills of the Rocky Mountains to the Pacific ocean (Koch 1996). Lodgepole pine is a softwood with long tracheids (3.19 mm average), and much larger differences in moisture content between heartwood and sapwood compared to aspen. The wood is light in color; soft; straight-grained; uneven in texture, with an abrupt transition from earlywood to latewood. Lodgepole pine contains longitudinal and transverse resin canals, and rays of two types, uniseriate or partly biseriate, and fusiform. It has low natural durability and is relatively difficult to treat with preservatives. Its principal use is as construction lumber for housing. It is also used for shelving, cabinetry, interior trim, fence posts and rails, transmission or telephone poles, house logs, veneer, plywood, pulpwood and firewood (Wiemann 2010).

Table 2.2 - Comparison of the physical and mechanical properties of aspen and lodgepole pine

Properties		Aspen	Lodgepole pine
Density (kg/m <sup>3</sup> )	Green	408	430
	12% MC	374	410
Specific gravity	Green	0.35	0.38
	12% MC	0.38	0.41
Moisture content (%)	Heartwood	95	41
	Sapwood	113	120
Oven-dry shrinkage (%)	Radial	3.5	4.3
	Tangential	6.7	6.7
	Volumetric	11.5	11.1
	Tang/Rad ratio	1.9	1.6
Static bending	Modulus of rupture (MPa)	Green	35
		12% MC	58
	Modulus of elasticity (GPa)	Green	5.9
		12% MC	8.1
Compression parallel to grain (MPa)	Green	15	18
	12% MC	29	37
Compression perpendicular to grain (MPa)	Green	1.2	1.7
	12% MC	2.6	4.2
Shear parallel to grain (MPa)	Green	4.6	4.7
	12% MC	5.9	6.1
Tension perpendicular to grain (MPa)	Green	1.6	1.5
	12% MC	1.8	2.0

References: Summit and Sliker (1980), Kretschmann (2010), Glass and Zelinka (2010).

Both lodgepole pine and aspen are similar in terms of their physical properties. Their overall volumetric shrinkage is almost identical, but aspen is more anisotropic than lodgepole pine. Lodgepole pine is stronger in most respects (except tension perpendicular to grain), and most importantly, its maximum crushing strength at 12% MC is 26% greater than that of trembling aspen.

Millions of hectares of mountain pine beetle-killed (MPB) lodgepole pine trees have become available in British Columbia, due to the largest epidemic of MPB in recorded history (Feng and Knudson 2007, Smook 2011). Dead lodgepole pine trees infected by the MPB dry out as the stems or logs age, causing defects such as checks. Severely checked MPB logs may not be suitable for lumber production (Lau et al. 2006).

However, they are increasingly used to manufacture OSB because of their favorable

wood density, tendency to plasticize when pressed at high temperatures, and ease of gluing. However, aspen remains the preferred wood species in Canada for the manufacture of OSB.

#### 2.1.1.2 Mixed species

OSB can be manufactured from wood obtained from a single species such as aspen or it can be made from a mix of wood species.

Au et al. (1992) tested the possibility of using paper birch in the core of OSB made from aspen. They found that the use of paper birch (a medium-density wood species) in the core led to decreased resin consumption, thus reducing production costs. They concluded that it was possible to make OSB with satisfactory properties from a mix of aspen and paper birch.

Zhang et al. (1998) made OSB by mixing the high-density softwood hinoki (*Chamaecyparis obtusa* Endl.) with lower density sugi (*Cryptomeria japonica* D. Don). They found that adding strands of hinoki to the surface layers of boards, with low proportion of face/core, improved parallel mechanical properties of the OSB.

Wang and Winistorfer (2000) also made OSB from a mix of different wood species. They were interested in the relationship between thickness swelling and layer characteristics of OSB panels made from the different species. They found that OSB made from 100% aspen flakes swelled 12.8% after 24 hours of water exposure; in comparison OSB made from 100% southern pine swelled 18.7%. Furthermore, the presence of aspen strands in either the face or the core layers of the panel resulted in decreased thickness swelling in those layers. Wang and Winistorfer (2000) attributed this positive effect of aspen on thickness swelling to the lower density of aspen, and its even cell structure that facilitated uniform compression during pressing. They suggested that 'internal swelling stress during water exposure is accordingly lower for aspen than for a different species with a higher density and more uneven cell structure'. However, they concluded that aspen and southern pine can be mixed or alternated in the

face/core, without compromising the quality of OSB.

Brunette (1993) studied the physical properties of OSB made from spruce (*Picea glauca* (Moench) Voss), jack pine (*Pinus banksiana* Lamb) or balsam fir (*Abies balsamea* (L.) Mill.) and found that internal bond strength of panels made from these species was equivalent to that of panels made entirely from aspen. Thickness swelling after 24-hour soaking was slightly lower for aspen panels than those of panels made from the three softwoods. Furthermore, adding and mixing softwood furnish with aspen tended to have a negative effect on thickness swelling of OSB panels.

### *2.1.2 Production of OSB strands*

The properties of wood influence its behaviour during stranding. Fischer (1972) describes the operation of the machines used to produce strands. His description is rather old, but it is still relevant today.

Disk-style flaker is often used in OSB plants to manufacture strands (Smook 2011). It consists of a metal disk with cutting knives mounted at regular intervals. As the disk rotates, billets are placed and held against the cutting surface by chain systems in the log in-feed. The cutting of strands occurs with high precision parallel to the wood grain of billets. According to Brunette (1993) the orientation of billets when they are fed into the strander (ie., radial cut vs. tangential cut) did not significantly affect physical properties (including thickness swelling) of OSB made from the different strands.

Conditioning ponds are used prior to the stranding process to improve strand quality by increasing log temperature and moisture content (Alberta Research Council 1990, Smook 2011). Woods with high moisture content usually yield more strands during stranding due to a reduced amount of fines generated by stranding wetter wood (Grant 1995). Woods with high moisture content however can produce strands with fuzzy surfaces, which leads to poor adhesion, as well as increasing operational costs associated with drying (Cloutier 1998). However, damage (crushing, cell wall buckling, splintering and cracking) develop in strands when parent logs are too dry. Hence,

ideally the moisture content of logs should preferably be slightly above the fiber saturation point prior to stranding (Kelly 1977).

OSB is made from strands that are typically 75 - 150 mm long, 15 - 25 mm wide, and 0.3 - 0.7 mm thick (Irle and Barbu 2010). These dimensions differ from those used for waferboard which are approximately as long as they are wide, and have random orientation in the panel (Mackes and Lynch 2001). OSB strands can be characterized by their thickness, width and length (Geimer 1976). According to Maloney (1977), the ratio between the length and width of the strands should be at least threefold to allow good orientation of strands in OSB mats. Another important parameter is the slenderness ratio (ratio of length to thickness), which has a large influence on the properties of OSB (Moslemi 1974a, Kelly 1977).

Strands produced for structural panel products vary according to species and strander operating characteristics. Species properties such as green density, modulus of rupture, modulus of elasticity and tensile strength perpendicular to the grain, as well as anatomical characteristics such growth ring characteristics, vessel length, fiber length, vessel volume and fiber volume all affect flake quality. According to Beer (1982), higher density hardwood species with ring and semi-ring porous growth rings are very difficult to convert into quality flakes because flakes split along the ring of large earlywood vessel elements.

### *2.1.3 Drying of strands*

After the stranding operation, strands are dried to remove moisture but before this occurs they are stored in wet bins to equalize their moisture content. This conditioning stage is necessary because large differences in moisture content between strands can be problematic. For example furnish that is too dry when it enters the dryers can be over-dried and ignite (Smook 2011). Some species such as lodgepole pine show large variations in wood moisture content between the sapwood and heartwood, as mentioned above, and for such species conditioning of strands prior to drying is highly recommended.

Generally, the target wood moisture content after drying of strands varies between two and seven percent (Maloney 1993). Drying is usually performed in a 3-pass dryer, which is basically a three-cylinder rotary drum. Drying infeed temperatures and strand retention time in the dryer are set according to the size, geometry, and moisture content of the strands (Smook 2011). The Alberta Research Council (1990) dried strands of aspen and black poplar (*Populus nigra* L.) at different temperatures and examined the quality of OSB made from the strands. High drying temperatures resulted in lower internal bond strength and diminished thickness swell for both species (Alberta Research Council 1990).

#### *2.1.4 Blending*

The blending operation blends resins and waxes with the furnish in rotating drums. As the strands tumble they are coated with atomized resin and wax (Maloney 1993). The aim of blending is to achieve a uniform distribution of resin on every strand (Thoemen et al. 2010). The adhesive acts as a binder during pressing and after curing of boards. The furnish gains moisture during blending since the resin is often mixed with alcohol and water. Wax added to the furnish during blending slows down water absorption of the panel (Borgin 1961).

##### *2.1.4.1 Resins (adhesive)*

The main adhesives used for the manufacture of OSB are: phenol formaldehyde (PF), methylene diphenyl diisocyanate (pMDI), and urea formaldehyde (UF) (Gomez-Bueso and Haupt 2010). The surface layers of OSB use either powdered PF or liquid PF. PF or pMDI resins are mainly used in the core layers of OSB (Cloutier 1998). Taylor et al. (2008) showed that using pMDI resin instead of PF reduced thickness swelling of OSB. The greater effectiveness of pMDI at reducing thickness swelling of OSB may be related to its ability to form both chemical and mechanical bonds with wood. The disadvantage of isocyanate adhesives is that they adhere to aluminum and some types of steel, causing production problems, for example, causing boards to stick to metal

platens. According to Galbraith et al. (1983) this problem has largely been solved using release agents.

Generalla et al. (1989) compared different ratios of phenolic resin in the manufacture of OSB, indicating an optimum (cost-benefit) amount of adhesives of 5% compared to the dry weight of flakes. In addition, they also claimed that the production of wood composites with an adhesive content greater than 7% was uneconomical. Avramidis and Smith (1989) tested the effect of different phenolic resin content levels (4, 5 and 6% based on oven-dry weight) and face-to-core ratios on some mechanical and physical properties of OSB. They showed that increased resin content levels and face-to-core ratios resulted in improved mechanical (MOE, MOR and IB) and physical properties (thickness swelling and linear expansion) of the OSB.

#### 2.1.4.2 Wax sizing

Wax is introduced into OSB furnish as a molten slack wax or as a water-based wax emulsion together with resin during blending as mentioned above (Eckert and Edwardson 1998). Wax improves OSB's water repellency and restricts absorption of liquid water by panels. However, it does not reduce absorption of water vapour and it only reduces rates of water absorption and thickness swelling (Maloney 1993).

Furthermore, there is a limit to the level of wax that can be added to OSB before it starts to interfere with bonding. For example, Kelly (1977) in his review of the influence of processing variables on the properties of particulate panels pointed out that wax contents above 1% (based on the dry weight of furnish) reduce panel strength by interfering with adhesive curing. In support of this suggestion Winistorfer et al. (1992) found an inverse relationship between wax level (0.5 - 1.0 - 1.5%) and the internal bond strength of OSB. However, higher wax levels were more effective at reducing the water absorption, thickness swelling and linear expansion of OSB. An additional benefit of adding wax to the OSB furnish is that it helps with the transfer of strands on forming lines and through the forming heads, and screw conveyors before pressing (Blau, K., Tolko Industries Ltd., personal communication, April 4, 2016).



### *2.1.5 Mat forming*

After the blending operation, strands are sent to mat formers where they fall between spinning disks or troughs before being laid down in linear layered mats along a conveyor system. The conveyor then carries the layered mats into the press (Stark et al. 2010). According to Thoemen et al. (2010), the orientation and proportion of long strands in the face layers has a marked effect on parallel bending properties. However, Geimer (1985) found that alignment of flakes in flakeboard mats had little influence on thickness swelling.

The effects of forming machine parameters (ie., free fall distance and plate spacing) and resource parameters (ie., flake geometry) on strand alignment and distribution (horizontal and vertical) of strands in the mat are factors that are most relevant to horizontal density profiles and thickness swelling of OSB (McNatt et al. 1992, Grant 1995, Brochmann et al. 2004).

### *2.1.6 Pressing*

Pressing compacts and consolidates the oriented and layered mattress of strands in a hot press at platten temperatures of 177°C to 204°C (350°F to 400°F) to cure the resins in 3 to 5 minutes. Resinated mats are pressed either in multiple-opening daylight presses or in a continuous press which conveys and compresses them between rollers (Stark et al. 2010).

The most important parameters involved in the pressing cycle are: pressure, temperature and pressing time. Pressure (4-6 MPa) is required to densify the mat to the final panel thickness, and also to ensure adequate surface contact between wood strands (Paridah et al. 2006). The temperature during pressing is set depending on the type of resin used. It is necessary to polymerize and cure the resin, and assist in compacting flakes to the final thickness of the mattress by plasticizing the wood, thereby reducing damage to strands caused by compression (Marra 1992). Geimer et al. (1985)

studied the influence of processing-induced damage on strength of flakes and flakeboards. They observed crushing and cell wall buckling, shearing, tension and bending failures in microtomed sections cut from flakes that had been pressed. Such damage may explain why the average strength and stiffness of flakes decreased as a result of pressing by 13 and 34 percent, respectively. One positive finding from Geimer et al. (1985) was that strength losses were inversely related to press temperatures. This was attributed to either a reduction in damage due to increased plasticization or a repair of damage by lignin flow.

Hot pressing should create a vertical density profile in the thickness direction of the board, and in flakeboard such a profile influences thickness swelling (Song and Ellis 1997). Ideally, the board should be denser at its surface, and lower in its core. Such a vertical density gradient can be altered by manipulating mat forming, moisture content of the mat, rate of press closing, temperature of the hot press and the reactivity of the resin. The compressive strength of the wood also influences vertical density profile (Kelly 1977).

## **2.2 Properties of OSB**

### *2.2.1 Physical properties*

#### **2.2.1.1 Density**

The density of particulate composites is important because it is correlated with most other properties, except linear expansion (Shuler and Kelly 1976, Haygreen and Bowyer 1996). Two factors influence the density of wood composites: (i) the density of the raw material; and (ii) the compaction ratio of the mat of strands or particles (Kelly, 1977).

According to Wang and Winistorfer (2000) density is the most important factor affecting the stress-strain relationship of the mat during hot-pressing, vertical density distribution and panel properties. The density of the wood used to make OSB, compaction ratios and density of resulting OSB panels are shown in Table 2.3.

Table 2.3 - Wood density, panel density and compaction ratio of OSB

Panel density (kg/m <sup>3</sup> )	Wood density (kg/m <sup>3</sup> )	Compaction ratio	Reference
630	480	1.31	Au et al. (1992)
650	400	1.63	Zhou (1989)
700	360	1.94	Avramidis and Smith (1989)
700	380	1.84	Avramidis and Smith (1989)
700	350	1.56	Avramidis and Smith (1989)
700	680	1.03	Sasaki et al. (1989)
480 to 960	430	1.11 to 2.23	Geimer (1982)
630 to 670	360	1.75 to 1.86	Macnatt et al. (1992)
630 to 670	480	1.31 to 1.39	Cloutier (1998)
670 and 730	390	1.71 and 1.87	Sobral Filho (1981)

Zhou (1990) reported that for most applications OSB should have a density between 650 and 700 kg/m<sup>3</sup>. Elevated compaction ratios can cause OSB panels to swell excessively when they come in contact with moisture (Maloney 1993). Thickness swelling generally increases as panel density increases, due to increased densification of strands in the board, and the release of compression strains when the panel comes into contact with water (Moslemi 1974b, Kelly 1977).

Xu and Suchsland (2007) simulated the effect of different densities on mechanical properties of OSB. Their model showed that when the compaction ratio of OSB panels was the same, a panel with only one layer of high-density wood strands had superior MOE to that of OSB made from low-density wood. However, when the density of the panels was the same, the MOE of panels made with high-density particles was inferior.

### *2.2.2 Thickness swelling of OSB and other particulate wood composites*

The dimensional stability of solid wood is related to its anatomy, hygroscopicity, chemical composition, hysteresis, amongst others (Glass and Zelinka 2010). Dimensional stability of wood composites is also related to these factors, however, additional factors including processing parameters (mentioned above) affect the dimensional stability of wood composites (Kelly 1997). According to Haygreen and Bowyer (1996) the additional factors that strongly influence the swelling of wood composites are: “(i) restraint of swelling by the different layers that make up the

composite; (ii) compaction ratio of the panel (plywood, particleboard, fiberboard) as mentioned above; and (iii) effect of adhesives and additives”.

The first factor mainly applies to plywood, although it may also be relevant to OSB, which has a structure that resembles that of plywood. The layout of plies perpendicular to each other in plywood restrains shrinkage and swelling of adjacent plies (Del Menezzi 2004). The adhesion between plies determines the extent to which the plies can resist dimensional changes (Haygreen and Bowyer 1996).

The second factor is mainly relevant to particulate composites (wafer, flake, chip and strand boards), for which the mattress of particles can be compressed up to 10 times their initial thickness, introducing compressive strains in finished panels. When the panel comes in contact with moisture, some of these strains are released, resulting in thickness swelling, which is often more pronounced at the edges of boards (Carll and Wiedenhoef 2009). Excessive pressure during the consolidation of plywood may also result in moisture-induced thickness swelling of plywood, but generally wood-veneer based composites are less prone to moisture-induced thickness swelling than particulate composite. Such moisture-induced thickness swelling resulting from the recovery of compressive strains is irreversible, in contrast to the reversible swelling of wood flakes in the composite.

The third factor that distinguishes dimensional changes in wood composite from those in solid wood is the presence of adhesives and additives. The most common additives used in wood composites are wax and preservatives. The effect of wax on the thickness swelling of OSB was described above. Adhesives reduce thickness swelling of the wood cell wall, thus acting as bulking agents (Haygreen and Bowyer 1996). For example, low molecular weight components of resin may be able to bulk the capillary system inside strands, without chemical bonding, consequently restricting moisture ingress by acting as physical barriers (Rowell and Banks 1985). Most importantly adhesives resist the forces that lead to thickness swelling.

Thickness swelling of OSB is an important property affected by numerous variables such as wood species, geometry and condition of strands, board density, adhesive content, bonding efficiency and pressing conditions (Halligan, 1970) as described above (Lehmann 1972, Vital et al. 1980). Thickness swelling of OSB is a serious problem, because it is associated with reductions in the physical and mechanical properties of panels (Suchsland 1973). Hence, standards specifying the property requirements of OSB invariably stipulate that the thickness swelling of the composite should fall below a certain value. For example in North America, the most used industry standard (Voluntary Performance Standard PS 2-04) requires the thickness swelling of OSB to be limited to 25% after 24 h of immersion in water (NIST 2004). In contrast a more restrictive thickness swelling tolerance has been adopted in Europe (12-25% depending on end-use, EN 2006).

## **2.3 Micro-checking of wood and wood composites**

In Chapter 1, I pointed out why micro-checks develop in solid wood, and also how micro-checks can increase the volume of solid wood and also other materials. The definitions and background research on micro-checking in solid wood and wood composites are presented in the next sections (2.3.1 to 2.3.5).

### **2.3.1 Definitions**

Checks that are visible to the naked eye are classified as macro-checks, whereas micro-checks can only be observed under the microscope. Flæte et al. (2000) defined checks as cracks, not penetrating wood deeper than 75 % of the board thickness. Micro-checking can be described as the separation, breakup or fracture of the wood cell wall as a result of mechanical stresses. Such micro-checks were described by Donaldson (2010) 'as delamination of the cell wall' (Figure 2.3), which can occur by intrawall fracture between adjacent tracheids or fibers (Figure 2.4), or in association with rays, or less commonly by transwall fracture, where the cell lumen is exposed (Donaldson 1997). Interwall fracture is a special case of intrawall fracture that occurs within the middle lamella (Côté and Hanna 1983).

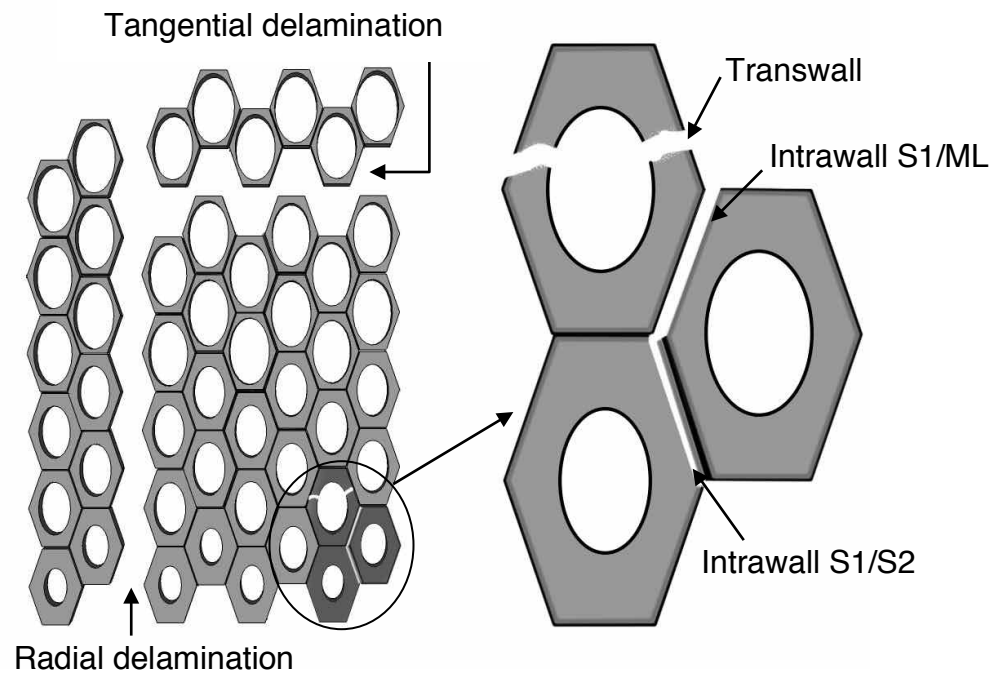


Figure 2.3 - Diagram of cell wall delamination in both radial and tangential planes, showing transwall and intrawall fracture types. (redrawn from: Donaldson 2010)

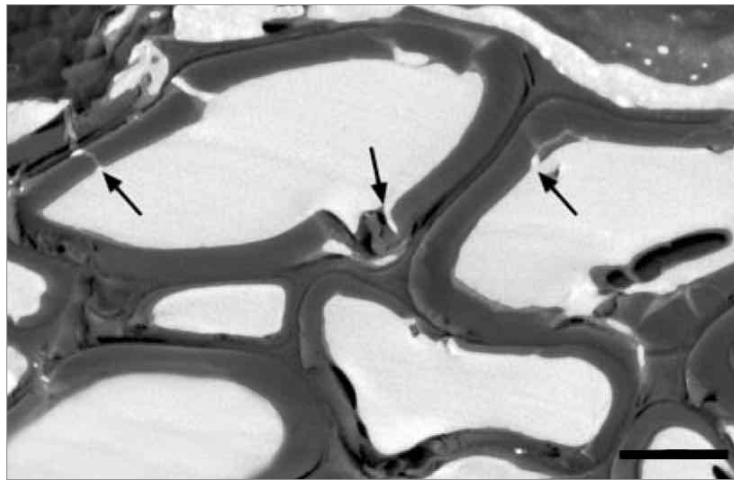


Figure 2.4 - FE-SEM back-scattered electron image of tracheids in plywood coated with a stain. Note coating penetration into micro-checks in the wood cell wall. Scale bar is 10  $\mu\text{m}$ . (redrawn from: Singh et al. 2007)

### 2.3.2 Location of micro-checks and variation of micro-checking in different species

Wood shows anisotropic fracture properties depending on the method of stress application (compression, tension or shear), and the direction of the applied force in relation to grain direction. Under compression, cell walls crumple, forming slip planes or compression failures (Kučera and Bariska 1982), while in tension shear fracture within (intrawall) or across (transwall) the cell wall occurs (Côté and Hanna 1983). Intrawall fracture is favored in thick cell walls with large microfibril angles, while transwall fracture is favored in thin-walled cells with small microfibril angles (Wardrop 1951, Fröhmann et al. 2003).

The development of micro-checks varies between wood species. For example, Coupe and Watson (1967) examined the location of micro-checks in softwoods and hardwoods subjected to accelerated weathering. In softwoods most micro-checks originated in latewood, while larger, but fewer micro-checks developed in earlywood. Flæte et al. (2000) examined check formation in two different species (aspen and Norway spruce (*Picea abies* (L.) Karst.)). Aspen developed a high number of relatively short checks; whereas Norway spruce developed fewer, but longer checks. However, Cheng (2015) found that check number and check length for trembling aspen were both less than in white spruce (*Picea glauca* (Moench) Voss).

### 2.3.3 Development of micro-checks during wetting and drying

The swelling and shrinkage of solid wood is often associated with the development of micro-checks because restraint of shrinkage at the surface of wood by wetter sub-surface layers causes tensile stresses to develop. When these stresses exceed the tensile strength of the wood, checks develop (Schniewind 1963). Most reports of the micro-checking of solid wood suggest that micro-checks develop during drying (Yamamoto et al. 2013, Sakagami et al. 2013) in rays and at the boundary of between latewood and earlywood due to uneven drying stress (Morén 1994, Hanhijärvi et al. 2003).

A considerable swelling pressure builds up when wood adsorbs moisture. In fact, the pressure exerted by swollen wood was used in ancient times to crack rocks (Niemz 2012). The density of wood and its swelling pressure are directly correlated. A higher swelling pressure was observed parallel to the grain than perpendicular to the grain. Wood composites also develop swelling pressures. For example, a swelling pressure of 0.2-0.4 N/mm<sup>2</sup> was noted for medium density fiberboard (MDF) (density: 600 kg/m<sup>3</sup>). Internal stresses vary in glued elements with different properties (different element thicknesses, different fibre and grain angles, differences in the EMC). These swelling stresses may also damage the adhesive bond between woody elements in wood-based panels (Donaldson 1997, Bucur 2011).

#### *2.3.4 Internal checking*

Internal checking, is defined as 'checking enclosed within the bulk of wood', and is characterised by radial delamination associated with wood's rays (Booker et al. 2000). Rays represent a natural point of weakness in wood because they are orientated perpendicular to the grain, have reduced lignification, and thin cell walls (Thuvander et al. 2000, Thuvander and Berglund 2000). Every tracheid is in contact with at least one ray (Zhang et al. 2003), so any radial checking must involve rays at some location (Bucur 2011). Whether checking develops at the ray or merely follows the path of least resistance is not known. According to Putoczki et al. (2007) checks typically result from delamination between adjacent tracheid, fiber or ray cell walls.

#### **2.4 Imaging of OSB and micro-checking**

Currently there is no universally accepted test methodology for assessing the micro-checking of wood (Ratu 2009). The micro-checking of wood can be directly examined by light microscopy. However, it is important to maintain the structural integrity of the material because sample preparation, for example, sectioning can damage the wood, introducing new micro-checks or obscuring existing ones (Donaldson 2010). Such damage can be avoided by embedding the sample in low-viscosity resin before



sectioning. According to Donaldson (1995), embedding will maintain the structural integrity of the wood sample without producing additional damage, and also allow thin sectioning for examination of fracture surfaces. Serial sectioning and 3D reconstruction has been used in combination with light microscopy to examine delamination at sawn wood surfaces (Donaldson et al. 2007). Another form of light microscopy, confocal reflectance microscopy, can be helpful for imaging cell wall layers at fracture surfaces (Donaldson and Frankland 2004). Higher resolution images of fracture surfaces and micro-checks can be obtained using scanning or transmission electron microscopy (Borgin 1971a, Putoczki et al. 2007, Evans et al. 2008). Images acquired from thermographic cameras, confocal profilometry, ultrasonography, X-ray computed tomography (CT), and nuclear magnetic resonance imaging can also be employed to study the micro-checking of wood and wood-composite materials (Thoemen et al. 2010, Evans et al. 2010, Evans et al. 2015a). Wood composites such as OSB possess complex microstructure, and there are difficulties involved in characterizing them. Lenth and Kamke (1996) developed a method of quantifying the cellular structure of a flakeboard mat using the cross-sectional void fraction, individual void geometry and distribution. An earlier study by Shaler (1986) used mercury porosimetry to determine the inter-strand void volume in flakeboard of different densities, flake orientations, species composition and resin levels. Voids in OSB can also be visualized and measured using light or electron microscopy in combination with computer image processing technology (Li et al. 2010). According to Muszyński and Launey (2010) these techniques are suitable for bridging the gap between experimentation and modelling taking into consideration the complexity of the internal structure of wood-based products.

#### *2.4.1 X-ray CT imaging*

X-ray photons have sufficient energy to penetrate through objects, so X-ray imaging can be used to non-destructively measure, characterize, or identify flaws such as cracks in many engineering materials (Zhang 2007). X-ray CT imaging has been used in medicine to visualize the inside of the human body since the 1970s (Hounsfield 1973,

Ambrose and Hounsfield 1973). Today X-ray CT can produce virtual cross-sectional images (tomograms) of the inner structure of the human body and other materials, based on transmission measurements of penetrating X-ray ionizing radiation (Witomski et al. 2010). The physical variable measured with this technique is the integrated X-ray linear attenuation coefficient caused by the material's density (Davis and Wells 1992). Attenuation is a measure of the ratio of transmitted to the incident beam (Ambrose and Hounsfield 1973). A greyscale value is associated with the attenuation, and an individual volume unit, the voxel. The voxel size is directly related to the resolution of the tomogram. X-ray CT with a resolution in the micrometer range is termed X-ray micro-CT (Banhart 2008).

X-ray CT imaging of wood has been used to characterize the internal structure of wood and detect internal defects, such as knots and cracks in logs and utility poles, as well as to generate optimized sawing patterns for the breakdown of logs (Taylor et al. 1980a,b, Funt and Bryant 1987, Davis and Wells 1992). X-ray CT has also been used to study wood composites, for example, the size and position of the macro-voids in Parallam were measured using medical X-ray CT (Sugimori and Lam 1999). More recently, Zhang et al. (2005) and Wu et al. (2006) used X-ray CT to image the internal void structure of OSB. Insulation boards made out of larch (*Larix decidua* Mill.) bark were scanned with an industrial X-ray CT to evaluate the effects of particle orientation on the thermal conductivity of panels (Kain et al. 2016).

X-ray micro-CT is now widely used to explore the microstructure of geological, biological, and engineering materials including wood (Maire 2012, Cnudde and Boone 2013, Maire and Withers 2014). X-ray micro-CT has been used to analyze weak links inside wood plastic composites (Shaler et al. 2003), and to detect anomalies at glue-line interfaces, adhesives distribution and characterize 3D density and moisture profiles in wood (Fromm et al. 2001, Kamke and Lee 2007). Morrison (2004) and Evans et al. (2010) analyzed the distribution of a melamine-urea-formaldehyde (MUF) adhesive in particleboard using X-ray micro-CT in combination with chemical labelling of the MUF adhesive. They were able to quantify the voids, adhesive and wood fraction within the

composite. The effects of thermo-hydro treatment on microstructural changes, such as mass loss and porosity in softwoods and hardwoods were recently analyzed using X-ray micro-CT by Biziks et al. (2016). Standfest et al. (2010) used sub-micrometer X-ray CT, to investigate correlations between the different physical and micro-structural properties of OSB, particleboard and MDF.

Internal micro-checks and voids in dry OSB consist of empty spaces, thus causing no attenuation to X-ray radiation, which allows for high-contrast thresholding between wood flakes and empty space (cell-lumen; voids and micro-checks). Thus it should be possible to use X-ray micro-CT to non-destructively visualize and measure the spatial distribution of checks and voids in OSB. However, manual segmentation may be required to distinguish between micro-checks and voids, since they consist of the same phase (empty space).

#### *2.4.2 Field emission scanning electron microscopy (FE-SEM)*

FE-SEM provides surface information at magnifications up to 300,000x, with virtually unlimited depth of field (Reed 2005, McKay 2015). Unlike the images generated by optical (light) microscopy, FE-SEM images are not seen directly; rather the images are formed on a monitor through the encryption of the signals generated by the interaction of electrons with the sample. FE-SEM is capable of observing structures as small as 1 nanometer (Reed 2005). Hence, FE-SEM is a powerful tool for examining the microstructure of OSB at very high-resolution, potentially making it possible to precisely locate where fracture events take place within wood cell walls. However, OSB is difficult to section especially after wetting and drying (Bucur 2011), and hence, according to McKay (2015), in SEM, a resin embedding stage may be necessary prior to imaging, as is the case for other biological materials (Spurr 1969, Donaldson 1995). The resin when cured and hardened forms a firm structure that supports and preserves the original structure of the sample during sample preparation (cutting and polishing prior to imaging).

## **2.5 Methods of reducing thickness swelling and micro-checking of wood and wood composites**

This thesis does not examine methods of reducing the thickness swelling and micro-checking of OSB, but some of my results suggest ways of reducing such degradation of OSB. Therefore, I briefly review the subject here. For more detailed reviews consult Forintek Canada Corp. (1998), Shmulsky and Jones (2011), and Lötter (2014).

### *2.5.1 Improving dimensional stability of wood and wood composites*

Improving the dimensional stability of the woody elements in wood composites is an obvious route to reducing their moisture-induced thickness swelling. There are several types of treatments that can be employed to improve the dimensional stability of wood: (1) bulking treatments (Rowell and Youngs 1981); (2) chemical modification (Hill and Malon 1998) and; (3) heat treatment (Chen and Workman Jr 1980). Modification to production processes, such as choice of raw material, changes to board composition and press parameters can also be used to modify the dimensional stability of particulate wood composites (Kelly 1977).

Modification treatments can be applied to wood particles or fibres before pressing and panel consolidation, including: vapour treatments (Hsu et al. 1988); acetylation (Rowell et al. 1986) or impregnation of strands with low molecular weight PF resin (Haygreen and Gertjeansen 1971). All these treatments bulk wood cell walls.

Alternatively, post-treatments such as heat treatments can be applied to consolidated panels to increase their dimensional stability (Roffael and Rauch 1973, Shen 1974, Hsu et al. 1989, Suchsland and Xu 1991). The goal of heat treatment is to release compression strains in the panel imparted during pressing of the mat. Heat treatments can also be employed as a pre-treatment to reduce the hygroscopicity of OSB strands (Moslemi 1974b). However, heat treatments can reduce the mechanical properties of OSB (Goroyias and Hale 2002).

Other ways of improving the dimensional stability of particulate wood panels, such as increasing their resin content (Halligan 1970, Shmulsky and Jones 2011), wax sizing (Hsu et al. 1990, Winistorfer et al. 1992), and cross-lamination (Rowell and Youngs 1981) were described (above) in Sections (2.1.3.1; 2.1.3.2; 2.1.4, respectively).

The application of surface coatings (paints and lacquers) and water-repellents are commonly used to improve the dimensional stability of solid wood. These products form a film on or in the wood, acting as a physical barrier to liquid water. They may also limit the adsorption and desorption of water vapour (Williams et al. 2005). He et al. (2000) coated the surfaces or edges of OSB samples using five different types of paint. Such coatings significantly reduced the thickness swelling and water absorption of OSB after 24 hour water soaking. Evans and Cullis (2008) assessed the effects of sanding and coating OSB with UV-cured finishes on the dimensional stability of OSB. They found that thickness swelling of coated boards after 72 hours immersion in water was less than one third of that of uncoated OSB.

Water-repellent preservatives are very similar to water repellents. They contain a fungicide, in addition to wax (water-repellent), resin and solvents. Wax and oil emulsion additives (waxes and oils) have been added to wood preservatives to increase the resistance of the treated wood to distortion and checking (Fowlie et al. 1990, McIntyre and Fox 1990). Mantanis and Papadopoulos (2010) dipped OSB samples in a water-repellent solution containing paraffin wax and found that it reduced water absorption and thickness swelling of OSB. The effectiveness of water-repellent preservatives at reducing thickness swelling of OSB was also tested by Baileys et al. (2003). Aspen furnishes used for the commercial manufacture of OSB were treated with water-repellent. The thickness swelling of treated OSB after 24 hours of water soaking was 8%, significantly lower than that of the control (23.8%) (Baileys et al. 2003). Water absorption was also greatly reduced as expected. Preston et al. (2008) patented a system in which green wood furnish was treated with water-repellent chemicals that are known to prevent solid wood from checking and swelling. Their results showed that the

treatment was effective at reducing both the thickness swelling and water absorption of OSB.

### *2.5.2 Reducing micro-checking of wood and wood composites*

Many environmental factors influence the checking of solid wood (Borgin 1971b). The most important ones are wood species and their properties (Schniewind 1963).

Therefore one of the most effective methods of reducing the surface checking of solid wood products is to select a species that is dimensionally stable and less susceptible to checking (Cheng 2015). Various physical methods can also be used to restrain checking, or chemical treatments can be used to dimensionally stabilize wood or make it water repellent (Ruddick and Ross 1979, Zahora 2000).

Surface grooving was used to reduce the checking of plywood (Deskey 1942).

According to Elmendorf (1950) the grooves allowed the surface of the boards to freely shrink and swell thus reducing surface checking. The surface micro-checking of wood composites such as OSB has received little attention.

## **2.6 Concluding summary**

The gaps in the literature that I identified in this thesis were the lack of information on the microstructure and micro-checking of OSB exposed to moisture-induced degradation. I also suggested that such microstructural changes may contribute to the irreversible thickness swelling of OSB. Subsequent experimental chapters will probe the microstructure of OSB subjected to wetting and drying to examine the changes that occur when OSB swells and dries.

## **Chapter 3: Surface Micro-Checking of Treated Wood and OSB Exposed to Wetting and Drying**

### **3.1 Introduction**

In this chapter, my aim is to develop a technique to investigate surface micro-checking of treated wood and OSB during wetting and drying. The relationship between the surface micro-checking and irreversible thickness swelling of OSB is explained, as well as the effectiveness of water-repellent treatments at restricting surface checking of treated wood. In Chapter 4, I explore the use of additional state-of-the-art technologies to investigate the *internal* micro-checking of OSB.

The dimensional stability of wood and OSB is easily measured, and methods have also been developed to automate measurement of the surface checking of solid wood (Christy et al. 2004). Such measurements are usually independent, whereas it would be better to simultaneously measure shrinkage/swelling and micro-checking to understand the relationship between surface strains and checking of treated wood and possibly OSB. The swelling and shrinkage of solid wood is often associated with the development of surface micro-checks because of the presence of moisture gradients and unbalanced strains (Schniewind 1963). Voids created by micro-checks can lead to permanent increases in the dimensions of solid wood (Torgovnikov and Vinden 2009), as well as in other materials (Cox and Etheridge 1989), as mentioned above. In the introduction to this thesis I hypothesized that micro-checking will develop in OSB exposed to wetting and drying. In this and the subsequent chapter I examine this hypothesis, and also examine whether micro-checking contributes to the thickness swelling of OSB exposed to wetting and drying.

Hydrophobic additives (waxes and oils) are commonly added to wood preservatives to increase the resistance of treated wood to distortion and checking, as described in Chapter 2 (Belford and Nicholson 1969, Levi et al. 1970). In this chapter I also describe an inexpensive high-resolution imaging system to visualize the swelling and shrinkage of water-repellent treated wood and OSB specimens in real-time. I use the system to

quantify the surface micro-checking of wood and OSB specimens, as mentioned above. The advantages of the system for quantifying the swelling and surface micro-checking of wood and OSB specimens, as well as its limitations are discussed.

## **3.2 Materials and methods**

### *3.2.1 Experimental design*

A randomized block design was used to examine the effect of wetting and drying on the thickness swelling, moisture content, surface checking and enlargement of voids in OSB. The same approach was used to examine the ability of water-repellent treatments to restrict the surface checking of treated wood.

The experiment was replicated six times (6 blocks), using OSB samples measuring 50.8 x 50.8 mm (length x width) and 10.5 mm in thickness that were obtained from different panels obtained from a commercial OSB mill in Western Canada. The OSB was web-stock used for I-joists, and was made from a mix of wood species (75% lodgepole pine and 25% aspen) bonded with PF (surface layers) and pMDI (core of boards) adhesives. During the manufacture of the OSB, powdered zinc borate biocide (1 to 2 % w/w) was added to the resinated wood flakes to increase the insect resistance of the OSB (Kirkpatrick and Barnes 2006, Han et al. 2012). The average density of the six OSB samples after conditioning at  $20 \pm 1^\circ\text{C}$  and  $65 \pm 5\%$  relative humidity (r.h.) to a moisture content of 9.9% (SD = 2.4) was  $650.5 \text{ kg/m}^3$  (SD = 53.1).

Two kiln dried southern pine (*Pinus* spp.) and aspen (Figure 3.1) boards donated by FPInnovations in Vancouver were conditioned at  $20 \pm 1^\circ\text{C}$  and  $65 \pm 5\%$  r.h., to reach moisture contents of 12.56% (SD = 0.29) and 11.49% (SD = 0.09, respectively. Their corresponding average densities were  $553.32 \text{ kg/m}^3$  (SD = 27.86) and  $520.31 \text{ kg/m}^3$  (SD = 41.74), respectively.



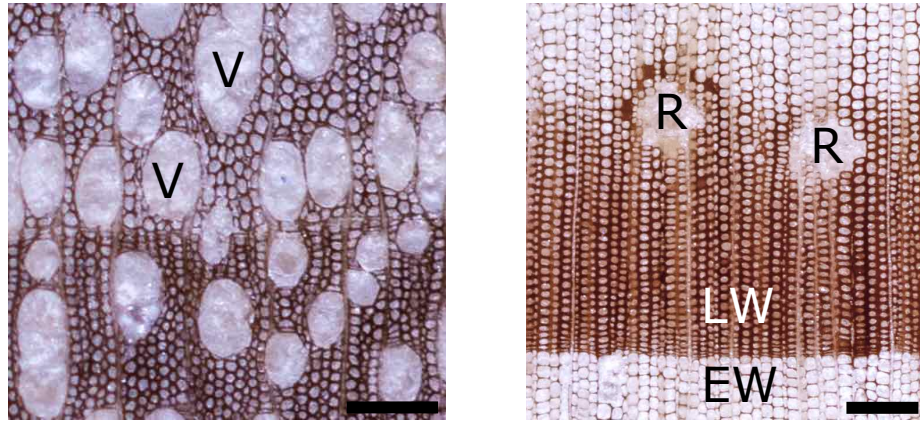


Figure 3.1 - Transverse section of aspen (left) and southern pine (right). Note the vessel elements (V) in aspen and the resin canals (R) and earlywood (EW) and latewood (LW) in pine. Scale bars are 150  $\mu\text{m}$

### 3.2.2 Preparation of specimens

OSB specimens measuring 20.0 x 2.5 mm (length x width) and a thickness of 10.5 mm (panel's original thickness, highlighted area in Figure 3.2) were cut from each parent sample with a 9 in. (22.86 cm) band saw (Ryobi BS902 - Ryobi Tools Limited, South Carolina, USA). A total of six samples (one per panel) were used for the experiment, as mentioned above. One side (thickness x length) of each specimen was sequentially hand-sanded with a series of abrasive papers (aluminum oxide, grit sizes: 100, 180, 280, 360) and then polished with an orbital sander using a series of Micro-mesh® (Micro-Surface Finishing Products Inc. Iowa, USA) sanding pads (grit sizes: 3200, 4000, 6000, 12000) until one side of each OSB specimen was smooth and free of sanding scratches and machining marks.

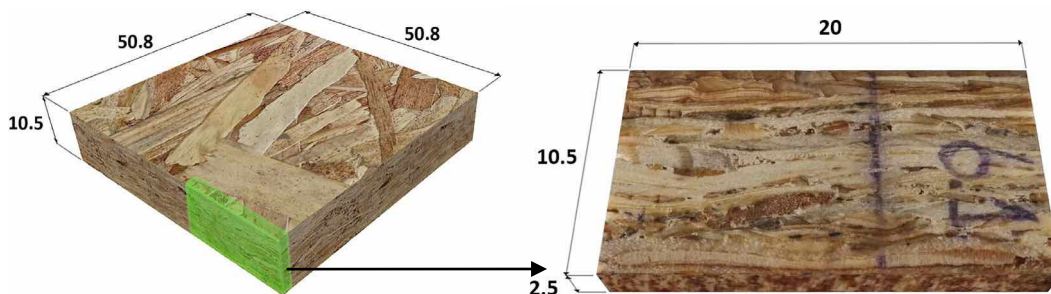


Figure 3.2 - Parent OSB sample (left) measuring 50.8 x 50.8 mm (length x width) and 10.5 mm in thickness and specimen (right) measuring 20.0 x 2.5 mm (length x width) and 10.5 mm in thickness

The two southern pine and two aspen boards were each cross-cut with a 9 in. (22.86 cm) band saw to produce four samples, each measuring 100 (longitudinal direction) x 40 (radial direction) x 25 mm (tangential direction) (Figure 3.3). The edges of samples were sealed with a white silicone sealant (GE Silicone II 100% Silicone # P-WGH291). One sample from each parent board was treated by vacuum/pressure impregnation with a commercial metal-free water-repellent preservative and the other sample acted as control. The samples were submerged in the water-repellent preservative (4,5-Dichloro-2-octyl-4-isothiazolin-3-one (DCOIT)) containing hydrophobic emulsion additive at a concentration of 800 ppm. Treatment involved one hour of vacuum (-5.52 kPa), followed by two hours pressure (401.28 kPa) in a laboratory Parr reactor (4522, Parr Instrument Company, IL, USA). Treated samples were conditioned at  $20 \pm 1^\circ\text{C}$  and  $65 \pm 5\%$  r.h. for two weeks and two matched samples were cut from the middle of each parent sample using a 9 in. (22.86 cm) band saw (Figure 3.3). These matched samples were then sanded using the same procedure described above for OSB samples. Specimens measuring 5 x 5 x 5 mm were cut from the sapwood of each matched sample (Figure 3.4) using hand-held, single-edged, carbon steel razor blades (Fisherbrand<sup>TM</sup>, Fisher Scientific, Pittsburgh, PA, USA). One specimen was used for swelling/shrinkage and checking measurements, and the other was used for measurement of sample moisture content. Figure 3.5 below shows the steps involved in the preparation of samples from treated wood.

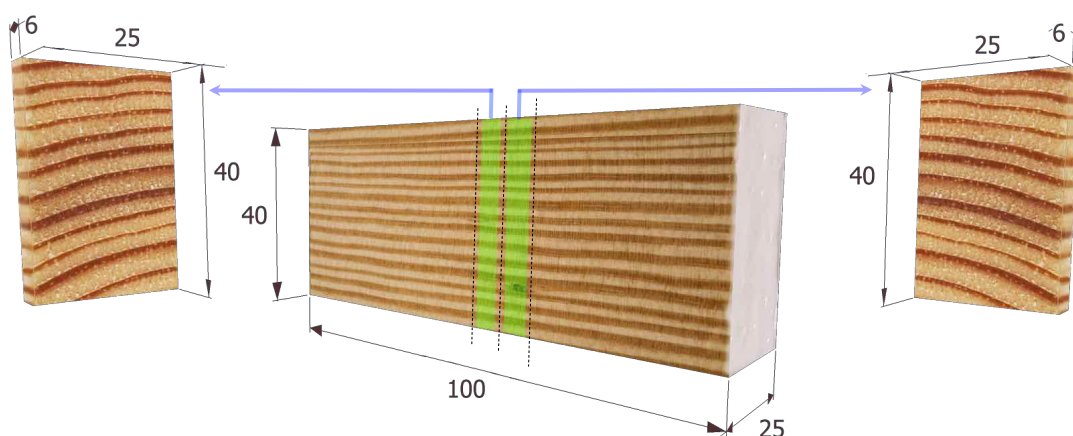


Figure 3.3 - Sample (middle) measuring 100 x 40 x 25 mm (longitudinal x radial x tangential) and matched samples (left and right) measuring 6 x 40 x 25 mm (longitudinal x radial x tangential). The edges of the sample were sealed with white silicone

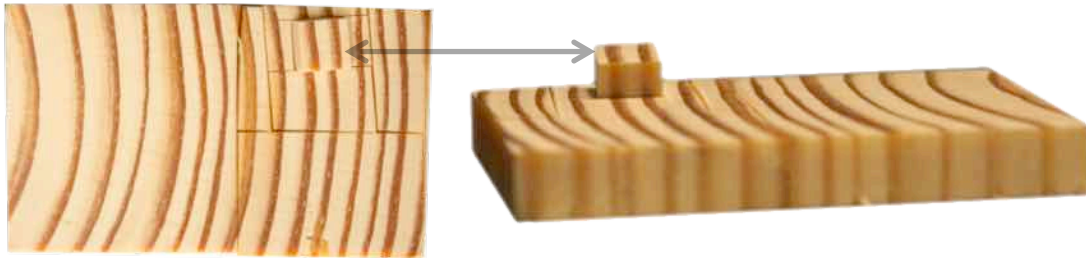


Figure 3.4 - Matched specimens (5 x 5 x 5 mm) used for swelling/shrinkage, checking and MC measurements. Top view on the left, and side view on the right

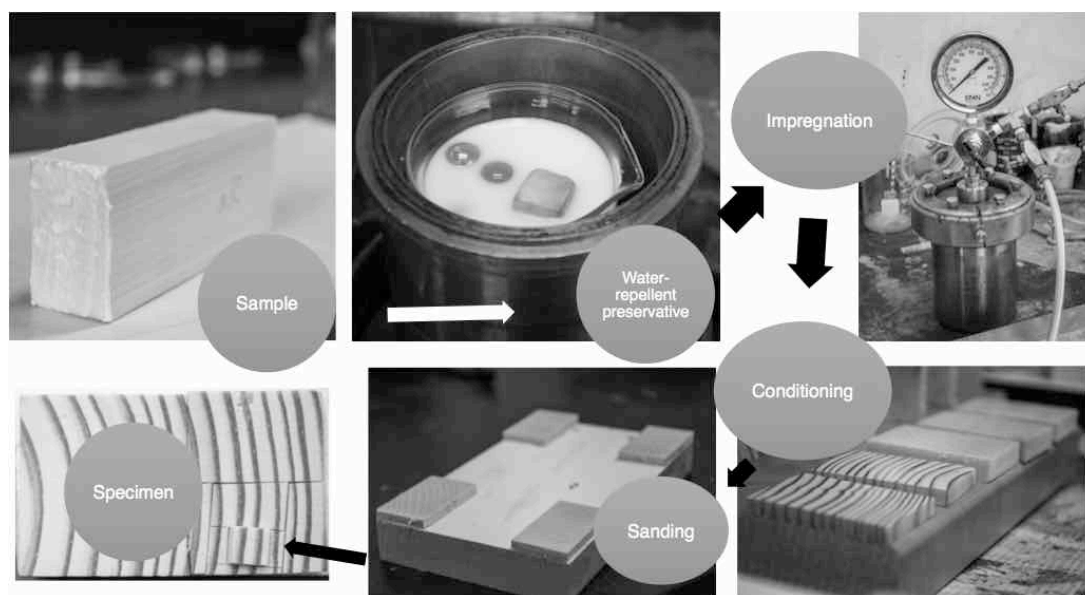


Figure 3.5 - Diagram showing all the steps involved in treating solid wood samples with a water-repellent preservative. The first step was to seal the edges of the samples using a silicone sealant (a), followed by impregnation (b), conditioning (c), sanding (d) and finally excising specimens (e) from treated samples using a razor blade

### 3.2.3 Moisture-induced degradation measurements

#### 3.2.3.1 Apparatus to quantify thickness swelling and micro-checking of OSB

The system I developed to measure thickness swelling and surface checking of OSB consisted of a digital single-lens reflex (DSLR) camera (Canon 5D Mark II - Canon Inc. Tokyo, Japan) and a state-of-the-art macro-lens (Canon MP-E 65mm f/2.8 1-5x) attached to a Polaroid MP-4 Land Camera Stage (Polaroid Corporation - Minnesota, USA) (Figure 3.6). An individual OSB specimen was firmly fixed on a stage

approximately 13 cm below the lens using a metal clamp holder equipped with a spring on the back to gently grip the specimen, while still allowing it to freely swell. Saturated air followed by desiccated air was blown across the polished surface of individual specimens via a transparent polymer hose located 10 mm away from the specimen. This wetting/drying cycle involved exposing specimens to two hours of warm (55°C) saturated air, followed by two hours of dry air at 65°C. Thermocouples attached to the surface of specimens indicated that they reached a maximum temperature of 35°C during drying. All measurements were made in a climate controlled room ( $20 \pm 1^\circ\text{C}$  and  $65 \pm 5\%$  r.h.).

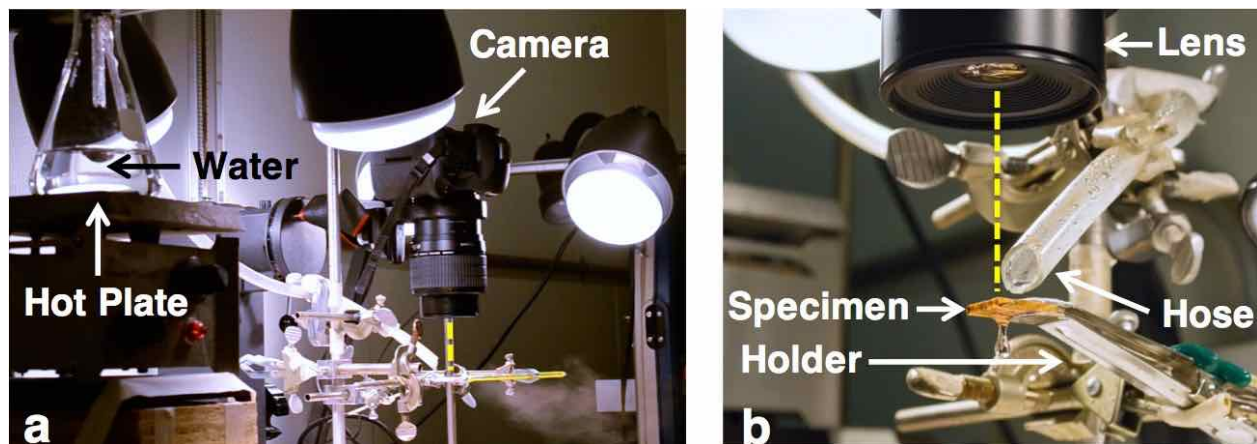


Figure 3.6 - Imaging system (arrowed a and b) used to visualize effects of wetting and drying on the surface microstructure of OSB and solid wood: hot plate (a- arrowed left) heats up water or air in a vented Erlenmeyer flask (a- arrowed left); saturated air is directed via a transparent hose (b- arrowed right-centre) onto a specimen (b- arrowed centre) held firmly using a metal clamp (b- arrowed bottom)

### 3.2.3.2 Measurements of thickness swelling and moisture content of OSB


High-resolution images (21.1 megapixels) of specimens cut from each of the six parent OSB samples (Blocks 1, 2, ..., 6) exposed to warm saturated air and then dry air were captured automatically every 10 seconds by the DSLR camera, and key frames were selected at 1, 2, 10, 30, 60 and 120 minutes during the wetting and drying phases of the test cycle (Figure 3.1). The specimens were removed from the stage after each key frame and weighed to obtain their moisture content (MC). Weighing of each specimen took less than a minute and they were then returned to the stage and reimaged. Each



specimen was exposed to wetting, and it then remained in a conditioning room overnight ( $20 \pm 1^\circ\text{C}$  and  $65 \pm 5\%$  r.h.) prior to commencement of the drying phase of the cycle. Oven drying was carried out before and after the test cycle by placing each OSB specimen in an oven at  $105 \pm 2^\circ\text{C}$  until they reached constant weight. The initial areas of the specimens that were captured by the DSLR camera measured 10.5 mm (panel's original thickness) x 10.5 mm (length). Raw photos (ISO 100, 1/25sec, f/5) of OSB were transferred to a computer, and image editing software (Adobe Photoshop CC 2015) was used to measure the thickness swelling (TS) of specimens during the test cycle (Frame A to Q) (Table 3.1).

Table 3.1 - Frames used for the analysis of thickness swelling and moisture content during wetting and drying of each specimen

<b>Wetting cycle</b>	A* (Conditioned) <b>Start</b>	B (Oven dried)	C (1min)	D (2min)	E (10min)	F (30min)	G (60min)	H (120min)	I (Conditioning overnight)
<b>Drying cycle</b>	Q* (Conditioned) <b>End</b>	P (Oven dried)	O (120min)	N (60min)	M (30min)	L (10min)	K (2min)	J (1min)	



Frames (A\* and Q\*) selected for the analysis of surface micro-checks and voids before and after wetting and drying cycles

### 3.2.3.3 Measurements of surface micro-checking and voids in OSB

The spaces caused by separation of strands within OSB specimens are termed voids (or inter-strand voids), as described in the literature (Furuno et al. 1983). Micro-checks refer to fractures *within* strands. Micro-checks and voids were measured before and after wetting and drying (Frames A and Q only). Photoshop was used to perform focus stacking of photos taken at the start (Frame A) and at the end of the test cycles (Frame Q). Focus stacking combined multiple images taken with different focal lengths and aperture settings (f/2.8, f/5.0, f/9.0, and f/16) to create sharp, distortion-free, images with good depth of field. These images were loaded into Photoshop and manual segmentation of checks and voids was carried out with the help of a drawing tablet (Wacom Intuos CTH680 - Wacom Co., Ltd. Saitama, Japan).

#### 3.2.3.4 Measurements of swelling/shrinkage, micro-checking and moisture content of aspen and pine wood treated with a water-repellent preservative

I used the same imaging system described above to measure the dimensional stability and micro-checking of treated wood. Wood specimens were mounted on a concertina-type stage and the height of the stage was adjusted so that the transverse surface of each wood cube was perfectly in-focus (Figure 3.7). The wetting/drying cycle involved exposing specimens to one hour to saturated air at 55°C, followed by one hour of dry air at 65°C.

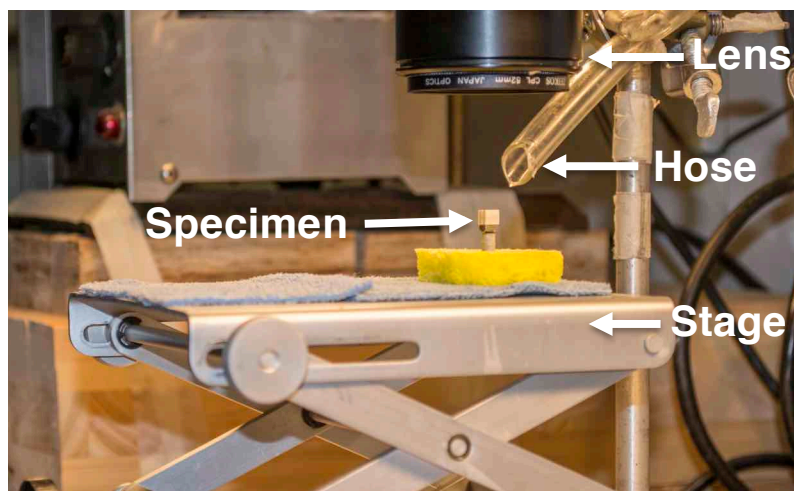


Figure 3.7 - Wood specimen mounted on a concertina-type stage and exposed to wetting and drying

Images of transverse wood surfaces exposed to saturated or dry air were captured automatically by the DSLR camera every 10 seconds. Images were transferred to a PC, and the image analysis software ImageJ was used to measure the dimensions of the transverse surfaces, as described above. The ability of ImageJ to detect checks depended on the difference in colour of the dark checks compared to the background colour of wood. When checks developed in darker latewood there was insufficient colour contrast between the checks and wood to automatically detect (threshold) checks. To overcome this problem, single key frames at 0, 1, 2, 5, 10, 15, 30 and 60 minutes were selected and checks were manually thresholded using Photoshop. Since I could not move samples when they were being imaged, the moisture contents of

matching samples exposed to wetting and drying were measured to assess the moisture contents of samples during the test cycle. The moisture contents of samples were measured after 0, 1, 2, 5, 10, 15, 30 and 60 minutes during both the wetting and drying phases of the test cycle. The initial and final moisture contents of samples during the test cycle are shown in Table 3.2.

Table 3.2 - Moisture content (MC) of untreated and water-repellent treated aspen and southern pine samples after wetting and drying

Measurement phase	MC of aspen (%)		MC of southern pine (%)	
	Untreated	Treated	Untreated	Treated
Start of cycle	12.7	13.8	13.9	14.1
End of wetting	69.5	67.2	64.7	60.8
End of drying	1.3	2.2	2.3	4.1

#### 3.2.4 Statistical analysis of data

Analysis of variance and linear regression were used to examine the effects of wetting and drying cycles on the following response variables: thickness swelling, moisture content, micro-checking and voids in OSB specimens. Statistical computation was performed using Genstat 17.1 (VSN International Ltd. 2014). Diagnostic tests were performed to determine whether data conformed to the assumptions of analysis of variance (normality with constant variance and independence of observation within and between samples). As a result of these tests, thickness swelling and moisture content data for OSB during wetting cycles was converted to natural logarithms before the final analysis. Statistically significant results are presented in graphs and differences between individual means can be compared using least significant difference (LSD) bars ( $p < 0.05$ ).

### 3.3 Results

#### 3.3.1 Thickness swelling and moisture content of OSB

The effect of exposure time on the thickness swelling and moisture content of OSB specimens during wetting and drying is shown in Figure 3.8. The moisture content and thickness of OSB specimens increase during wetting, and decrease during drying, as expected. The thickness swelling and moisture content data varied a lot during wetting,

but there was less variation during drying. Significant differences ( $p < 0.05$ ) in thickness swelling and moisture content at different measurement times occurred during the first 30 minutes of the wetting and drying cycles. Thereafter there was no significant ( $p > 0.05$ ) change in thickness swelling and moisture content. Linear regression of thickness swelling versus moisture content was highly significant ( $p < 0.001$ ,  $R^2 = 98.7$ ), as expected. The average irreversible thickness swelling of OSB specimens after one wetting and drying cycle was 15.97% (SD 3.94).

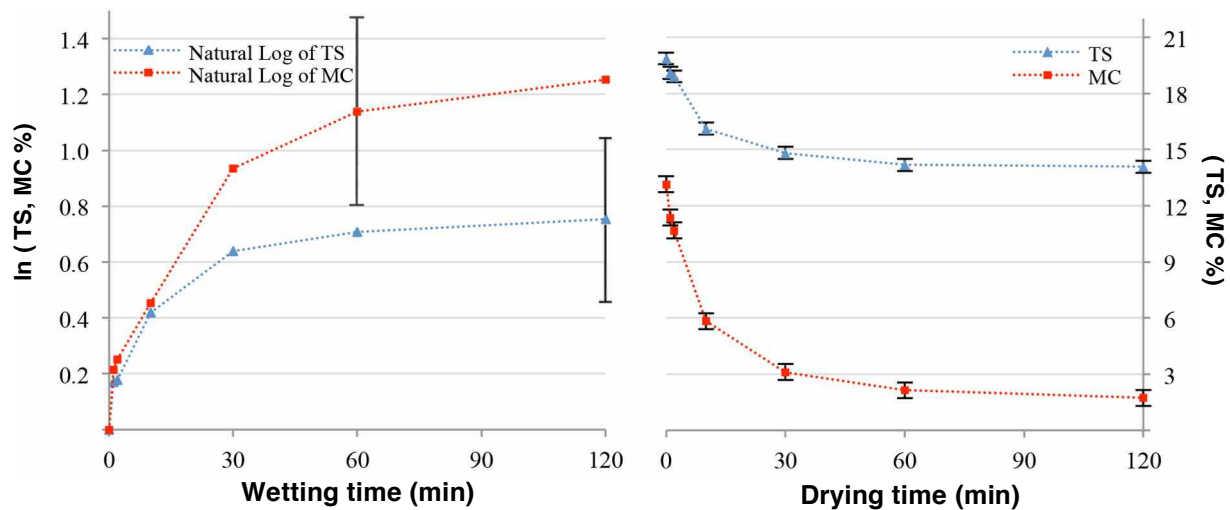


Figure 3.8 - Average percentage thickness swelling (TS) and moisture content (MC) of OSB specimens during wetting and drying

Images of an OSB specimen during wetting and drying cycles are shown in Figure 3.9. Thickness swelling of the specimen is obvious after 30 minutes exposure to moist air (Frame F), and is pronounced after 1 and 2 hours of exposure (Frames G & H). Thickness swelling after 2 hours was 29.85% (72.47% MC) (Frame H). The specimen decreased in thickness during the subsequent conditioning and drying phases, but at the end of the drying cycle the specimen had not returned to its original dry dimensions, and 19.4% of its swelling was irreversible (permanent). Such permanent swelling or springback of specimens after wetting and drying was also visualized at high magnification (Figure 3.10). Figure 3.10 shows the recovery of buckled tracheids in compressed flakes in a separate OSB specimen exposed to wetting and drying. In Figure 3.10 it is also possible to see delamination between flakes after wetting and drying.



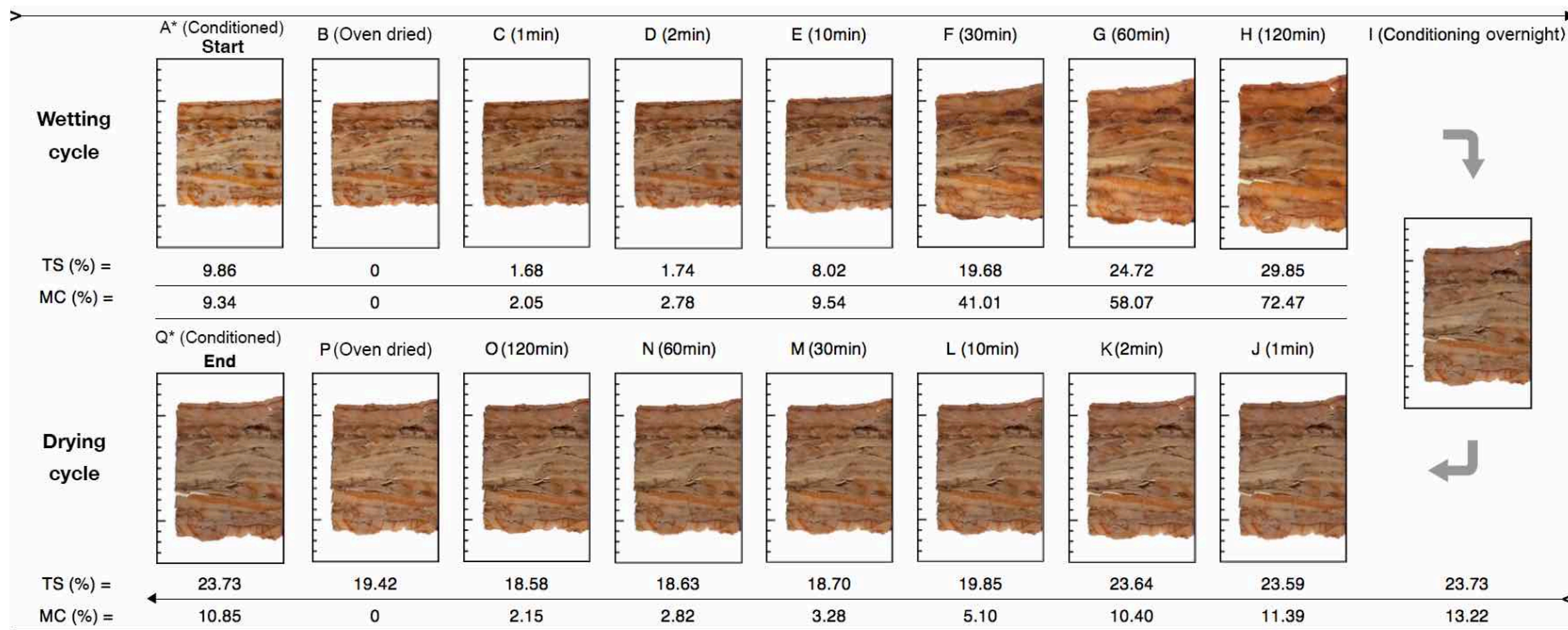


Figure 3.9 - Thickness swelling, moisture content, and associated images of an OSB specimen during wetting and drying. The start and end points of the cycle were (A\*) and (Q\*), respectively. Vertical scale on frames (y axes) in millimeters

### 3.3.2 Surface checking and formation of voids in OSB

Surface checks developed during wetting, enlarged as OSB dried, and in some cases partially closed towards the end of the drying cycle (Figures 3.11 and 3.12). Radial and tangential micro-checks developed in softwood flakes (Figure 3.13) and, less commonly, in the rays of aspen flakes. They also commonly occurred at the interface between latewood and earlywood in softwood flakes (Figure 3.14). In one OSB specimen a bark inclusion checked badly (Figure 3.15). Analysis of variance confirmed that there were significant ( $p < 0.05$ ) differences in the area of internal voids and micro-checks present in specimens before and after the wetting and drying cycle (Figure 3.16).

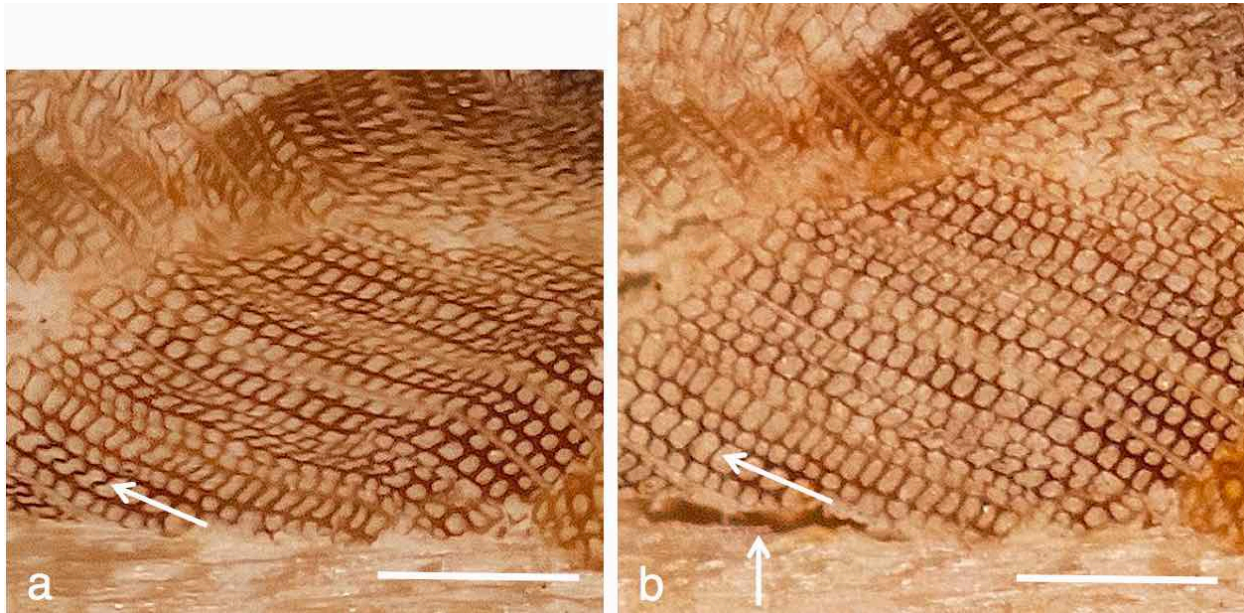


Figure 3.10 - Springback of part of a softwood flake in an OSB specimen after moisture-cycling: (a) Specimen before wetting and drying showing compressed and buckled tracheids; (b) Specimen after wetting and drying. Note the recovery of buckled tracheids (arrowed left), as well as delamination (arrowed bottom left) causing adjacent flakes to separate by approximately  $20\mu\text{m}$ . Scale bars are  $200\mu\text{m}$

Figure 3.17 highlights the voids (white) and surface checks (black) in an OSB (greyscale) specimen before and after a wetting and drying cycle. The area taken up by checks in the specimen before and after the wetting and drying cycles were 0.56 and 2.02%, respectively. Comparable figures for the internal voids were 0.77 and 3.60%. The area of surface checking in OSB specimens, averaged across *all* specimens, increased more than three times during the wetting and drying cycle, from 0.37 to 1.17%, and the area of voids increased nearly twofold (from 3.05 to 5.98%). Voids and checks in the remaining OSB specimens are highlighted in figures appended to this thesis (Appendix 1). Linear regression indicated that the area of micro-checks in OSB specimens following wetting and drying was a good predictor of irreversible thickness swelling ((F1,10), = 39.1,  $p < 0.001$ ), with an adjusted  $R^2$  of 77.6, whereas there was no significant ( $p > 0.05$ ) relationship between void area and irreversible thickness swelling.



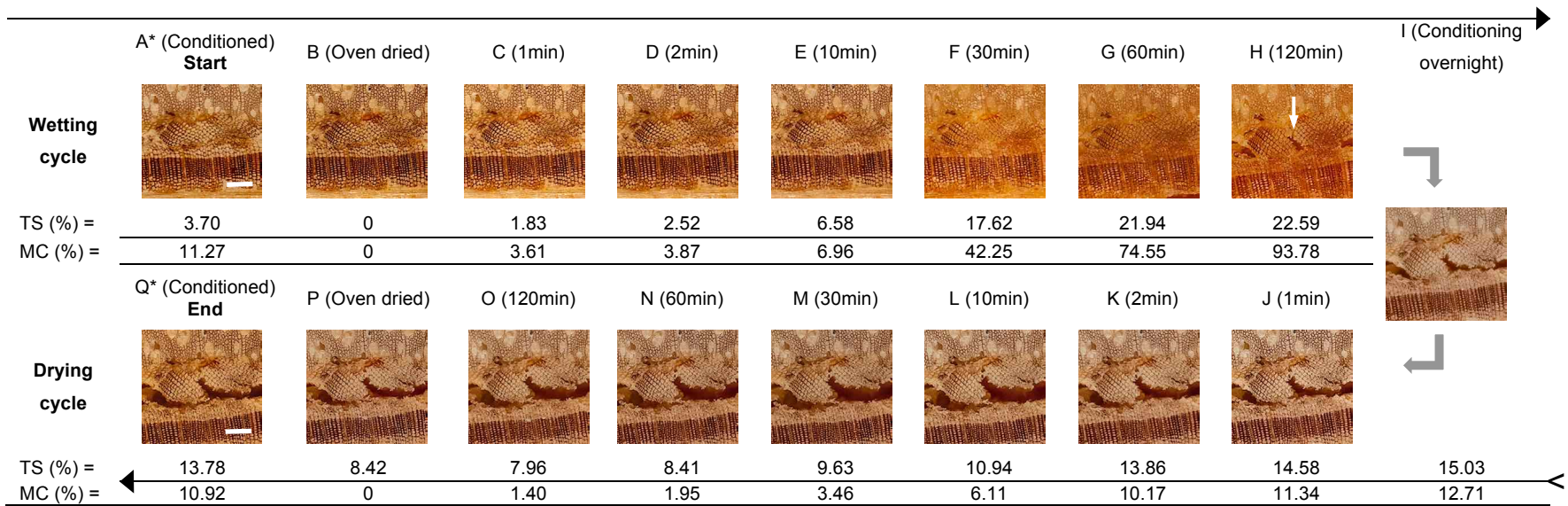


Figure 3.11 - Formation of micro-checks and delamination taking place during wetting (Frame H) near the core of an OSB specimen (as in Figure 14), and subsequent propagation and enlargement of micro-checks during drying (Frames I to P). Scale bars (Frames A and Q) are 200  $\mu\text{m}$

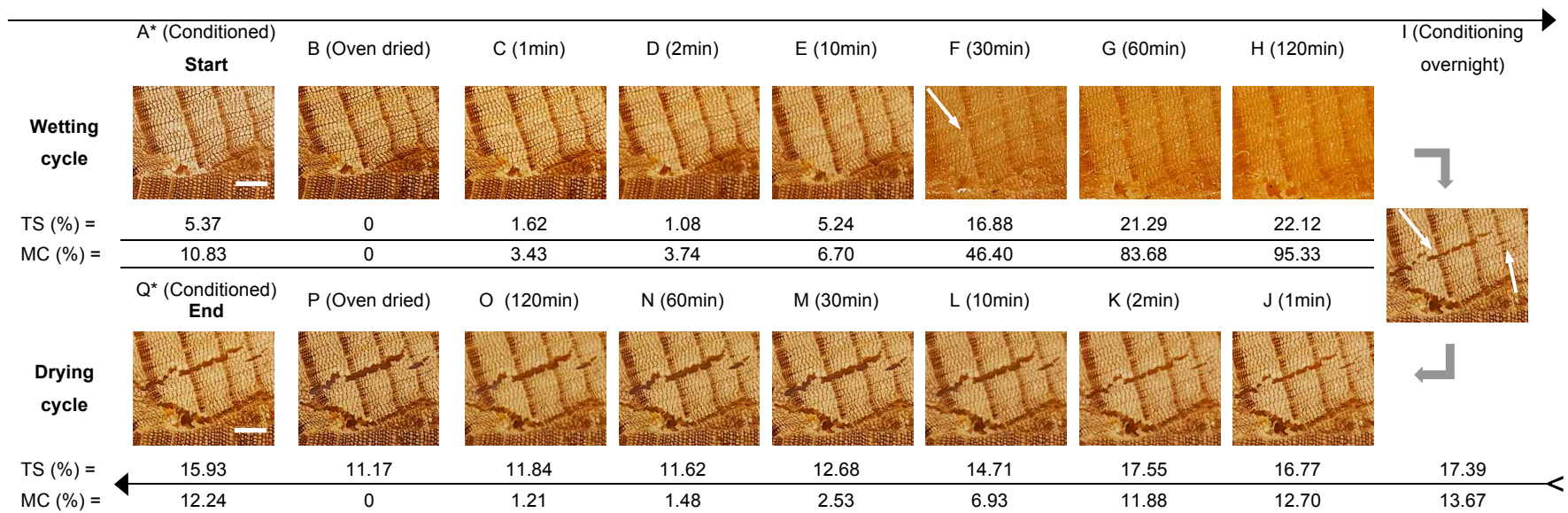


Figure 3.12 - Micro-checking of rays (Frame F) taking place during wetting near the surface layers of an OSB specimen (as in Figures 3.10 and 3.13), and subsequent propagation and enlargement of micro-checks during drying (Frames I to P). Scale bars (Frames A and Q) are 200  $\mu\text{m}$



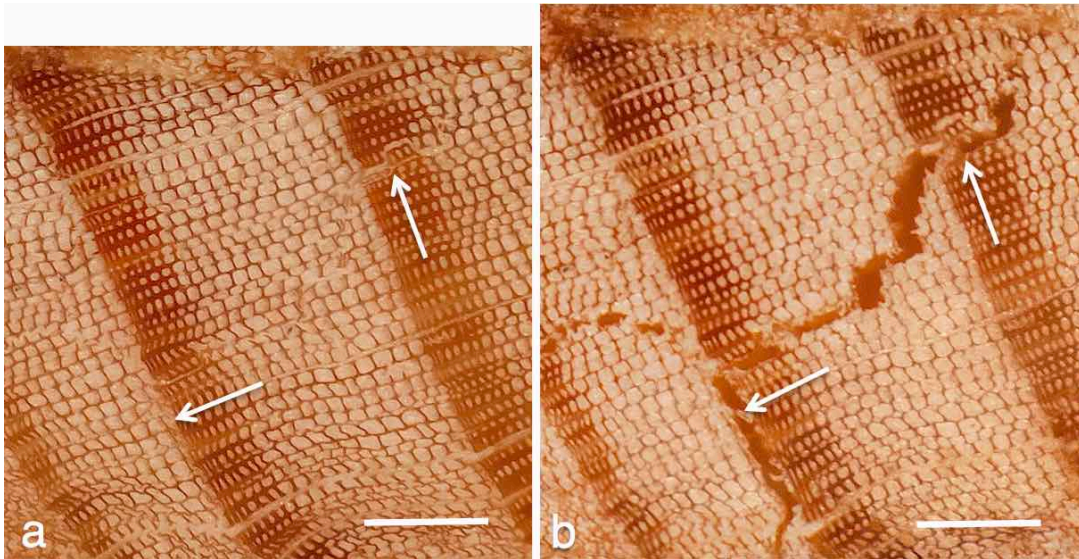


Figure 3.13 - Micro-checking of part of a softwood flake in OSB before (a) and after wetting and drying (b): (a) Tangential micro-check (bottom left) at the latewood-earlywood interface and a radial micro-check (top right); (b) Propagation and enlargement of micro-checks that formed during wetting (arrowed). Scale bars are 200  $\mu\text{m}$

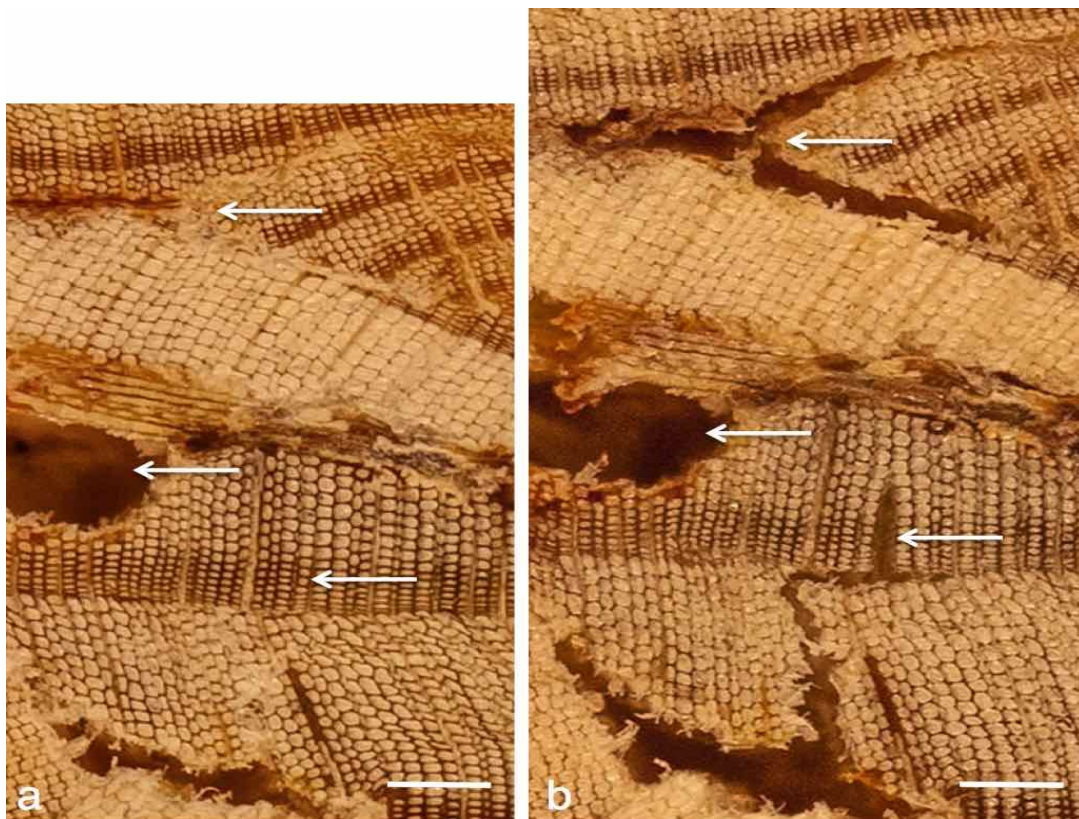


Figure 3.14 - Delamination (arrowed top) and micro-checking (arrowed bottom) of softwood flake in OSB before (a) and after (b) wetting and drying. Large void between softwood flakes (arrowed left of centre). Scale bars are 200  $\mu\text{m}$

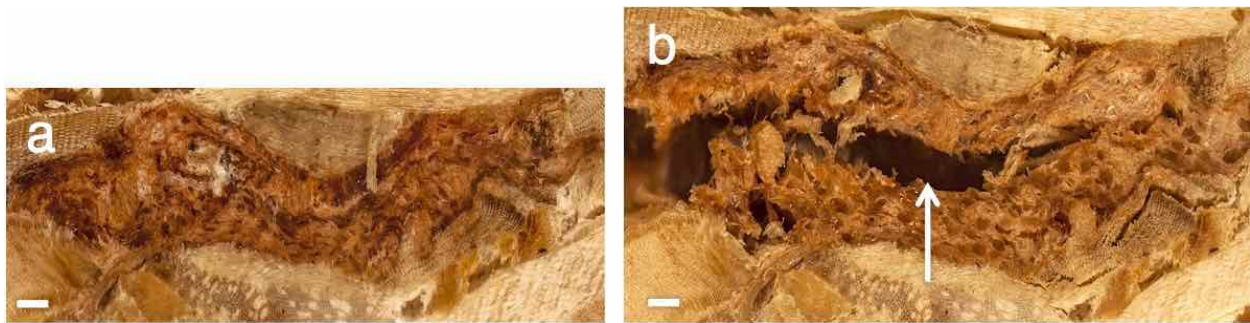


Figure 3.15 - Bark inclusion between two wood flakes in OSB before (a) and after (b) wetting and drying. Note the development of a large check within the body of the bark inclusion. Scale bars are 200  $\mu\text{m}$

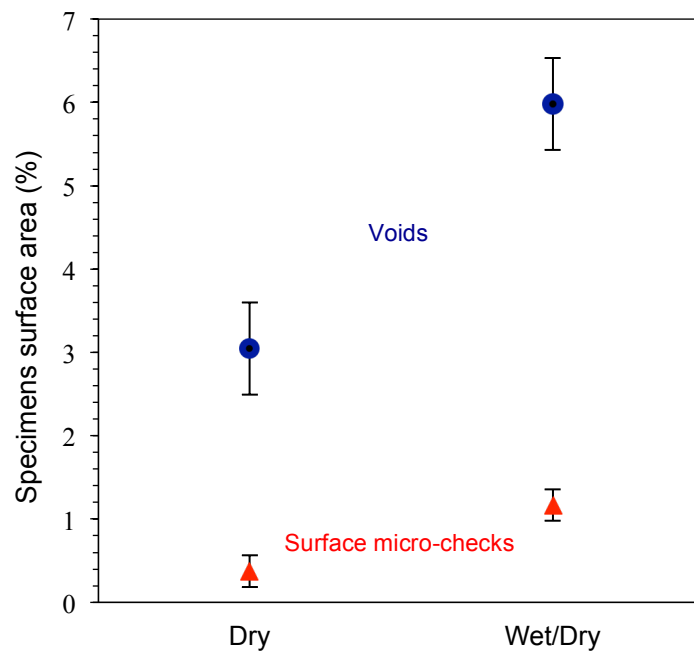


Figure 3.16 - Area of OSB specimens before (Dry) and after moisture cycling (Wet/Dry) that can be attributed to surface micro-checks (triangles) occurring within wood flakes (bottom) or voids (circles) occurring between flakes. Non-overlap of error bars indicates that individual means are significantly different ( $p < 0.05$ )



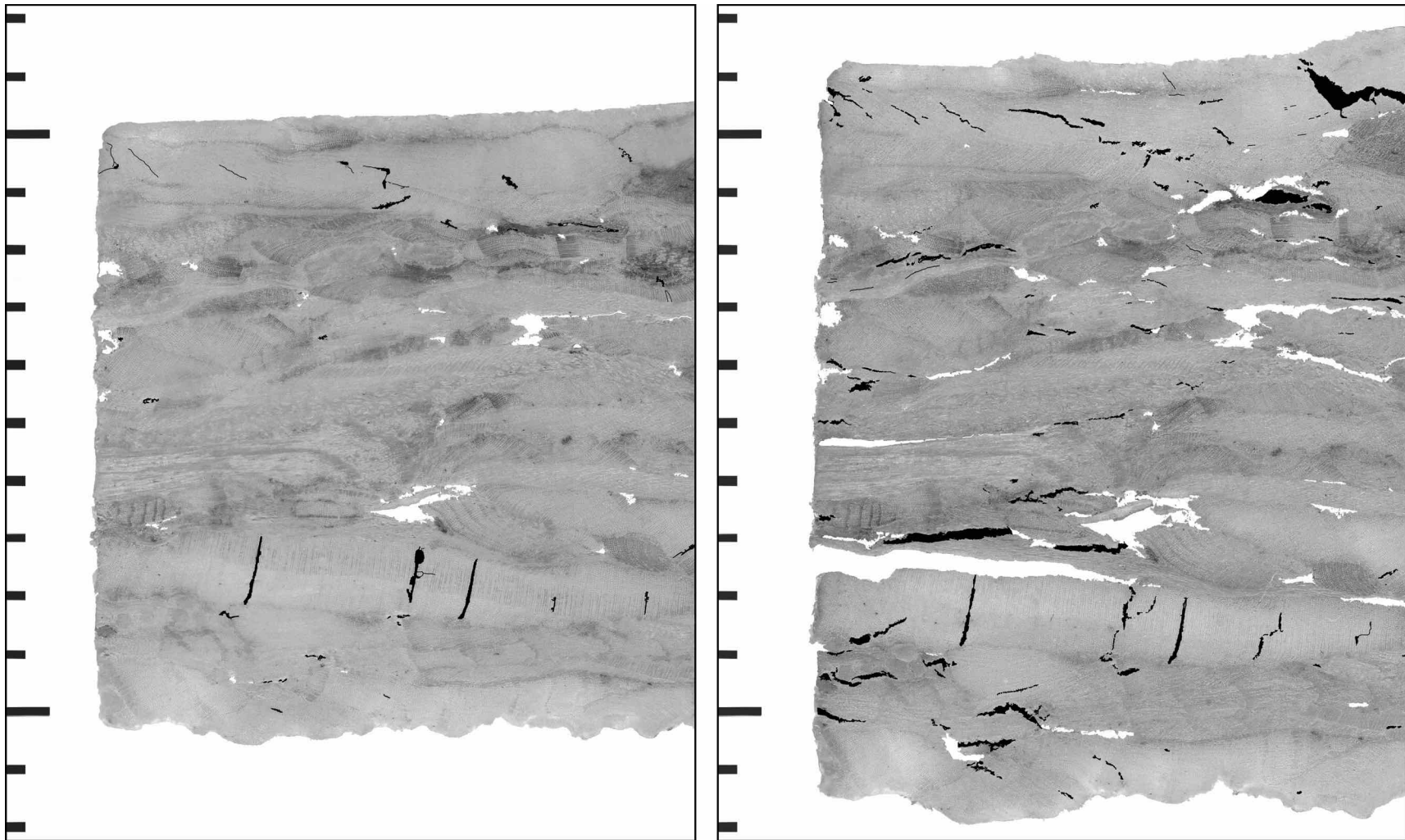


Figure 3.17 - Surface checking (black) and voids (white) in part of an OSB (greyscale) specimen (as in Figure 3.9) before (left) and after (right) wetting and drying. The area occupied by checks is 0.56 and 2.02% of the specimen's area before and after swelling, respectively. The area occupied by voids is 0.77 and 3.60% of the specimen's area before and after swelling, respectively. The irreversible swelling of the specimen was 19.4%. Vertical scale in mm

### 3.3.3 Dimensional stability, checking and moisture content of treated wood

Figure 3.18 shows the changes in dimensions of untreated (blue rectangles) and water-repellent treated (light tan triangles) southern pine samples during wetting and drying cycles. The left-hand side of the graph shows the swelling of two samples and the right-hand side shows shrinkage. The right hand side of the graph also shows the checking of untreated (red dashes) and treated (yellow triangles) samples. Two images are present on the right hand side of Figure 3.18. These images show a transverse surface of an untreated sample (top image) and a transverse surface of a treated sample (bottom image). Both images contain earlywood and latewood bands. Checks are coloured blue.

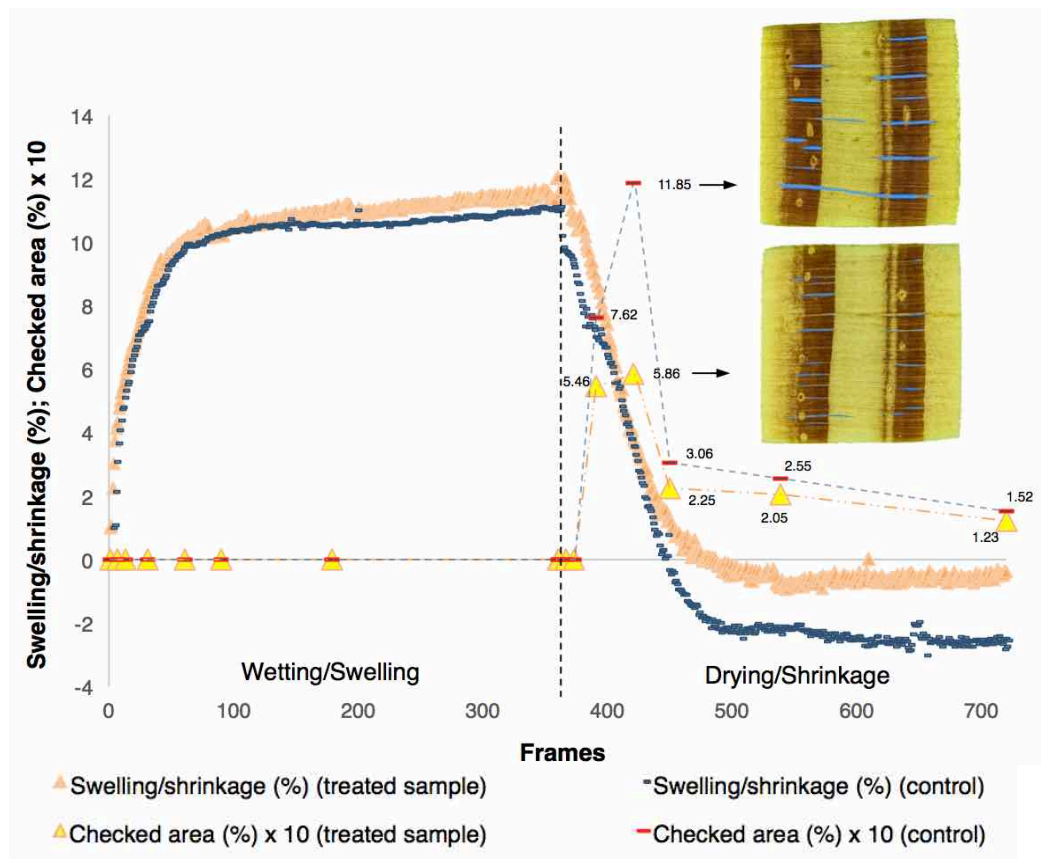


Figure 3.18 - Swelling/shrinkage and area of checks in treated and untreated southern pine samples during wetting and drying

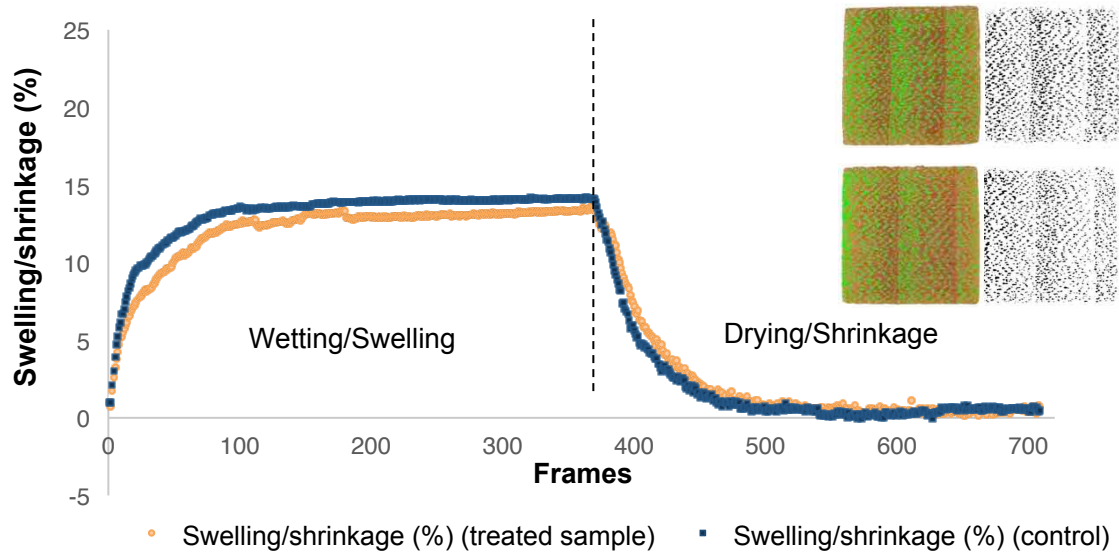


Figure 3.19 - Swelling and shrinkage of treated and untreated aspen samples during wetting and drying

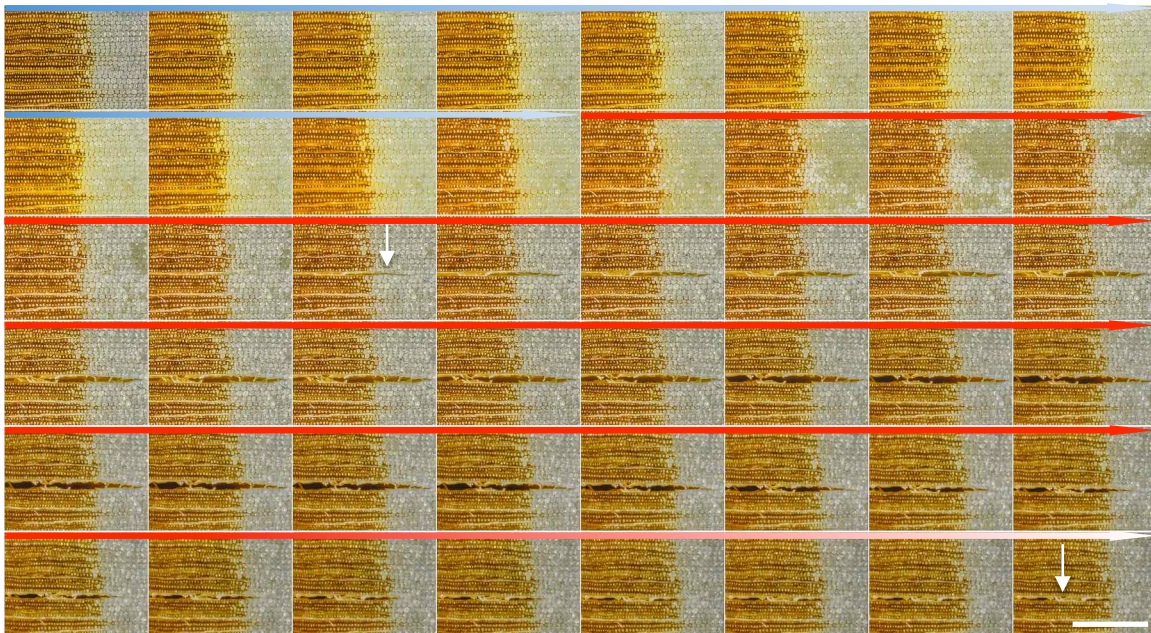


Figure 3.20 - Check in a southern pine sample (frames top left to bottom right) that developed during wetting (blue arrows) and drying (red arrows). Check initiated at the beginning of drying (arrowed left), at the interface between latewood and earlywood, and partially closed-up at the end of drying (arrowed right). Most frames during wetting were omitted because no changes were visualized. Scale bar is 0.5 mm



There is a large difference in the behaviour of treated and untreated southern pine samples at the start of the drying cycle (right-hand side of Figure 3.18), but, surprisingly, the surface swelling of the samples was similar during the wetting phase (left-hand side of Figure 3.18). However, when the untreated sample was first exposed to dry air its transverse dimensions changed rapidly as can be seen by the vertical plunge in the dimensions of the sample. At the same time checks developed in the untreated sample. These checks are aligned with the rays and are mainly found in latewood, although some of them traverse earlywood (Figure 3.18).

The behaviour of the treated Southern pine sample resembled that of the untreated sample, but it showed less rapid changes in dimensions at the start of the drying cycle and the level of checking in the initial part of the drying phase was approximately half that of the untreated southern pine specimen. Checks in both untreated and treated samples closed-up as they dried (Figure 3.20), and at the end of the drying phase the levels of checking in both types of samples were similar. Overall shrinkage of the untreated specimen was greater than that of the treated specimen, which may reflect the lower moisture content of the former at the end of the drying cycle compared to that of the treated specimen (Table 3.2).

The aspen samples behaved differently to the southern pine samples. Firstly, the water repellent preservative restricted rate of swelling and shrinkage, which is more in line with expectations. Secondly, checks did not develop either in the treated or untreated samples (Figure 3.19).

### **3.4 Discussion**

In this chapter I observed that surface micro-checking of OSB resembles the micro-checking of solid wood in some respects, but differs in others. Aspen flakes in OSB were less susceptible to micro-checking than pine flakes, in accord with my observations of the checking of solid aspen and pine wood and those of Cheng (2015). Checking of flakes in OSB mainly occurred in rays and at the

boundary between latewood and earlywood, again in accord with my observations of the checking of solid wood and those of other researchers (Morén 1994, Hanhijärvi et al. 2003). Furthermore, micro-checks in OSB increased in size during the drying phase of the wet and dry cycle, as they do when solid wood is exposed to wetting and drying (Sakagami et al. 2009). However, an unexpected finding was that checks in OSB developed during the wetting phase of the wet and dry cycle, whereas most reports of the micro-checking of solid wood suggest that micro-checks develop during drying (Sakagami et al. 2013, Yamamoto et al. 2013). I also observed that checks developed in solid wood during the drying phase. This difference in micro-checking of OSB and solid wood may be explained by heterogeneous structure of OSB and creation of spatially unbalanced positive and negative strains when the surface is exposed to moisture. Further research using digital strain analysis to quantify and visualize the strains that evolve when OSB is exposed to wetting and drying would be needed to confirm this hypothesis.

The transverse surfaces of both untreated and treated southern pine samples swelled rapidly when they were exposed to moist air and there was little difference in swelling between them. This observation does not accord with those of previous studies, which have found that water repellents are effective at restricting the rate of volumetric swelling of treated wood exposed to water (Fowlie et al. 1990, Zahora 1991). My method of assessing swelling recorded changes in dimensions of the transverse *surface* rather than overall volumetric change, which may explain the discrepancy between my findings and those of previous studies.

My results confirm that the thickness swelling of OSB exposed to water is due in part to recovery of elastic deformation of wood cells that occurs when OSB is pressed, and also to delamination of glue-lines and creation of voids between flakes (Kelly 1977, Hsu and Bender 1988, Wu and Suchsland 1997). Voids also developed in OSB as a result of the micro-checking of flakes during wetting and drying, as I hypothesized. The area of such micro-checks in OSB specimens

increased threefold during the wetting and drying cycle. The area of voids between flakes increased twofold during the wetting and drying cycle. Furthermore, many of the micro-checks were oriented parallel to the Z (thickness) direction of OSB specimens, like the voids resulting from delamination. These observations suggest that micro-checking may contribute to the thickness swelling of OSB, but this suggestion requires further research to examine whether voids created by micro-checking also develop beneath the surface of OSB exposed to wetting and drying. This is a topic I examine in the next chapter.

My results also demonstrate that the system I developed to simultaneously measure dimensional change and structure of OSB and solid wood (treated and untreated) exposed to wetting and drying has sufficient resolution to observe changes at the cellular level, for example recovery of compressed tracheids during wetting. On the other hand, it has a large enough field of view (maximum of 36 x 24 mm) to visualize macroscopic changes in the structure of OSB samples, including the ability to quantify swelling of OSB and solid wood specimens in real-time. The system is inexpensive, robust and easier to use compared to the confocal laser and environmental SEM systems that have been used in the past to non-destructively examine the micro-checking of wood during wetting or drying, or exposure to weathering (Hatae et al. 2012, Yamamoto et al. 2013). A video that provides more information on the system is available at web-link <http://bit.ly/1UksLjA>.

### **3.5 Conclusions**

Surface micro-checking develops when OSB is exposed to wetting and drying, but unlike solid wood, some of the micro-checks develop during the wetting phase of the wet/dry cycle. Further research is needed to understand this difference in micro-checking of OSB and solid wood. The results from this chapter suggest that micro-checking contributes to the irreversible swelling of OSB. I also observed that aspen wood and also aspen flakes in OSB were less

susceptible to micro-checking than pine flakes, which may explain why OSB made from aspen flakes is more dimensionally stable than OSB made from a mix of different wood species. The measurement system I developed was able to detect differences in the dimensional stability and checking of untreated southern pine and aspen wood and matched samples treated with a water repellent, as well as simultaneously measure dimensional change and microstructure of OSB exposed to wetting and drying. The system has sufficient resolution to observe changes at the cellular level, but its field of view is large enough to visualize macroscopic changes in the structure of OSB samples, and to quantify swelling of OSB specimens in real-time. The system has potential to help with the development of treatments designed to improve the dimensional stability of OSB and other strand based composites, but automation of post processing of data would be desirable, particularly the time-consuming measurement of voids and micro-checks in OSB.

## **Chapter 4: Internal Changes to the Microstructure of OSB Exposed to Wetting and Drying**

### **4.1 Introduction**

In Chapter 3, I observed that surface micro-checking occurs in both solid wood and OSB during wetting and drying. Surface micro-checking appeared to be associated with irreversible thickness swelling of OSB. Surface micro-checking was observed using an inexpensive imaging system, but it was incapable of visualizing micro-checking within the body of OSB specimens. Hence, it is unclear whether the surface micro-checking I observed extends beneath the surface of OSB, possibly contributing to irreversible thickness swelling of OSB when it is exposed to wetting and drying. In this chapter, I probe the internal microstructure (including micro-checking) of OSB at high-resolution using state-of-the-art technologies (helical X-ray micro-computed tomography and field emission scanning electron microscopy).

High-resolution imaging including X-ray micro-CT has been applied to wood, as well as to materials with a similar internal structure to OSB, for example particleboard (Evans et al. 2010). However, high-resolution imaging of the effects of moisture-induced swelling on the microstructure of OSB has not been explored. In this chapter, I use X-ray micro-CT in combination with FE-SEM and image analysis to examine the changes in the microstructure of OSB exposed to wetting and drying. Based on findings in Chapter 3 I hypothesize that micro-checks will develop in OSB as a result of wetting and drying. I discuss the effectiveness of X-ray micro-CT and FE-SEM at visualizing and quantifying the changes in microstructure of OSB specimens. I also examine the extent to which changes in the internal microstructure of OSB such as micro-checks contribute to thickness swelling.

## 4.2 Materials and methods

### 4.2.1 Materials

The same parent OSB samples used in Chapter 3 were used in this chapter. The supplier of the OSB, and the dimensions, composition and properties of the boards are described in Chapter 3 (3.2.1).

### 4.2.2 X-ray micro-CT

X-ray micro-CT was used to probe the microstructure of two rectangular specimens and also a single cylindrical OSB plug. The rectangular specimens measured 30 x 16 x 10.5 mm (unleached) and 30.5 x 15.4 x 13.1 mm (leached), and the plug was 10 mm diameter and 10.5 mm in length (board's original thickness) (Figure 2.1). The rectangular specimens were cut with a band saw and the plug was removed from a parent OSB panel using a 10 mm diameter steel plug cutter (Samona International; Delta, BC, Canada) attached to a drill press (Delta 16.5"; Delta International Machinery; Guelph, ON, Canada). The plug was scanned twice using X-ray micro-CT: first the plug was scanned in its *dry* or original state (first conditioning); then it was soaked in tap water (Figure 4.2) for 48 hours and conditioned at  $20 \pm 1^\circ\text{C}$  and  $65 \pm 5\%$  r.h. until it reached a constant moisture content, and re-scanned. The two different rectangular specimens were scanned once (1, conditioned; 2, conditioned after wetting). Thus four data sets (*dry* and *wet/dry*) were obtained. These data sets were each analyzed to obtain information on the microstructure of OSB specimens before and after moisture-induced swelling. A total of 22 2D slices (width x thickness) were selected from data sets from the OSB plug for image analysis (11 frames each from the *dry* and *wet/dry* data sets). The 2D depth-profile slices through each specimen represent 0, 10, 20, 30, 40, 50, 60, 70, 80, 90, and 100 % of the length of the plug (see Figures 4.1 and 4.3). Each frame was analyzed to quantify the microstructure of the plug in both *dry* and *wet/dry* data sets. Thickness swelling of the plug was measured using the quantity of pixels (area)

within 2D frames (width x thickness) from the *dry* and *wet/dry* data sets. Image analysis was used to quantify the area of pixels in each frame.

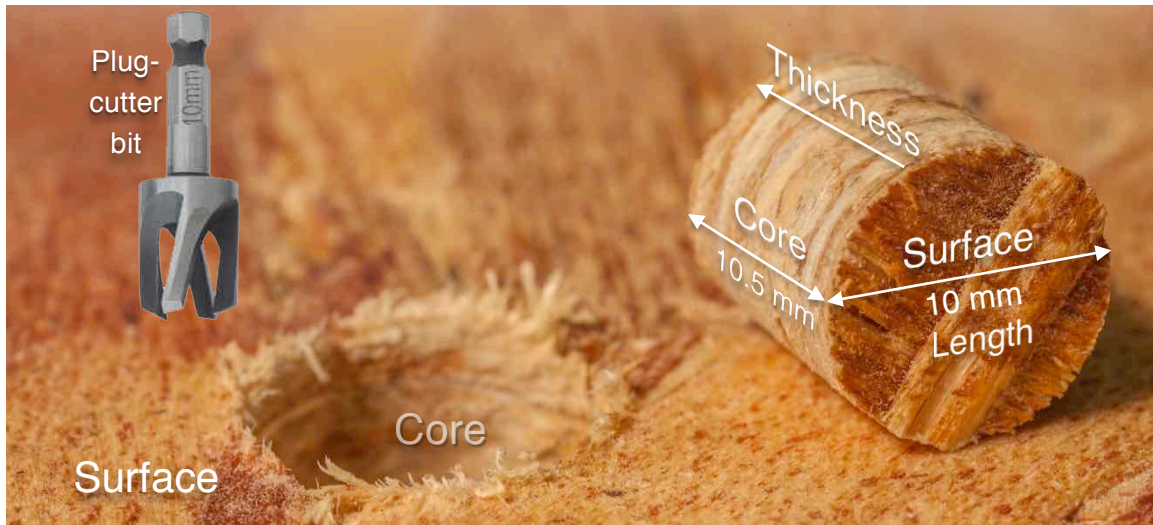


Figure 4.1 - Plug (right) extracted from an OSB board using a 10 mm diameter steel plug cutter (top left - not to scale)

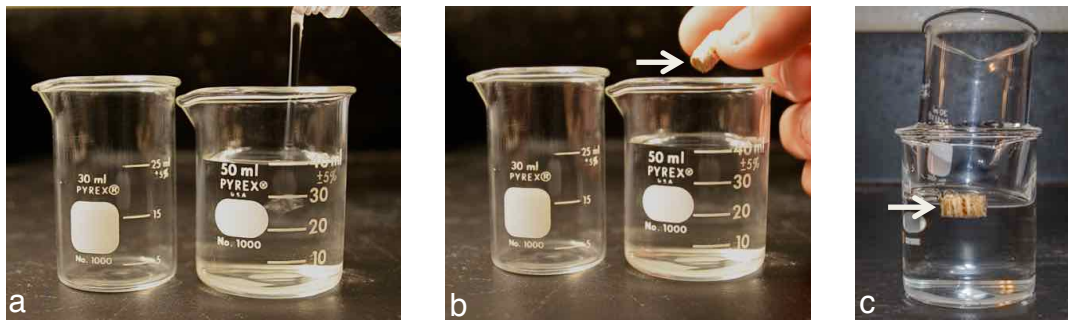


Figure 4.2 - Steps involved in soaking the OSB plug in water for 48 hours. Two beakers (30 mL and 50 mL) were used to soak the plug in water; the larger beaker was filled with 40 mL of tap water (a); the plug was placed on the water in the larger beaker (b- arrowed centre); and finally the smaller beaker was placed into the larger beaker (c- arrowed right) to force the plug under the water in the larger beaker

Frames in the plug before and after swelling were carefully matched to ensure that the same areas were observed, thus making it possible to more precisely examine the effect of moisture-induced swelling on the microstructure of OSB.



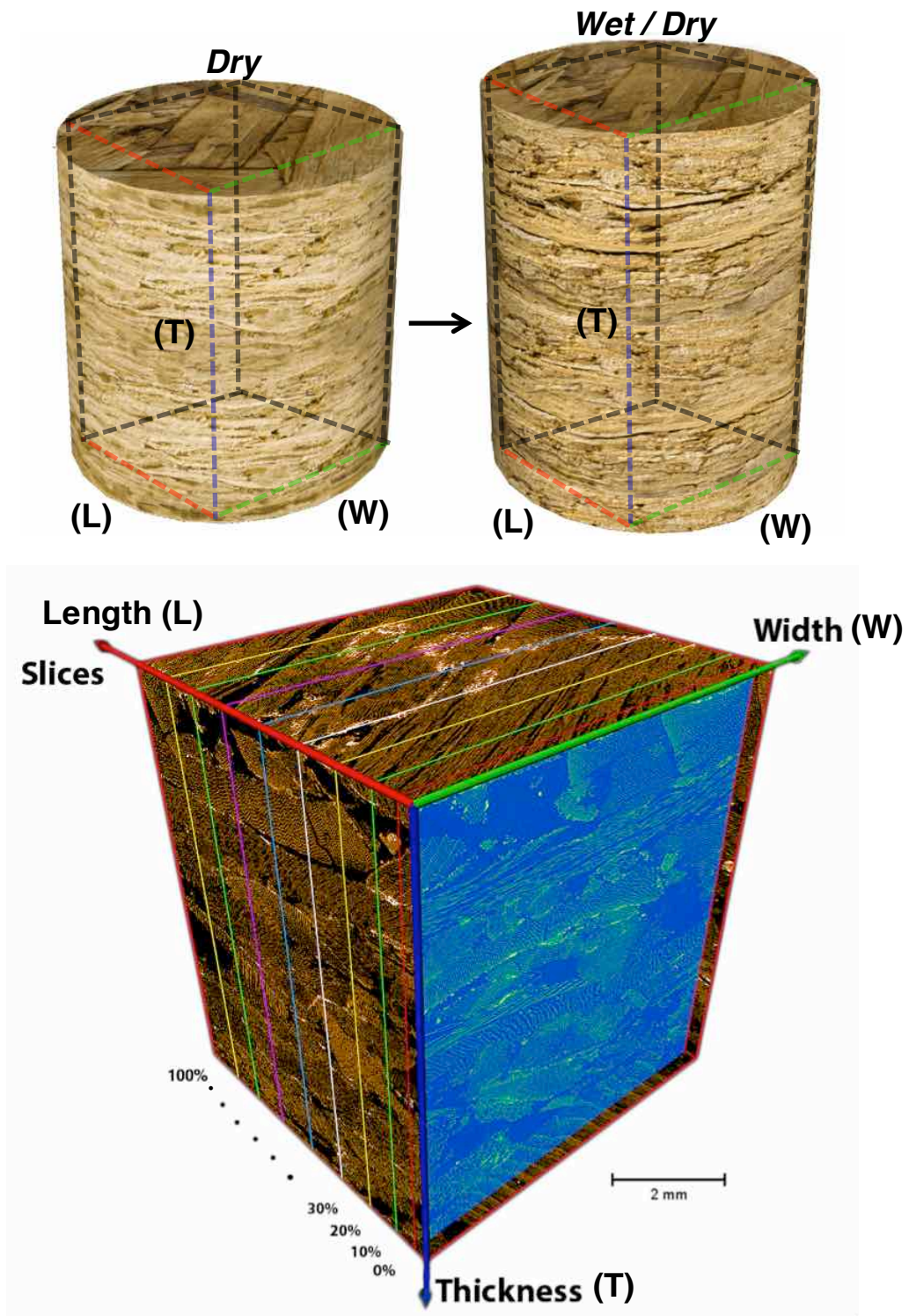


Figure 4.3 - Diagram showing a 3D image (bottom) of part of an OSB plug and the 2D slices (width x thickness - highlighted blue) at 0, 10, 20, 30, 40, 50, 60, 70, 80, 90, and 100 % of plug's length, which were subject to image analysis. A total of 22 slices (frames) were selected from data sets for the analysis (11 frames from both *dry* (top left) and *wet/dry* (top right) data sets)



#### 4.2.2.1 Conventional CT system

A conventional X-ray micro-CT system was used to probe the microstructure of two rectangular OSB specimens. One specimen was in a dry (conditioned) unleached state and the other had been soaked in water, redried and then conditioned as described by Evans et al. (2015a). The specimen was imaged using a 3 m long X-ray micro-CT device (Figure 4.4) (Sakellariou et al. 2004, Evans et al. 2015a). The device is one of the early generation of micro-CT devices developed by a group of researchers in the Department of Applied Mathematics at The Australian National University (ANU). It consists of an X-ray source (X-Tek RTF-UF225), rotation stage (Newport RV120PP), and a flat panel X-ray detector (PerkinElmer XRD 1621 xN) that has a 2048 x 2048 pixel array mounted on a parallel optical rail (Sakellariou et al. 2004). Each OSB specimen (unleached and leached) was placed separately on a rotation stage, located 95 mm from the source, with the detector position 1800 mm from the source, and probed individually with a polychromatic X-ray beam (Bremsstrahlung radiation) generated by a focused electron beam (60 kV and beam current of 140  $\mu\text{A}$ ) as described by Evans et al. (2015a). A CCD camera recorded the X-ray transmission radiograph (projection data). The specimen stage was rotated through 360 degrees over a period of 20 hours for each specimen, and a total of 2880 radiographs were obtained as described by Evans et al. (2015a). Projection data were processed with a Feldkamp-Davis-Kress (FDK) reconstruction algorithm to generate a tomogram (Feldcamp et al. 1984), which is a three dimensional representation of the variation of density within the specimen. Each three-dimensional point in the tomogram is called a voxel, as mentioned above. The voxel size in the reconstructed tomograms for the OSB specimens was approximately 10.5  $\mu\text{m}$ . The quality of each tomogram was optimized using a range of measures to overcome the limitations imposed by using a polychromatic X-ray cone beam, as described by Evans et al. (2010). These included pre-filtering the X-ray beam to minimize beam hardening, and using a small cone beam angle ( $0.8^\circ$ ). The projection data must represent linear interactions

between the specimen and the X-rays to generate a tomogram (Sakellariou et al. 2004). For X-ray tomography, however, the interaction is not linear because X-rays are attenuated, but Beer's law can accurately describe such attenuation, and can be easily manipulated into a linear form, provided the X-ray beam is mono-energetic (Sakellariou et al. 2004). This linearization also works with the poly-energetic X-rays employed in this instrument, but beam hardening artifacts are introduced into the tomogram. These artifacts were minimized by reducing the energy distribution of the X-rays using pre-filtering. In my case a 2 mm thick glass filter was used when imaging the OSB specimens, as described by Evans et al. (2015a). The tomograms produced had sufficient quality to unambiguously segment the wood, void, and zinc phases (Figure 4.7). Hence, they were used to examine effects of leaching on the micro-distribution of zinc in OSB (see Evans et al. 2015a for more details). However, the microstructure of wood flakes was not clearly visible in the tomographic images, so another X-ray micro-CT device was used to obtain higher resolution tomograms of OSB subjected to moisture-induced swelling.

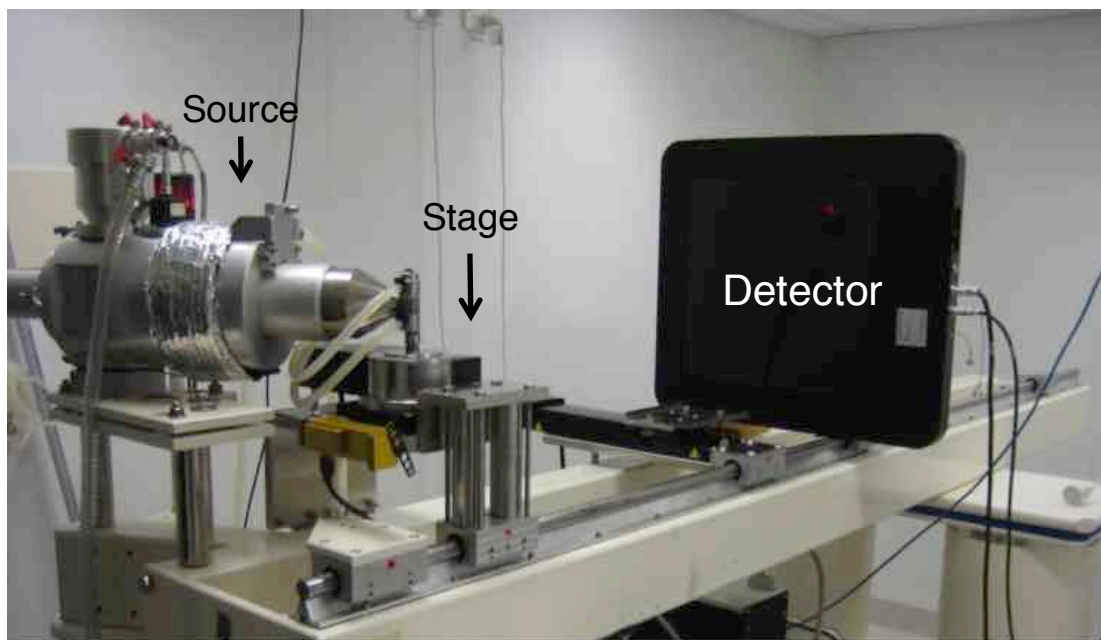


Figure 4.4 - Conventional X-ray micro-CT system initially used to probe the effects of moisture on the microstructure of OSB. (photograph c/o McKay 2015)

#### 4.2.2.2 Helical scanning CT system

Helical scanning micro-CT results in significantly higher signal-to-noise ratio with reduced scanning times compared to 'conventional' X-ray micro-CT (Varslot et al. 2011) (Figure 4.6). The high-cone-angle helical X-ray micro-CT system (Figure 4.5) I used was also designed and built at the Department of Applied Mathematics at The ANU. The system consists of an X-ray source that generates Bremsstrahlung radiation with an accelerating voltage in the range of 80-120 kV. A cone-shaped X-ray beam originating from a tungsten target penetrates the specimen, and a series of radiographs are captured on a detector as the specimen rotates and moves vertically on a stage (Figure 4.5). To obtain a full data set using this system requires the specimen to rotate through 2880 positions. As in the conventional CT device described above, projection data were processed with the FDK reconstruction algorithm to generate a tomogram (Feldcamp et al. 1984), and the same pre-filtering technique described above was used to minimize beam hardening of the X-ray beam. The helical CT system scans objects helically with a high-cone-angle and a smaller distance between the radiation source and the object and CCD detector. As a result the voxel size was smaller in reconstructed tomograms than that in tomograms produced by the conventional micro-CT system: approximately 4.4  $\mu\text{m}$  for the OSB specimen (plug) before and after wetting and drying. The higher resolution and clearer radiographs produced by the helical scanning technology is noticeable in Figure 4.6, where images of OSB obtained using the conventional CT device (Figure 4.6a) and the helical scanning system (Figure 4.6b) are shown side-by-side. Using the helical scanning technology, higher resolution images of OSB were obtained and it was possible to see the cellular structure of individual wood flakes (Figures 4.8 and 4.9). Therefore, in this thesis, the data sets produced by the helical X-ray micro-CT system were selected in preference to those produced by the conventional CT device for subsequent analysis of the microstructural changes in OSB exposed to wetting and drying. A further advantage of the data sets obtained using the helical CT device is that they were obtained from the

same specimen, making it possible to accurately compare the effects of moisture cycling on the microstructure of the OSB sample.

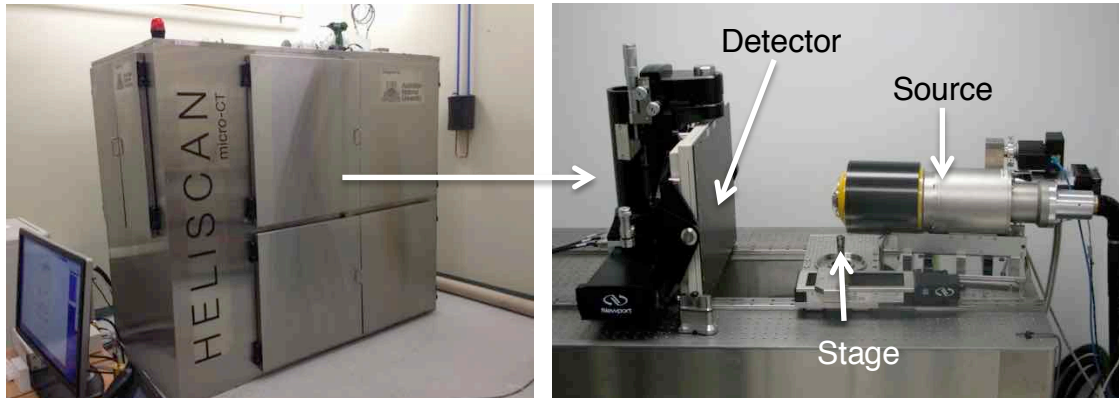


Figure 4.5 - State-of-the-art high-cone-angle helical micro-CT system (HELISCAN) developed in the Department of Applied Mathematics at The Australian National University. Photo source: Professor Tim J. Senden

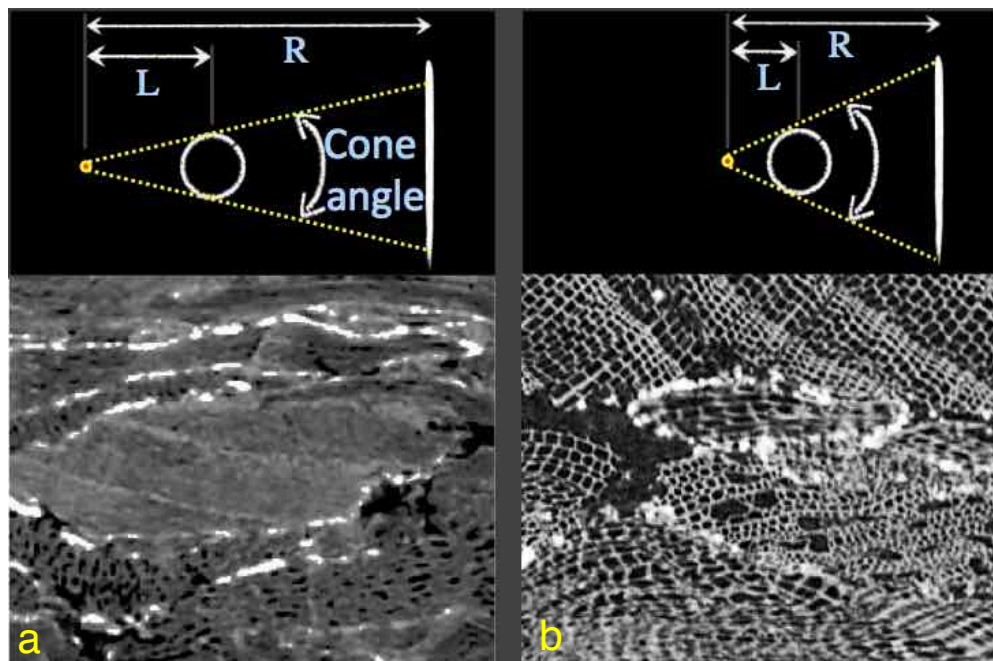


Figure 4.6 - Acquisition geometry of a conventional micro-CT device (a) compared to higher resolution helical scanning micro-CT device (b).  $L$  is the sample-distance, and  $R$  is the camera-length. Higher signal-to-noise ratio is achieved with high-cone-angle helical scanning (b) (redrawn from: Evans et al. 2015b)

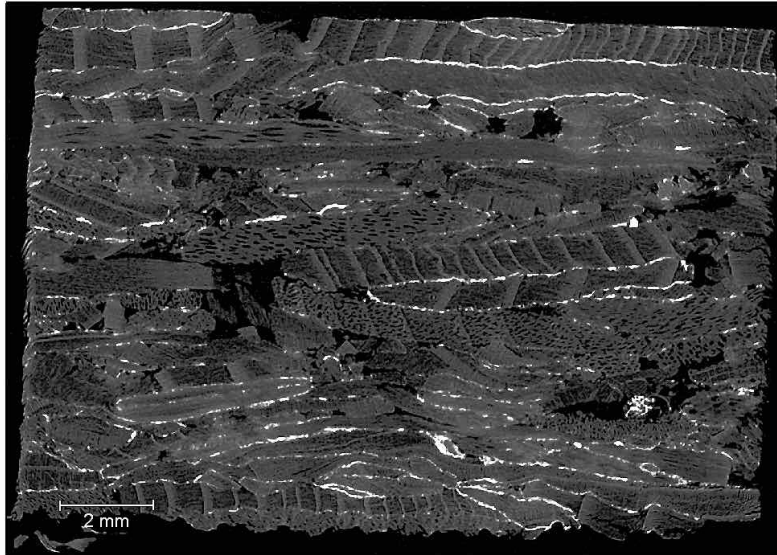


Figure 4.7 - In-plane greyscale image (1524 x 1344 pixels or 15.4 x 13.1 mm, 10.5  $\mu\text{m}$  voxel size) of an unleached OSB specimen obtained using a conventional X-ray micro-CT device. Denser material (zinc) is white; wood is grey and voids/air space are black. (Source: Evans et al. 2015a)



Figure 4.8 - Orthogonal greyscale image (2520 x 2520 pixels, 4.4  $\mu\text{m}$  voxel size) of an OSB plug (10 mm diameter) obtained using a high-cone-angle helical micro-CT device. Denser material (zinc) is white; wood is grey and voids/air space are black



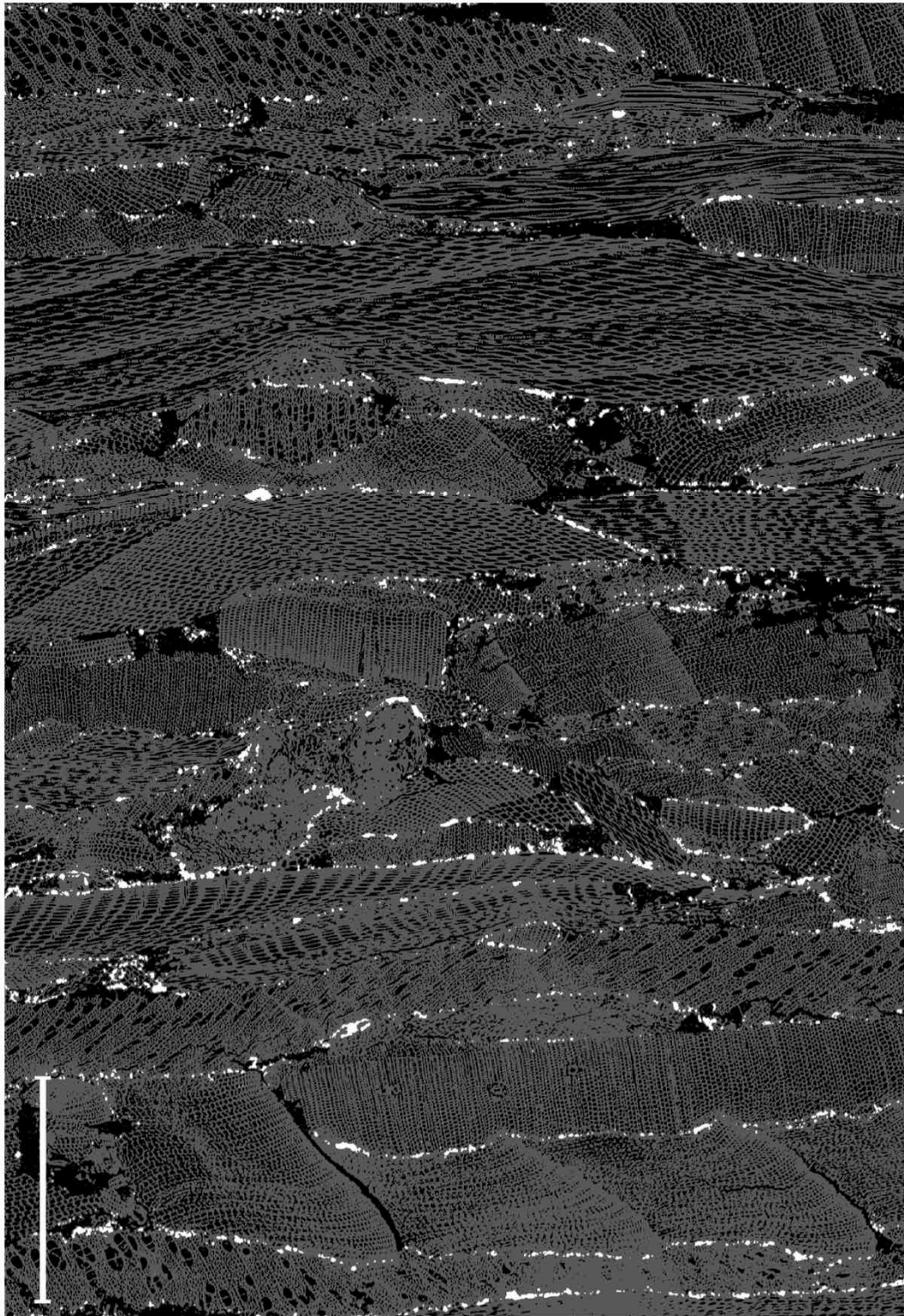


Figure 4.9 - In-plane rendered greyscale image of a dry OSB plug obtained using a high-cone-angle helical micro-CT device imaged at  $4.4 \mu\text{m}$  voxel size. Denser material (zinc) is white; wood is grey and voids/air space are black. Scale bar is 1.25 mm

#### 4.2.2.3 Visualization and segmentation of different phases in OSB

Three-dimensional volumes were used to generate intensity histograms for cell-lumen/air space (low density), wood (mid-density) and zinc (high-density), within specimens. Thresholding of the peaks in these intensity histograms allowed the different phases (wood, air space and zinc) in the tomographic images to be identified. Data sets were visualized in 2D and 3D using volume rendering in which a transfer function assigns each voxel a colour and transparency (Knackstedt et al. 2006). Volume rendering was performed using the software Drishti, which is an open source volume exploration and presentation tool for visualizing tomographic data and is available at <http://sf.anu.edu.au/Vizlab/drishti/> (Limaye 2012). Image processing and volume rendering of OSB's 3D microstructure was also carried out using the software Avizo Fire 8.0 (Visualization Sciences Group; Burlington, MA, USA). The image processing process involved: alignment of the image stack; image enhancement with the removal of noise by applying a non-local means filter according to Buades et al. (2005); and segmentation by greyscale thresholding, which calculates the variance of the intensity distribution by applying factorization as a measure of dispersion. Histograms with segmented phases for *dry* and *wet/dry* OSB plug, respectively, are shown in Figure 4.10. All data processing (pre-processing and reconstruction) used a Compaq AlphaServer super-computer located at the Australian Partnership for Advanced Computing at The ANU, Australia's national supercomputing facility. Visualization of tomographic data with Drishti and Avizo software used a high-end desktop computer (3.40 GHz Intel Core i7 2600K processor with 24GB of random-access memory (RAM) and a GeForce GTX 590 (NVIDIA; Santa Clara, CA, USA) graphics card).

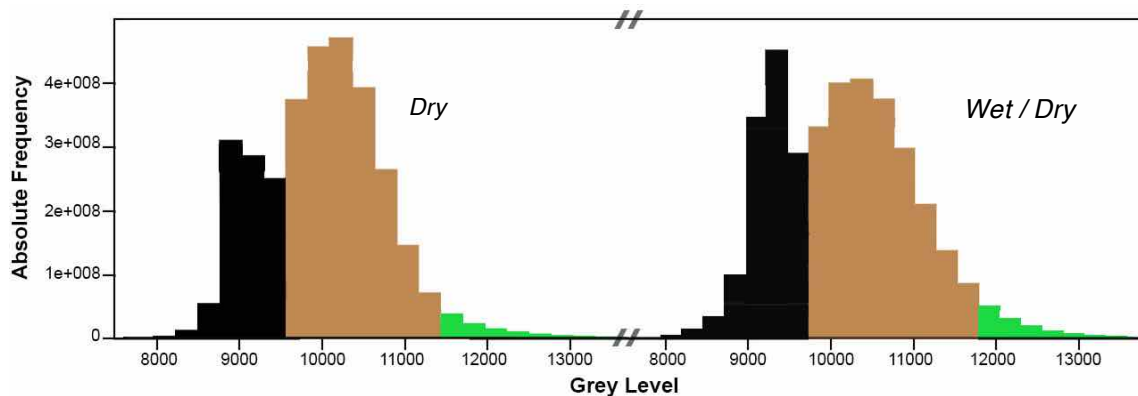


Figure 4.10 - Histograms of *dry* (left) and *wet/dry* (right) OSB plug; the phases automatically detected are: air space/voids (black); wood (brown) and zinc (green)

The nomenclature used to describe the microstructure of OSB is the same as that used in Chapter 3. The spaces caused by separation of strands within OSB specimens are termed voids. Micro-checks refer to fractures *within* strands. The air-space phase is due to the presence of cell-lumens, voids and micro-checks. Automated thresholding did not separate the different air-space phases.

Therefore, manual segmentation was needed to separate cell-lumens from micro-checks and voids in both *dry* and *wet/dry* data sets produced by the helical X-ray micro-CT system. Manual segmentation involved loading the in-plane images of *dry* and *wet/dry* OSB into Photoshop; followed by manual segmentation of checks and voids using a drawing tablet (Figure 4.11) (Wacom Intuos CTH680; Wacom Co., Ltd. Saitama, Japan) as in Chapter 3.

When comparing 2D frames from data sets of the specimen *dry* or *wet/dry*, their microstructure could not be identically matched, because of in-plane movement of wood flakes due to swelling/shrinkage. Zinc borate particles trapped between well-bonded strands were used to identify and match frames in the *dry* and *wet/dry* OSB data sets. The distribution of zinc borate before and after wetting and drying is concisely reported in this chapter. A more comprehensive description of the work has been published by Evans et al. (2015a,b).





Figure 4.11 - Manual segmentation of checks and voids carried out with the help of a drawing tablet and a laptop computer (MacBook Pro 2.5 GHz Intel Core i5 with 8 GB of RAM; Apple; Cupertino, CA, USA) running Photoshop

#### 4.2.3 FE-SEM

FE-SEM was used to examine the microstructural changes occurring at the surface and core of boards following wetting and drying. The factors involved in the experiment were (1) *Treatment* (a, control, b, wetting and drying (as in Chapter 3 - Figure 4.12), and c, 72 hrs. water soaking (Figure 4.13)) & (2) *Location* (surface v. core). The experiment was replicated five times (5 blocks), using samples measuring 20.0 x 2.5 mm (length x width) and 10.5 mm in thickness (as in Chapter 3 - Figure 4.14a).

The preparation of OSB samples prior to FE-SEM (cutting and sanding) followed the same procedures described in Chapter 3 (3.2.2). After the OSB samples were subjected to the treatments, small specimens (Figure 4.14b) were cut from the core and surface (second factor) of their parent OSB samples using hand-held, single-edged, carbon steel razor blades (Fisherbrand™; Fisher Scientific, Pittsburgh, PA, USA). A total of 30 specimens were prepared (3 treatments x 2 locations x 5 blocks). These specimens were dried (Figure 4.15) in an oven at  $70 \pm 2^{\circ}\text{C}$  until they reached constant weight. They were then embedded with a low-viscosity epoxy resin in polyethylene capsules (BEEM® embedding capsules,

size 3; PolyySciences, Inc. Warrington, PA, USA) mounted in a capsule holder (Figure 4.16). Embedding was necessary because it ensured that the OSB's integrity was maintained when it was sanded and polished prior to FE-SEM. The epoxy resin was prepared according to Spurr (1969), with some modifications as follows (Table 4.1): (1) 20% w/w of a dopant agent (epibromohydrin) was added to the resin-mix before embedding, to enhance contrast between wood flakes and voids/cracks, by increasing the density of the resin so that it could be more easily differentiated from voids and wood (McKay 2015); (2) acetone was added to the embedding capsules and specimens before the epoxy resin was transferred to the capsules and the procedure was carried out in a desiccator to reduce the absorption of moisture by specimens. After 24 hours during which time the low-viscosity resin infiltrated the specimens, they were placed under vacuum for several days until they were fully saturated with resin (Figure 4.17). The resin-impregnated specimens were cured by heating them in an oven at  $70 \pm 2^{\circ}\text{C}$  for two days (Figure 4.17). One side of each resin-embedded-specimen was sequentially sanded with an orbital sander using a series of abrasive papers (aluminum oxide, grit sizes: 180, 280, 360). Each specimen was then polished using a series of Micro-mesh® sanding pads (grit sizes: 3200, 4000, 6000, 12000) (Micro-Surface Finishing Products Inc; Wilton, IA, USA) until one of their sides was smooth and free of sanding scratches (Figure 4.18). After polishing and cleaning, the specimens were mounted on aluminum stubs using double-sided adhesive tape (Figure 4.19). One stub containing a set of non-embedded specimens was also prepared for comparison.

Table 4.1 - Concentration of ingredients used to make up a low-viscosity epoxy resin embedding medium

Ingredients	Concentration (%)	Function
Nonenyl succinic anhydride (NSA)	61.61	Hardener
3,4 epoxy cyclohexyl methyl 3,4 epoxy cyclohexyl carboxylate (ERL 4221)	23.70	Medium
Diglycidyl ether of polypropylene glycol (DER 736)	14.22	Softener
Dimethylamino-ethanol (DMAE)	0.47	Cure accelerator

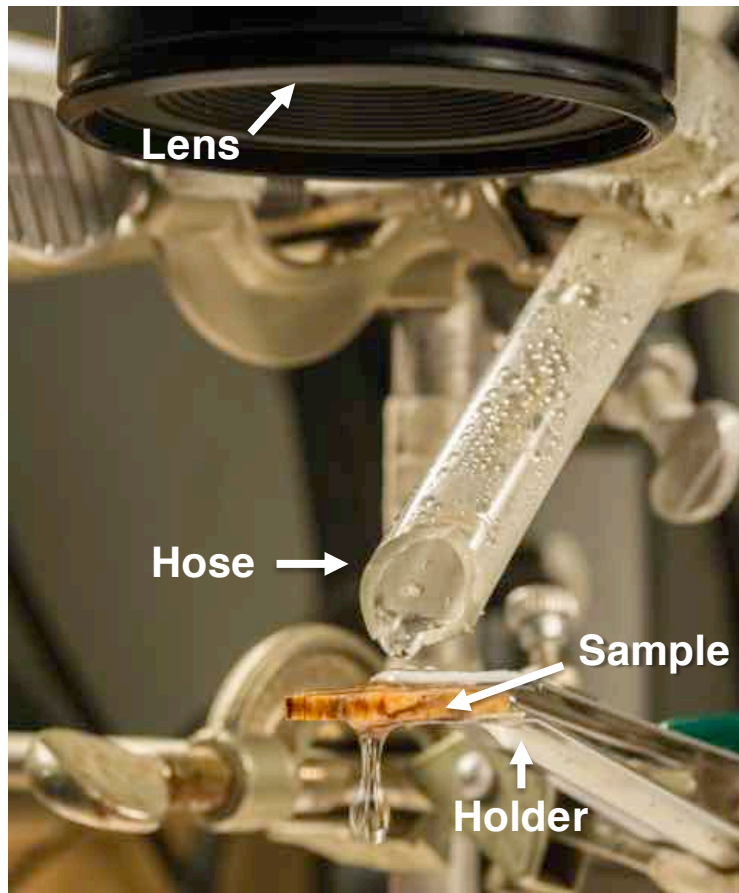


Figure 4.12 - OSB sample exposed to the wetting & drying cycle which was identical to that used in Chapter 3 (Section 3.2.3.2)

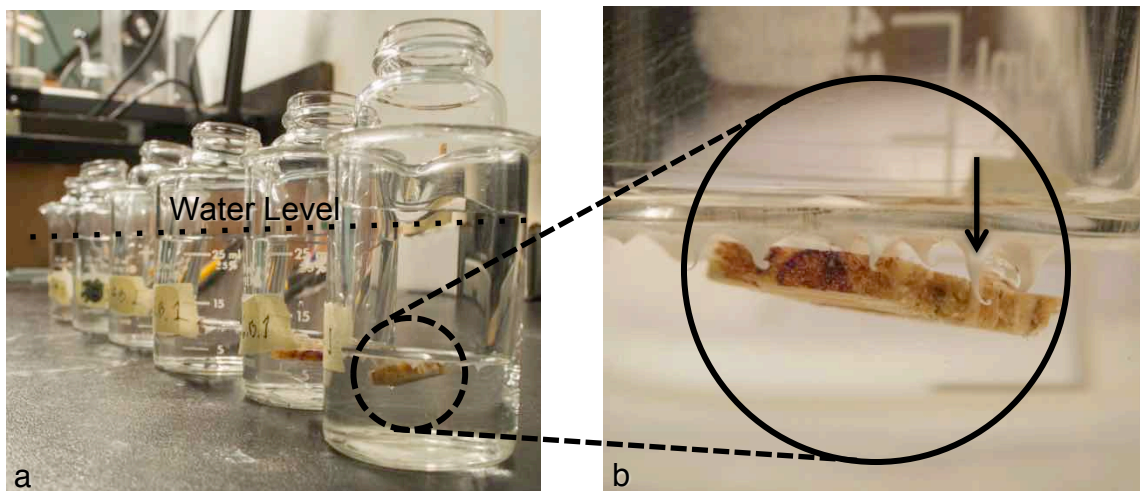


Figure 4.13 - Samples soaked in distilled water for 72 hours: (a) glass flasks were placed into 30 mL beakers to submerge samples in water. Note the silicon bumps at the bottom of the glass flask (b- arrowed right) to ensure that samples were fully submerged in water

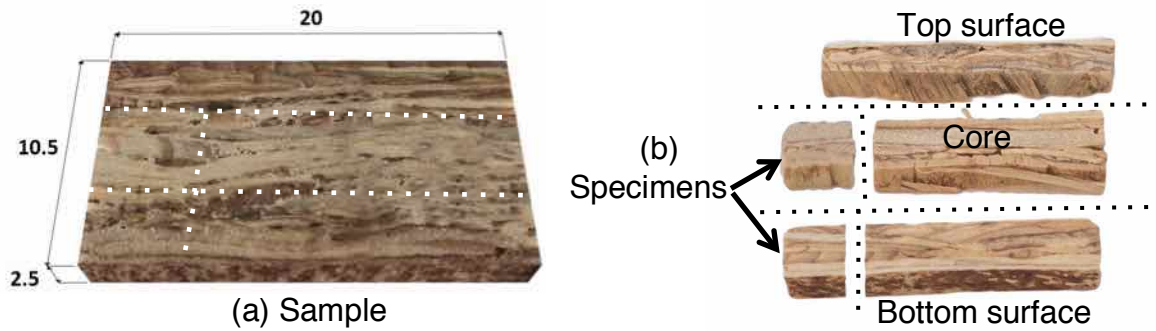


Figure 4.14 - Cutting pattern for OSB specimens: (a) the sample measuring 20.0 x 2.5 x 10.5 mm (length x width x thickness) was subjected to one of the three treatments (control, water soaking or wetting and drying), and it was then cut into three parts using a hand-held, single-edged, carbon steel razor blade; (b) two specimens, each measuring approximately 3.0 x 3.0 x 2.5 mm (thickness x length x width), were cut from the core and surface layers with the same razor blade



Figure 4.15 - Oven drying of specimens for 3 days at  $70 \pm 2^\circ\text{C}$  prior to embedding them with a low-viscosity epoxy resin



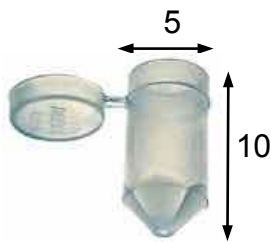


Figure 4.16 - Specimen embedding capsules (5 x 10 mm) (left) placed on a plastic holder (right); a low-viscosity epoxy resin was transferred into the capsules using a pipette until the capsules containing OSB specimens were completely filled with resin



Figure 4.17 - Capsules containing a fully saturated OSB specimen (arrowed left). Hardened epoxy resin-embedded-specimens after curing in an oven at  $70^{\circ}\text{C} \pm 2^{\circ}\text{C}$  for two days (right)



Figure 4.18 - Preparation of FE-SEM specimens in a fume hood (a); hardened resin-impregnated specimens were sanded and polished (b) until the surface was smooth and free of scratches. Inspection of specimens was carried out using a binocular microscope while specimens were clamped at the base of the microscope (c)

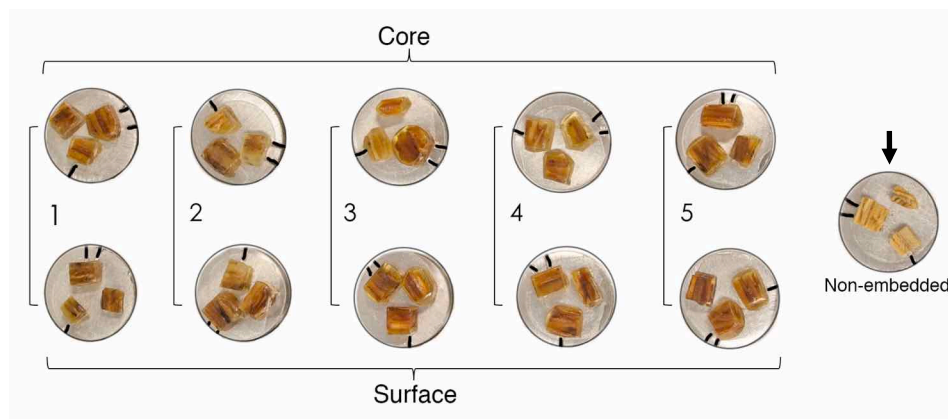


Figure 4.19 - Finished epoxy resin-embedded-specimens (3 treatments x 2 locations x 5 blocks) mounted on aluminum stubs using double-sided tape. A set of resin-free non-embedded specimens was also prepared (arrowed right)

Specimens were sputter coated with an 8 nm layer of gold and probed using a Zeiss UltraPlus analytical FE-SEM (Carl Zeiss International, Germany) (Figure 4.20), operating with an accelerating voltage of 15 kV and a working distance of 11.4 to 11.9 mm. Secondary electron images of the specimens were acquired, and saved as TIFF files. Image analysis of FE-SEM photos was performed using Photoshop.



Figure 4.20 - Zeiss UltraPlus field emission scanning electron microscope (FE-SEM) (Carl Zeiss International. <http://www.zeiss.com/microscopy>)

### 4.3 Results

In the following sections (4.3.1 & 4.3.2) I describe my principal findings using the different techniques described above. These findings are mainly in the form of visual images, supported by quantitative analysis of data on micro-checks and voids.

#### 4.3.1 X-ray micro-CT

##### 4.3.1.1 Conventional X-ray micro-CT system

Using the conventional X-ray micro-CT system it was possible to visualize the microstructure of OSB with good resolution. 3D and orthogonal rendered X-ray micro-CT images obtained using the conventional CT system are shown in Figures 4.21 and 4.22. Figure 4.21 clearly shows the presence of growth rings in

softwood and vessel element in hardwood flakes, as well as the distribution of voids, which are larger in the core of leached OSB. The presence of checks in the leached OSB sample was also observed (Figures 4.21 and 4.22).

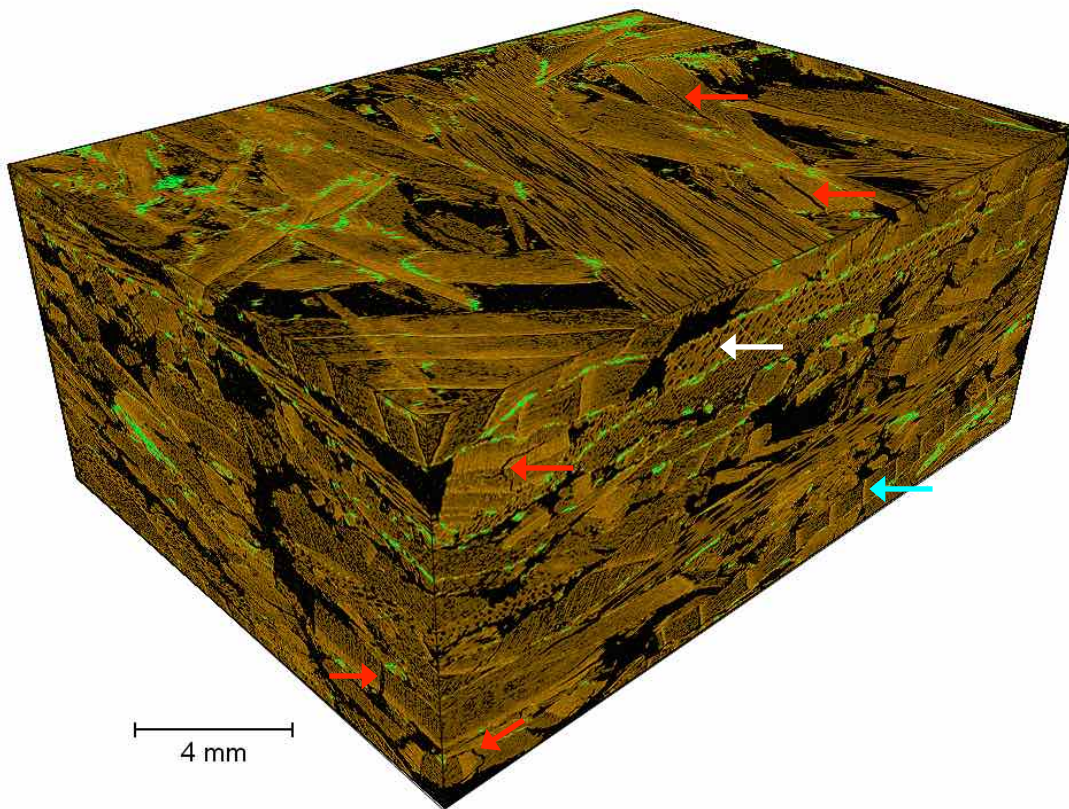


Figure 4.21 - 3D rendered X-ray micro-CT image of a leached OSB specimen obtained using a conventional micro-CT system. Wood is rendered brown; voids are black; and zinc is green. Note checks arrowed red; aspen vessel element arrowed white; and latewood band in pine arrowed cyan



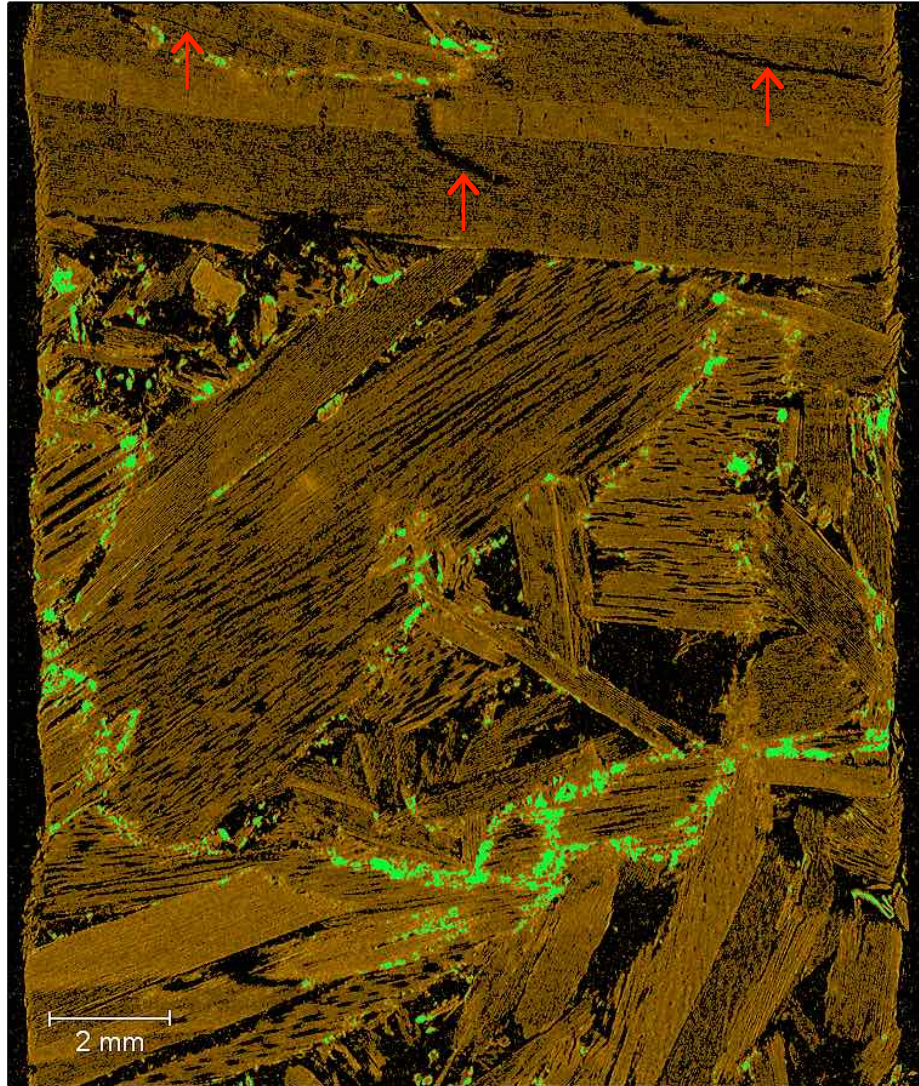


Figure 4.22 - Orthogonal rendered X-ray micro-CT image of a leached OSB specimen obtained using a conventional CT system. Note the presence of micro-checks arrowed red in the wood flake. Wood is rendered brown; voids are black; and zinc is green

The conventional CT scanning system provided sufficient resolution to allow mapping of the 3D micro-distribution of zinc in both unleached and leached specimens. The spatial distribution of zinc in unleached OSB is shown in Figure 4.23. It is clear that zinc forms a network in the composite, creating interrupted lines of zinc oriented in the x-y plane. Further information on the distribution of zinc in the unleached and leached OSB specimens can be found in Evans et al. 2015a.

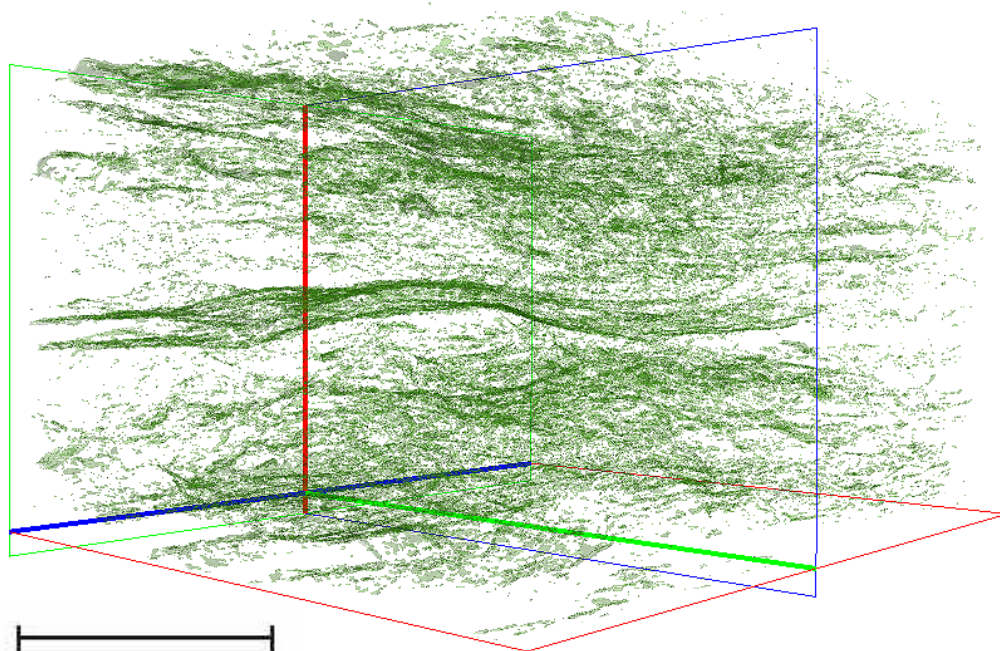


Figure 4.23 - 3D rendered X-ray micro-CT image of an unleached OSB specimen obtained using a conventional CT system. Red axis (z) represents the thickness of the board, and zinc is rendered green. Note that zinc forms a fine network in the composite, oriented in the x-y plane. Scale bar is 4 mm

#### 4.3.1.2 Helical X-ray micro-CT system

An OSB plug was analyzed using X-ray micro-CT before and after wetting/drying (Figures 4.24 and 4.25) with a helical X-ray micro-CT device, as mentioned above. The thickness of the specimen (plug's height) increased from 10.5 mm (dry) to 12.8 mm (wet/dry) as a result of moisture cycling. Hence, the irreversible thickness swelling of the specimen was nearly 22%. The irreversible thickness swelling of the OSB plug after wetting and drying is obvious in Figures 4.24 and 4.25. In Figure 4.26, it is possible to see images of *dry* (a) and *wet/dry* (b) OSB obtained from the same location; wood is rendered brown; voids are black; and zinc is white. Red arrows indicate existing internal checking in the *dry* OSB data set (Figure 4.26a), and green arrows represent internal checking in the *wet/dry* OSB data set (Figure 4.26b). Note the formation of several new internal micro-checks (arrows in Figure 4.26b), as well as the enlargement of existing ones.





Figure 4.24 - Dry OSB plug (left) and the same plug after wetting and drying (right) - the thickness of the plug increased from 10.5 mm (*dry*) to 12.8 mm as a result of wetting and drying. The irreversible thickness swelling was 21.98%



Figure 4.25 - Perspective view of OSB plug before (left) and after wetting and drying (right)

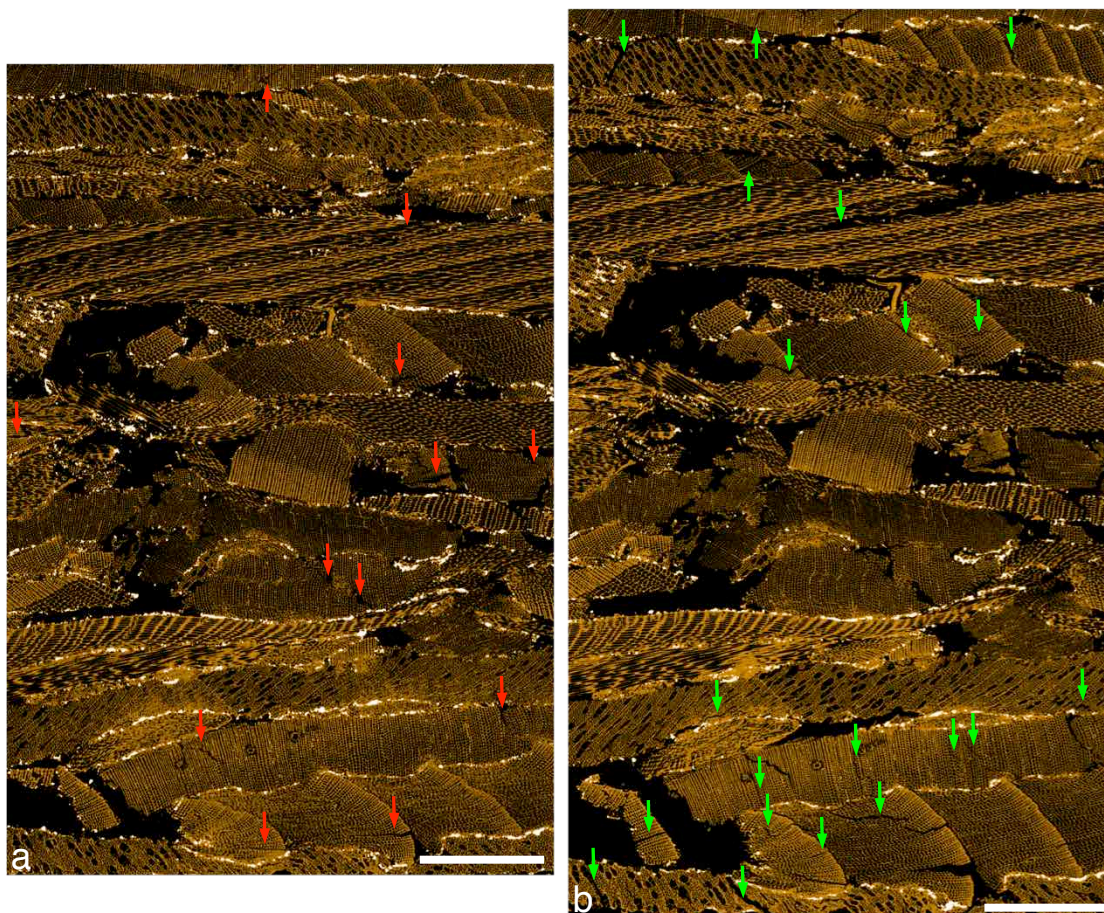


Figure 4.26 - Matched in-plane rendered helical X-ray micro-CT images of part of an OSB plug before (a) and after wetting and drying (b). Red arrows indicate existing internal checking in *dry* OSB (a), and green arrows represent internal checking formation in *wet/dry* OSB (b). Note the formation of several new internal micro-checks (arrows in b), as well as the enlargement of existing ones. Scale bars are 1 mm

It was possible to visualize check formation in both hardwood and softwood flakes in images from matched *dry* and *wet/dry* data sets. Checking appeared to be associated with vessel elements in aspen (Figure 4.27). In pine checking occurred at the interface between latewood and earlywood (tangential delamination) and in rays (radial delamination), as well as adjacent to resin canals. Non-linear transwall cracking propagation in tracheids was common in softwood flakes in surface layers. Latewood bands in pine also changed their angle of orientation. The partial recovery of deformation of flakes and enlargement of voids was also detected after wetting and drying. For example, aspen vessel elements were clearly bigger in the *wet/dry* data set (Figure 4.27b).



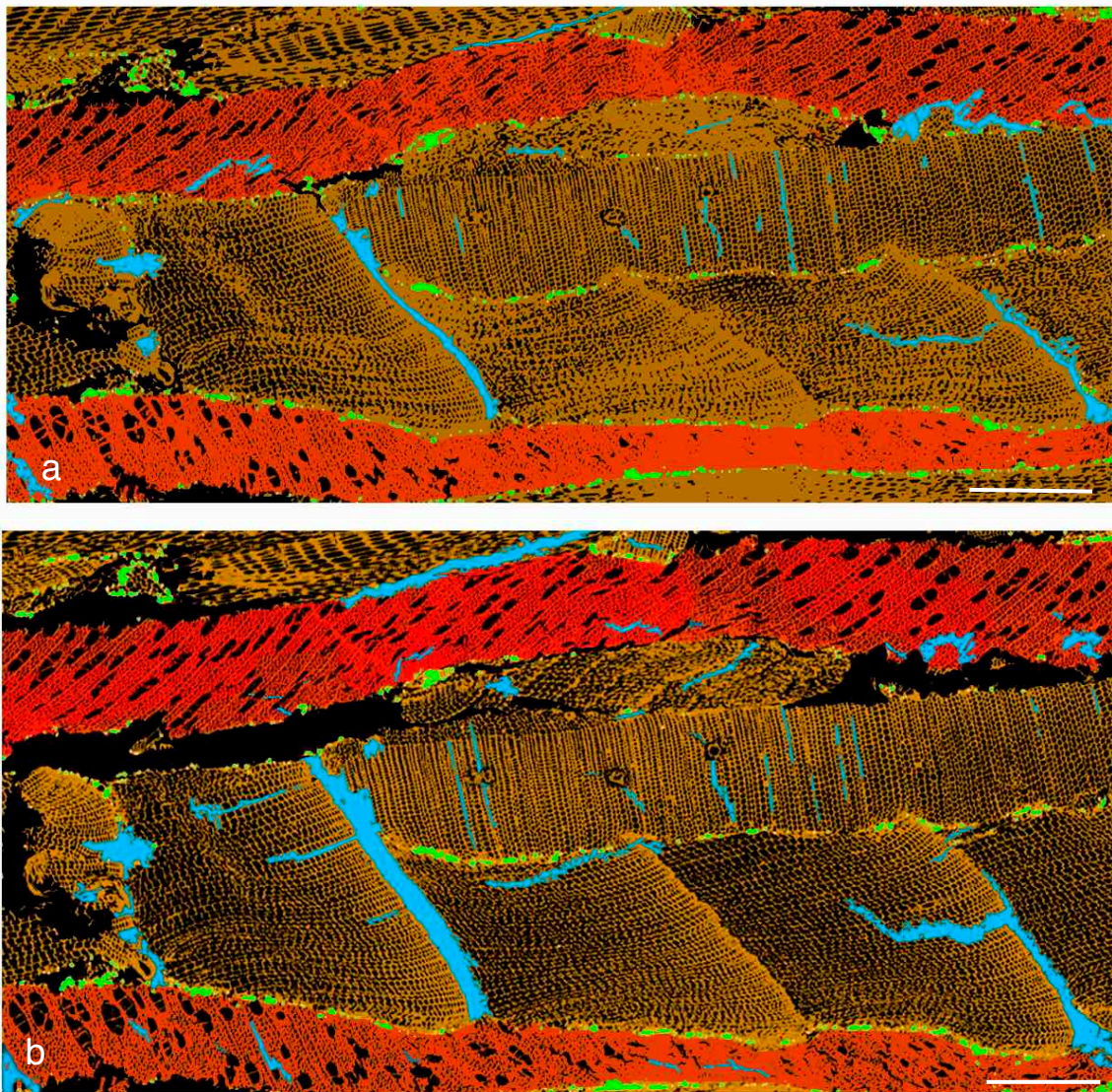


Figure 4.27 - In-plane rendered helical X-ray CT images showing part of an OSB sample. Note individual aspen and pine flakes delineated by adhesive bond lines containing zinc (rendered green). Aspen flakes highlighted red in *dry* (a) and *wet/dry* (b) data sets. Note larger checks (blue) in pine flakes (brown), compared to aspen flakes (red) in both *dry* and *wet/dry* data sets. Partial recovery of vessel elements in aspen's upper flake after wetting and drying is clear in (b). Scale bars are 0.5 mm

After manual segmentation of all the phases in OSB, image analysis was used to measure the area occupied by each phase, Figure 4.28 shows an in-plane rendered helical X-ray micro-CT image of the centre (slice at 50%) of a *wet/dry* OSB data set. The areas within the cross-section (width x thickness) occupied by the different segmented phases are: 55.13 % wood (brown), 32.20 % cell-lumen



(black), 8.40 % voids (magenta), 3.32 % cracks (cyan), and 0.95 % zinc (white). Figures 4.29, 4.30 and 4.31 show how the different segmented phases change as a result of wetting and drying of the OSB plug.

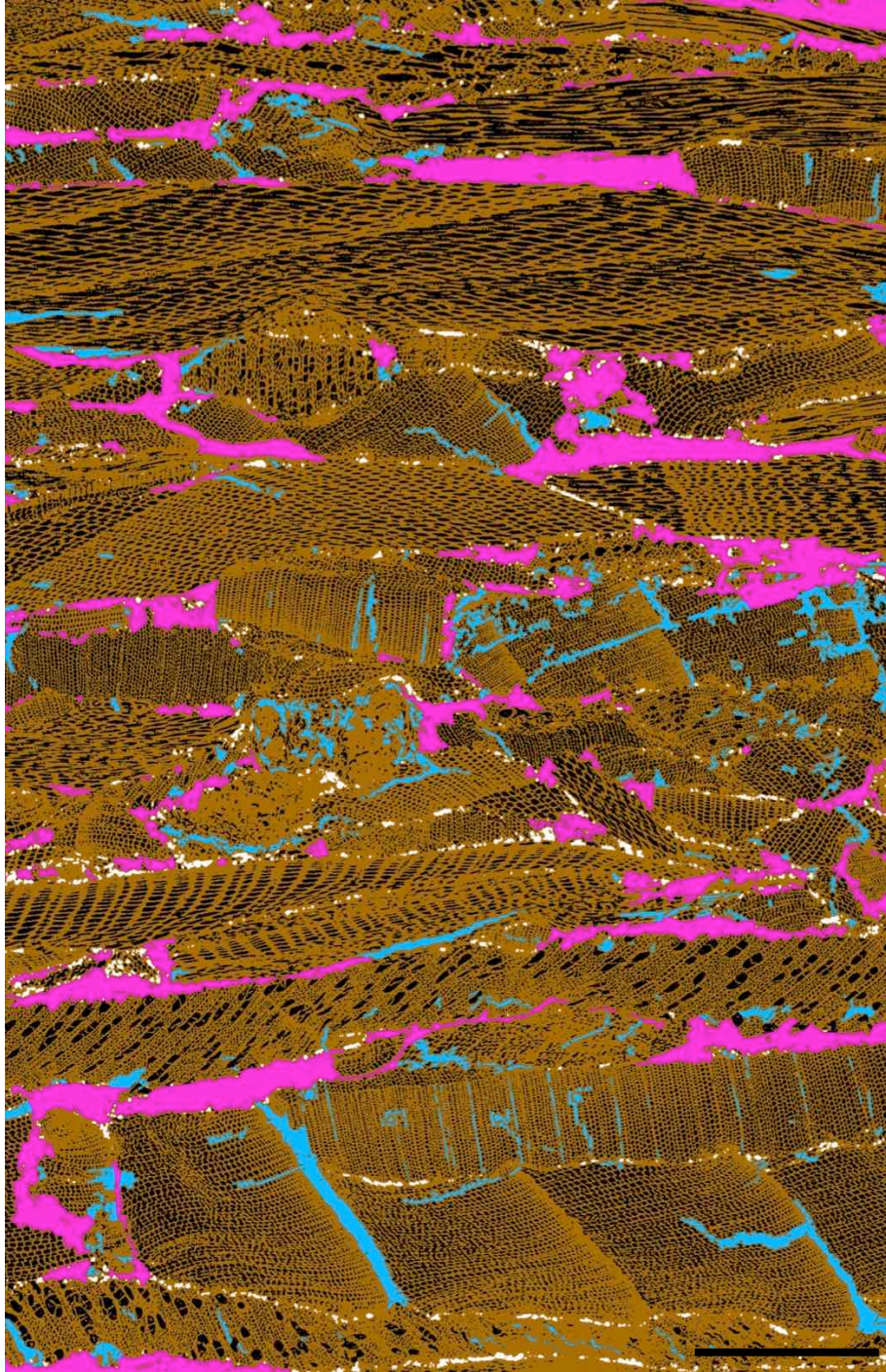


Figure 4.28 - In-plane rendered helical X-ray micro-CT image of the centre (slice at 50%) of a *wet/dry* OSB data set. Wood is rendered brown; lumens are black; voids magenta; cracks cyan; and zinc is white. Scale bar is 1 mm



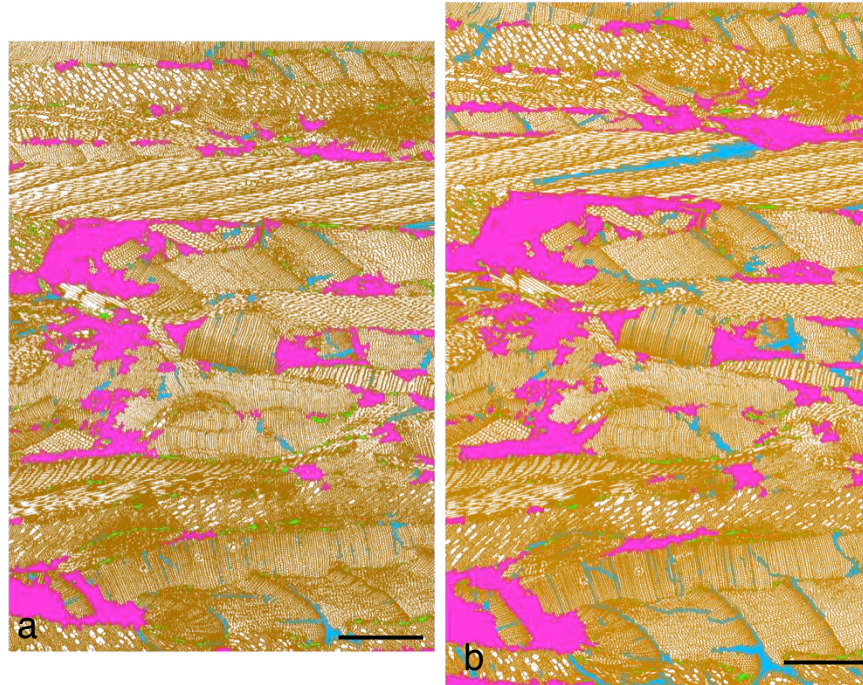


Figure 4.29 - Matched in-plane rendered helical X-ray micro-CT images of part of the OSB plug before (a) and after wetting and drying (b). The phases shown are: wood (brown), zinc (green), voids (magenta) and cracks (cyan). Scale bars are 1 mm

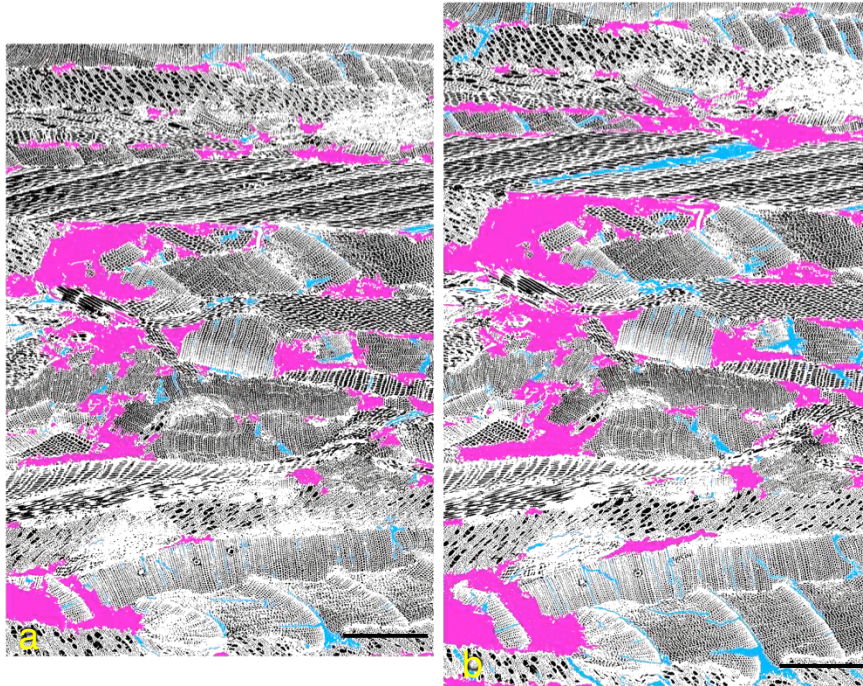


Figure 4.30 - Matched in-plane rendered helical X-ray micro-CT images of part of the OSB plug before (a) and after wetting and drying (b). The phases shown are: cell-lumen (black), voids (magenta) and cracks (cyan). Scale bars are 1 mm

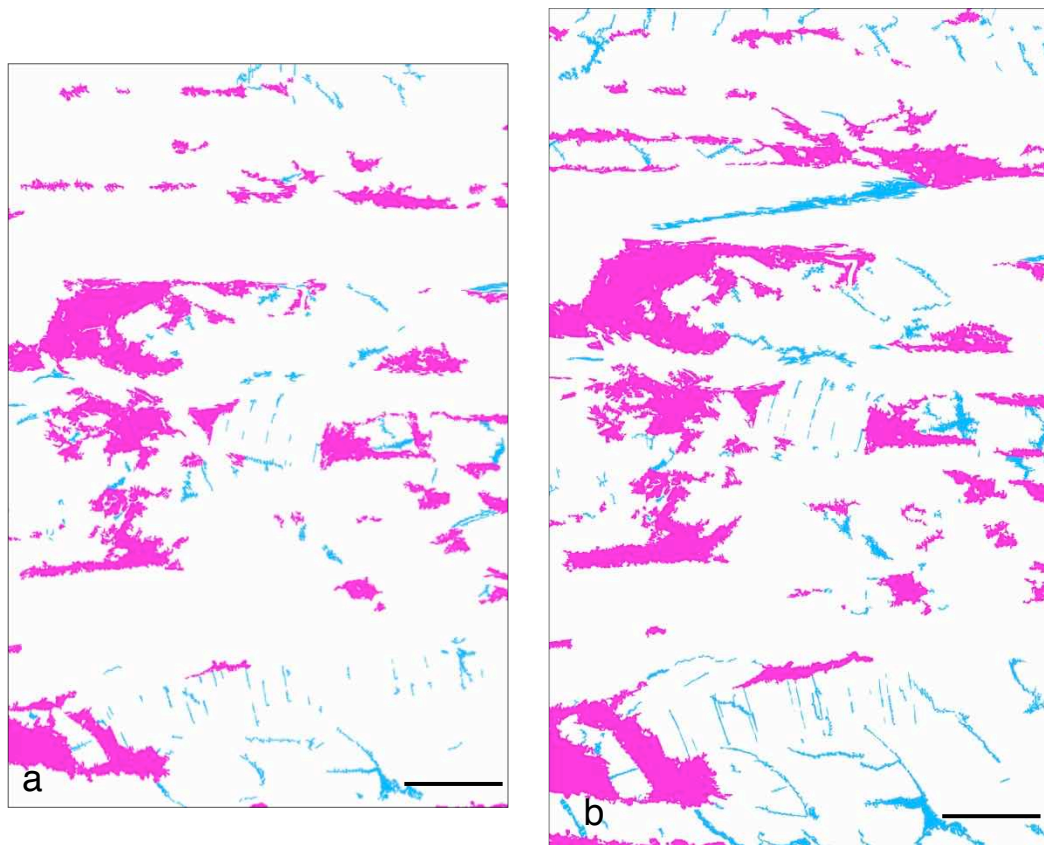


Figure 4.31 - Matched in-plane rendered helical X-ray micro-CT images of part of the OSB plug before (a) and after wetting and drying (b). The phases shown are: voids (magenta) and cracks (cyan). Scale bars are 1 mm

It is possible to see in Figures 4.30, 4.31 and 4.32 that voids present in the OSB before wetting and drying got bigger and some coalesced (joined up) (Figure 4.31b), and existing micro-checks got bigger. Furthermore, new micro-checks developed mostly in the x-y plane.

In-plane rendered helical X-ray micro-CT images of the remaining slices from the data sets are appended to this thesis (Appendix 2). Figures 4.32, 4.33 and 4.34 summarize how the area of different phases (strands, cell-lumen, voids, checks and zinc) in the OSB plug changed as a result of wetting and drying. These graphs provide numerical information across the frames for the *dry* and *wet/dry* data sets. An increase in area of voids and checks across the frames is apparent. A decrease in zinc associated with wetting and moisture-induced swelling of the OSB plug is clear in Figure 4.34. Figure 4.35 compares the



average percentage area of the different phases from all slices from the *dry* and *wet/dry* data sets. Voids and cracks occupy a greater proportion of the overall area in the *wet/dry* data set compared to the *dry* data set. For example, micro-checks occupy almost twice the area in the *wet/dry* data set compared to the *dry* data set.

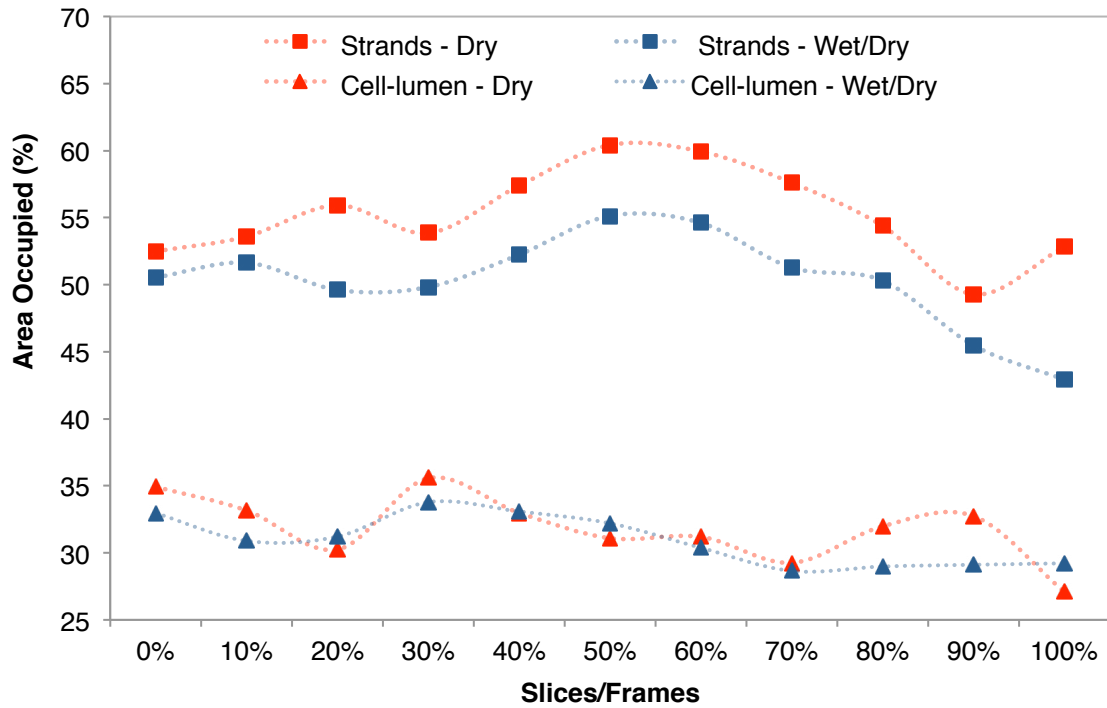


Figure 4.32 - Area occupied by the phases representing strands (square) and cell-lumens (triangle) in the *dry* v. *wet/dry* OSB data sets (slices from 0-100 %) across the specimen's length

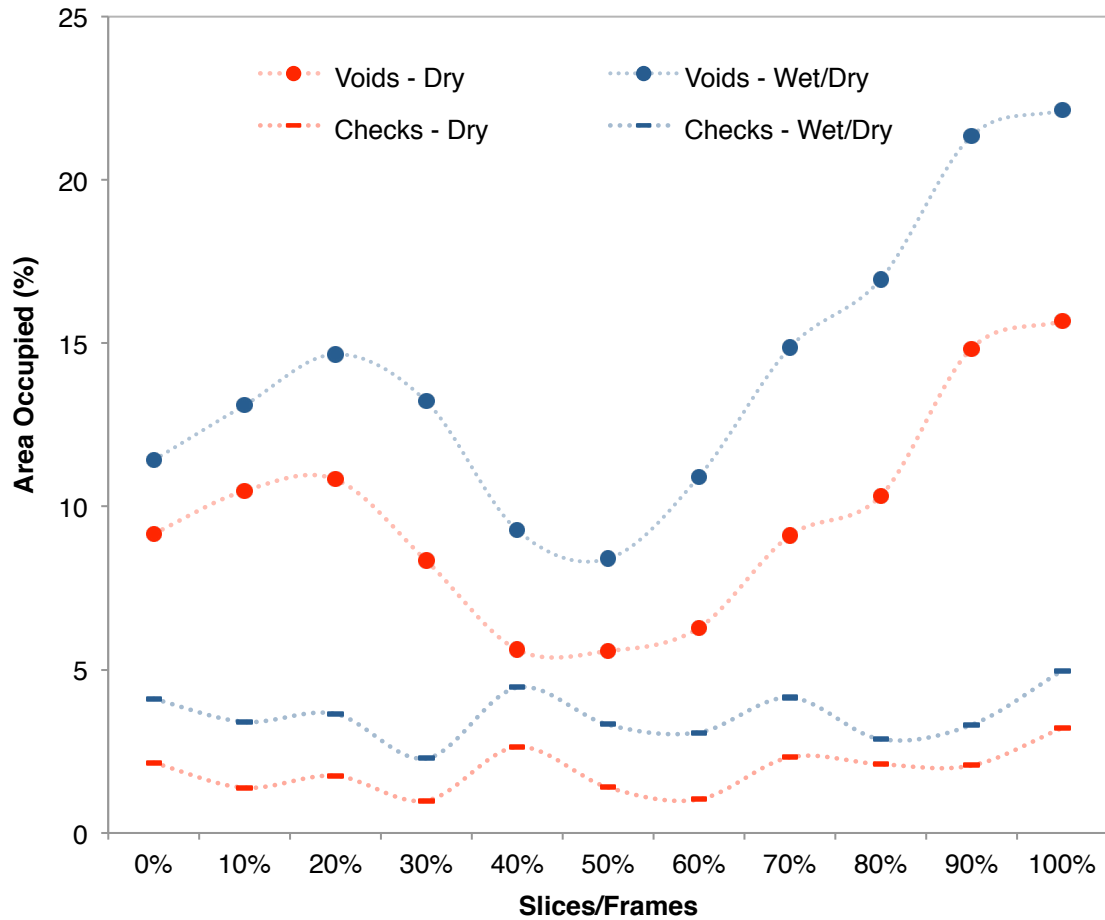


Figure 4.33 - Area occupied by phases representing voids (circle) and checks (dash) in the *dry* v. *wet/dry* OSB data sets (slices from 0-100 %) across the specimen's length. Changes in voids or checks appeared to be proportional in frames

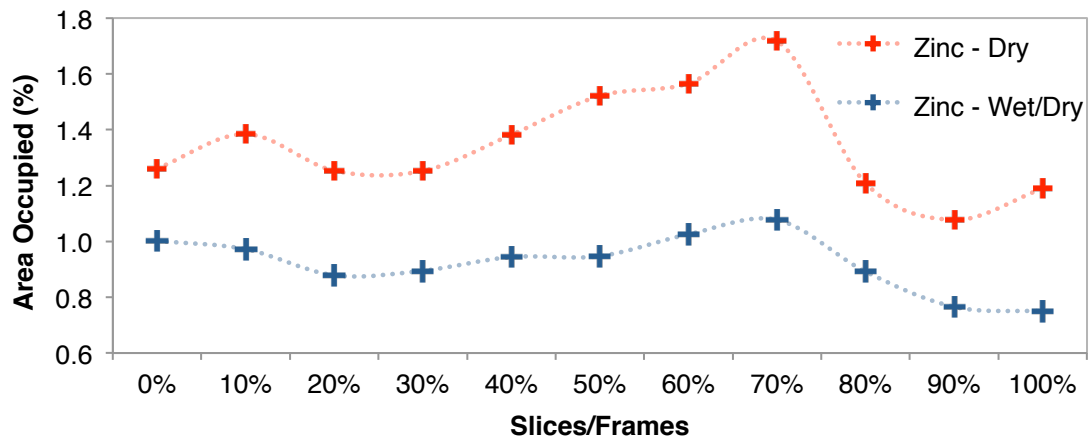


Figure 4.34 - Area occupied by the zinc phase in the *dry* v. *wet/dry* OSB data sets (slices from 0-100 %) across the specimen's length. Note the decrease in area occupied by zinc associated with wetting and drying

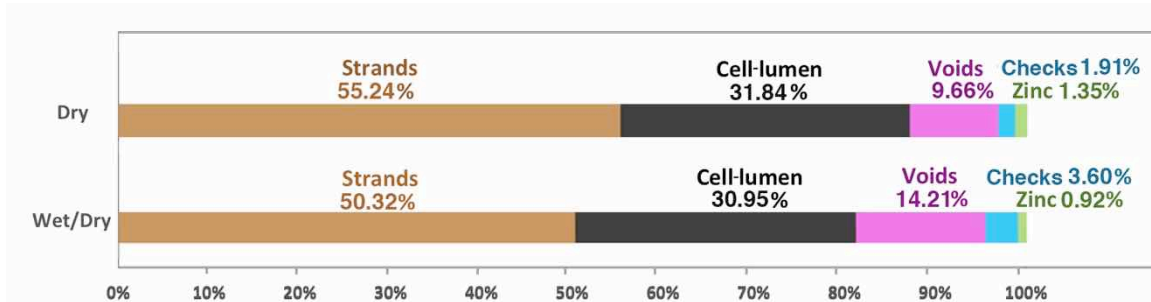


Figure 4.35 - Graph showing the average area of phases from all slices from the *dry* and *wet/dry* data sets. Note that voids and cracks occupy a greater proportion of the overall area in the *wet/dry* data set

Differences in area occupied by phases such as “strands” and “cell-lumen”, as well as the others in *dry* and *wet/dry* images are summarized in Figure 4.35. Some of the difference may be due, in part, to a shift in the internal structure of the data sets due to a complex (in-plane and out-of-plane) swelling behaviour of the OSB plug.

Statistical analysis of phase data for the different frames showed that the area occupied by voids and cracks increased significantly ( $p < 0.001$ ) from *dry* to the *wet/dry* state, whereas the area occupied by wood flakes and zinc decreased significantly ( $p < 0.001$ ). The area occupied by cell-lumen did not change significantly ( $p = 0.138$ ). Figure 4.36 plots these results.

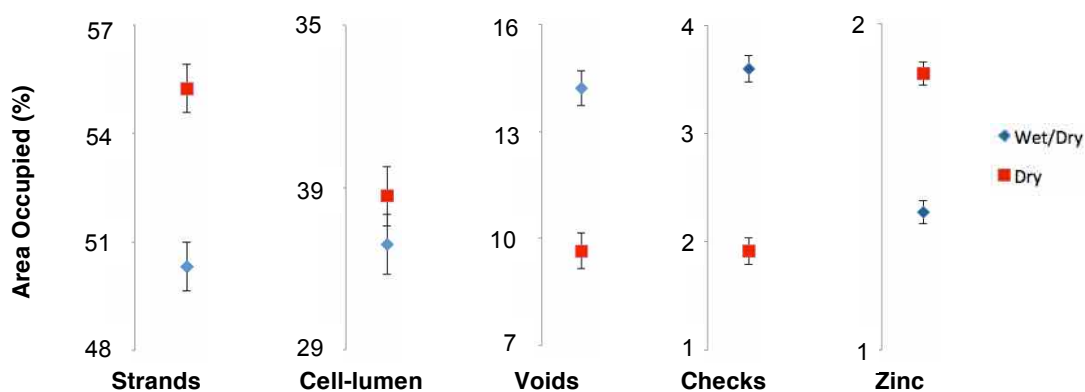


Figure 4.36 - Area of phases from replicate slices from the *dry* (red) v. *wet/dry* (blue) data sets. Non-overlap of error bars indicates that individual means are significantly different ( $p < 0.05$ )

The spatial distribution of zinc in *dry* and *wet/dry* OSB images is shown out-of-plane in Figures 4.37 and 4.39. It is clear that zinc is present around the flakes of the *dry* specimen, and also in the specimen after wetting and drying (Figures 4.37b and 4.39b). However, there appears to be less zinc present in the specimen after wetting and drying. Figure 4.38 shows a matched orthogonal image of part of an OSB plug before (Figure 4.38a) and after (Figure 4.38b) wetting and drying. These images highlight the possibility of matching frames by identifying common features in both data sets, such as vessel element and zinc particles.

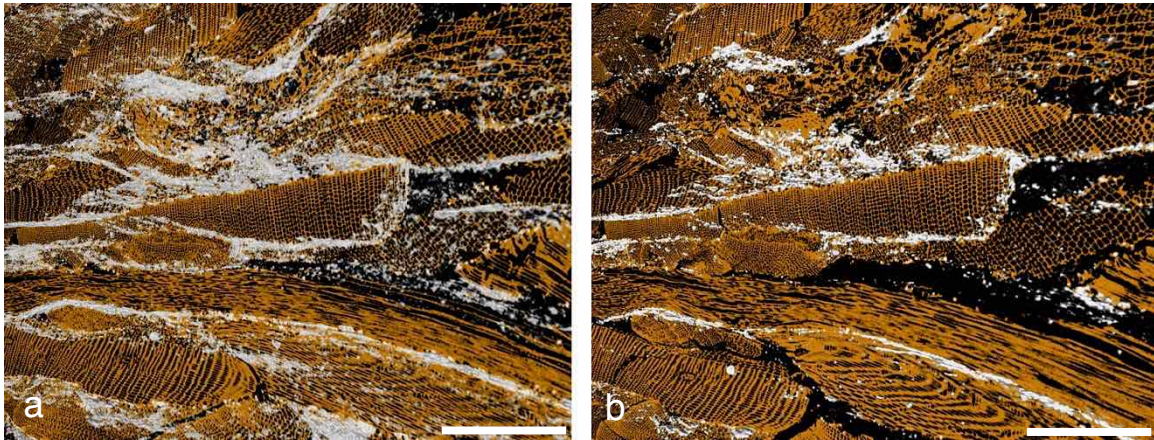


Figure 4.37 - Matched out-of-plane rendered X-ray micro-CT images of part of an OSB plug before (a) and after wetting and drying (b). Wood is rendered brown; voids are black; and zinc is white. Note that less zinc is present in the image after wetting and drying. Scale bar is 0.5 mm

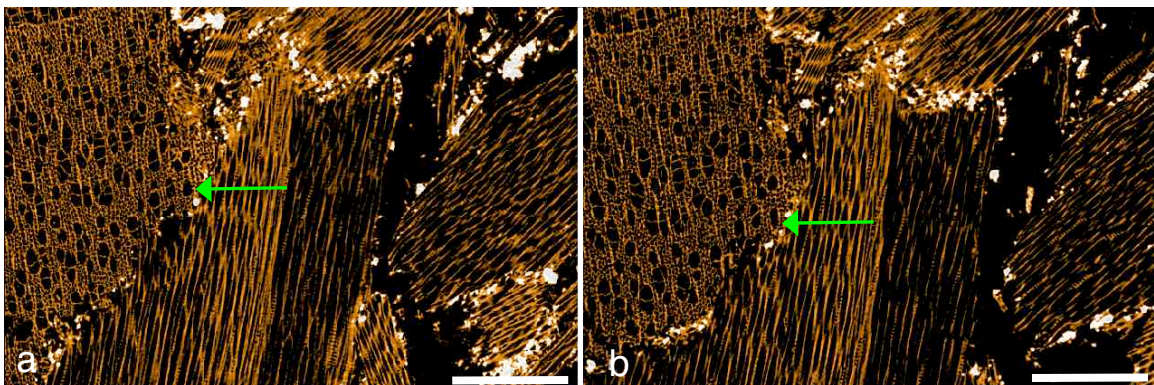


Figure 4.38 - Matched orthogonal rendered X-ray micro-CT images of part of an OSB plug before (a) and after wetting and drying (b). Wood is rendered brown; voids are black; and zinc is white. Green arrows point to the same aspen vessel element. Scale bars are 0.5 mm



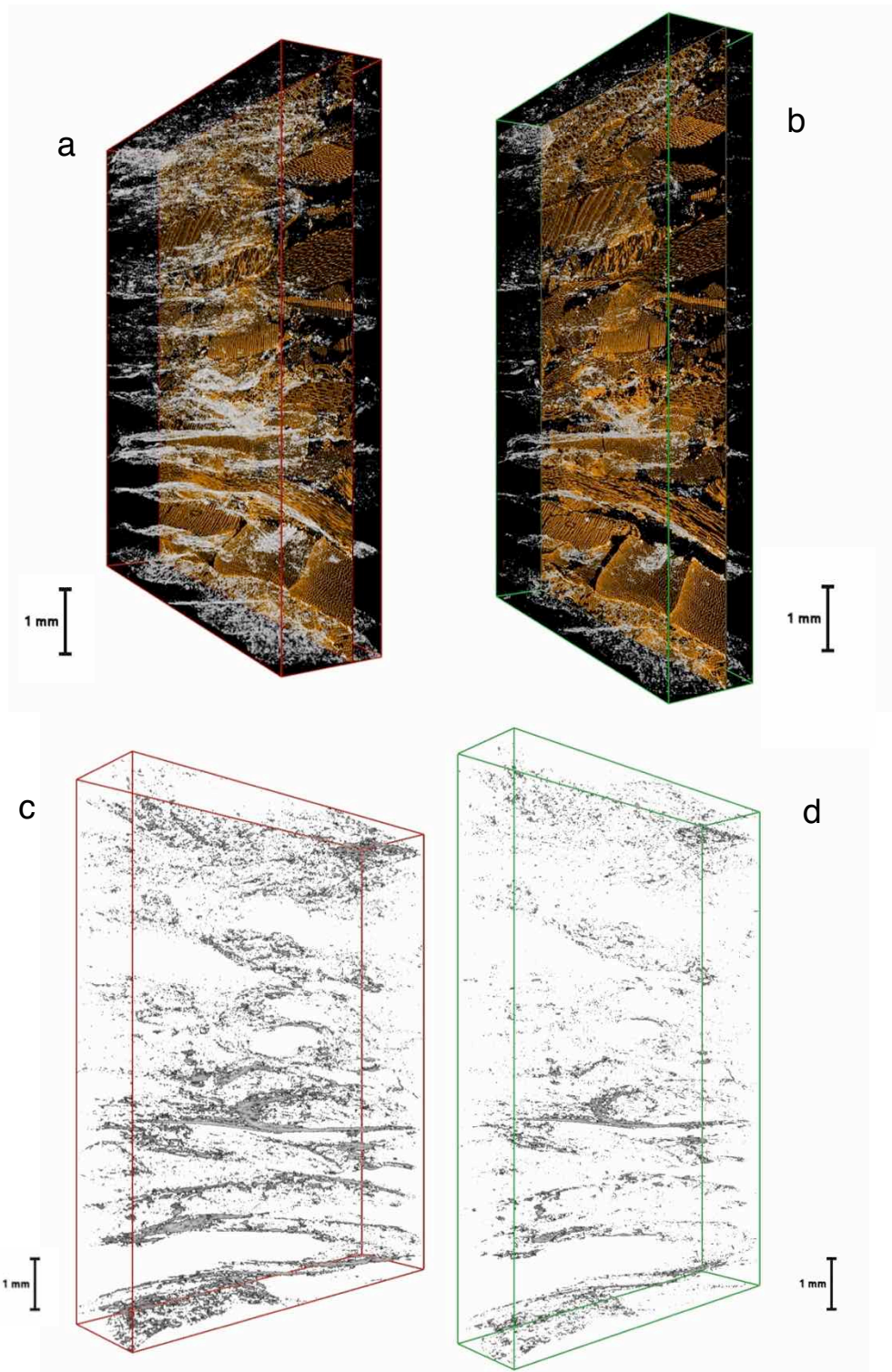


Figure 4.39 - Out-of-plane images showing the 3D distribution of zinc in both *dry* (a & c) and *wet/dry* (b & d) data sets. Images on the bottom (c & d) only show the presence of zinc. Note that the *wet/dry* data set (d) suggests that wetting and drying reduced the level of zinc in the OSB specimen

#### *4.3.2 Field emission scanning electron microscopy*

Using FE-SEM, I sought to find out the origins of micro-checking in OSB. There was little difference in the micro-checking of sub-samples taken from the surface and core of OSB and my principal finding is that fracture surfaces of micro-checks in pine occur in or close to the middle lamella (interface between the wood cells), which is rich in lignin (Panshin and De Zeeuw 1980) (Figures 4.40 and 4.41). The epoxy embedding medium appeared to be able to infiltrate the void structure of OSB, although the earlywood of pine was more easily infiltrated than the latewood (Figure 4.42). Micro-checks were more visible in pine than in aspen (Figures 4.43, 4.44 and 4.45). Embedding the specimens with a low-viscosity epoxy resin made it possible to obtain a clear, defect free surface. In contrast, specimens that were not embedded in the epoxy resin were very difficult to section, and the resulting images were poor (Figures 4.46, 4.47, 4.48 and 4.49). All of the FE-SEM images from OSB specimens are appended to this thesis (see Appendix 3).



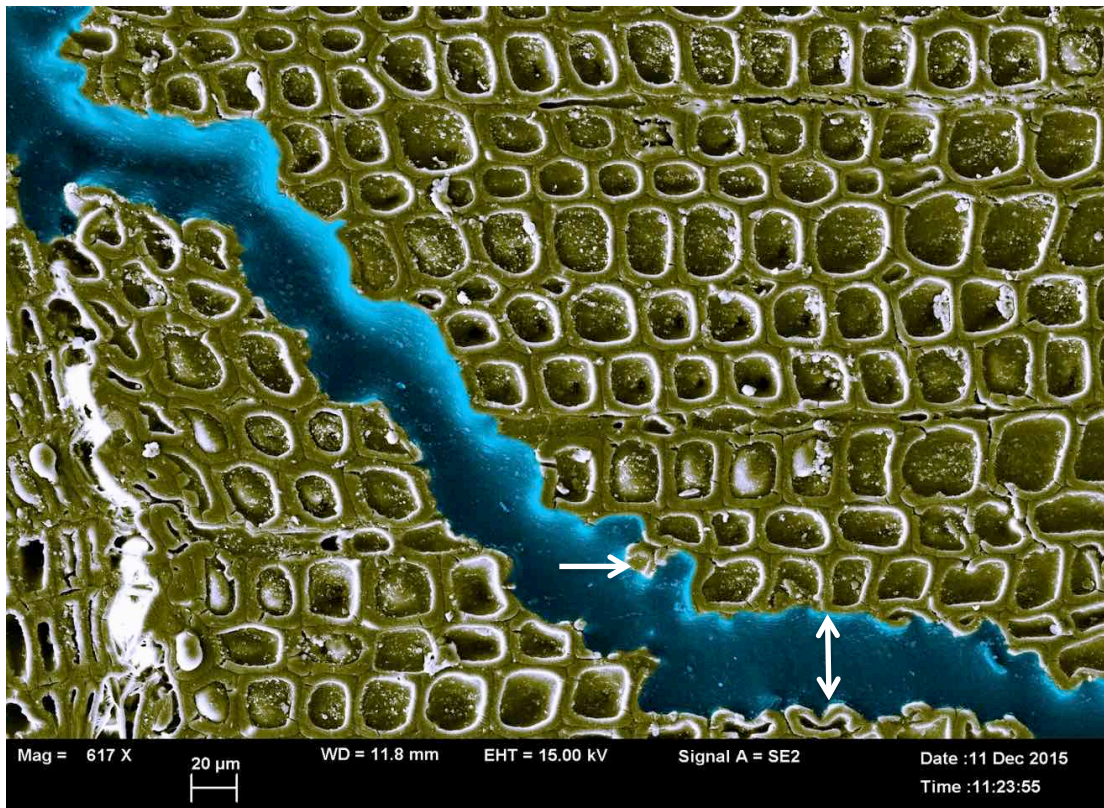


Figure 4.40 - FE-SEM image from an OSB specimen exposed to 72 h of water soaking and subsequent drying. Note the within wall (arrowed left) and inter-wall (arrowed right) fractures (highlighted cyan) in pine latewood

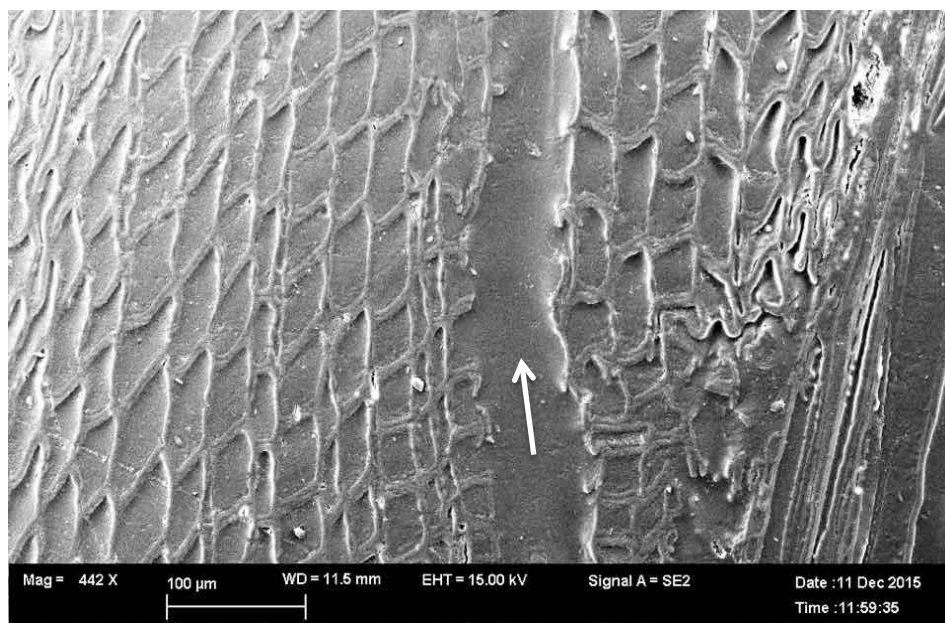


Figure 4.41 - FE-SEM image obtained from an OSB specimen exposed to the wetting & drying cycle used in Chapter 3. Note the within wall micro-check in the earlywood of a cross-section of a pine flake (arrowed centre)

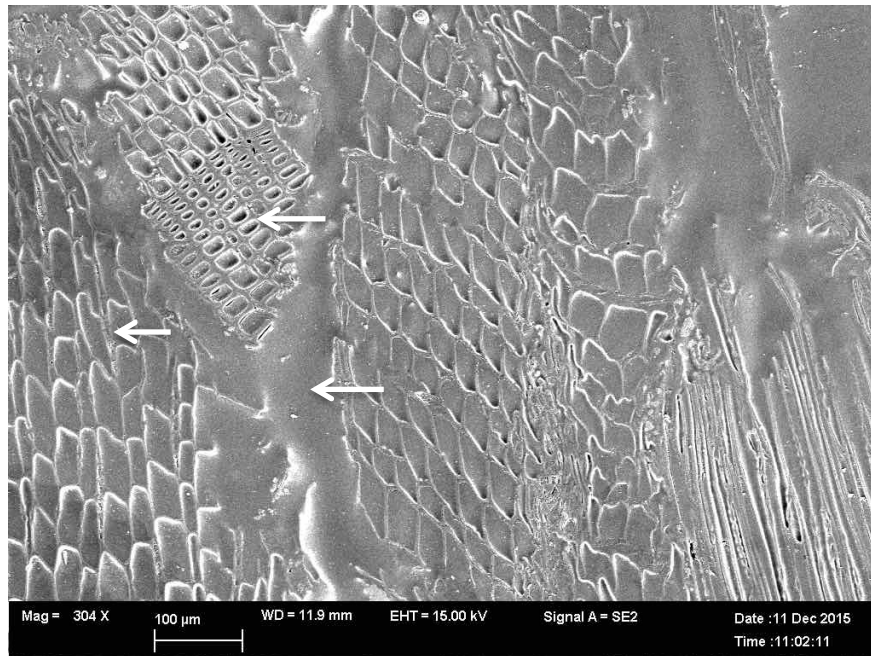


Figure 4.42 - FE-SEM image of an OSB specimen exposed to 72 h of water soaking and subsequent drying; effective infiltration of embedding medium in voids (arrowed right) and in earlywood has clearly occurred (arrowed left), but infiltration does seem to be as complete in latewood (arrowed centre)

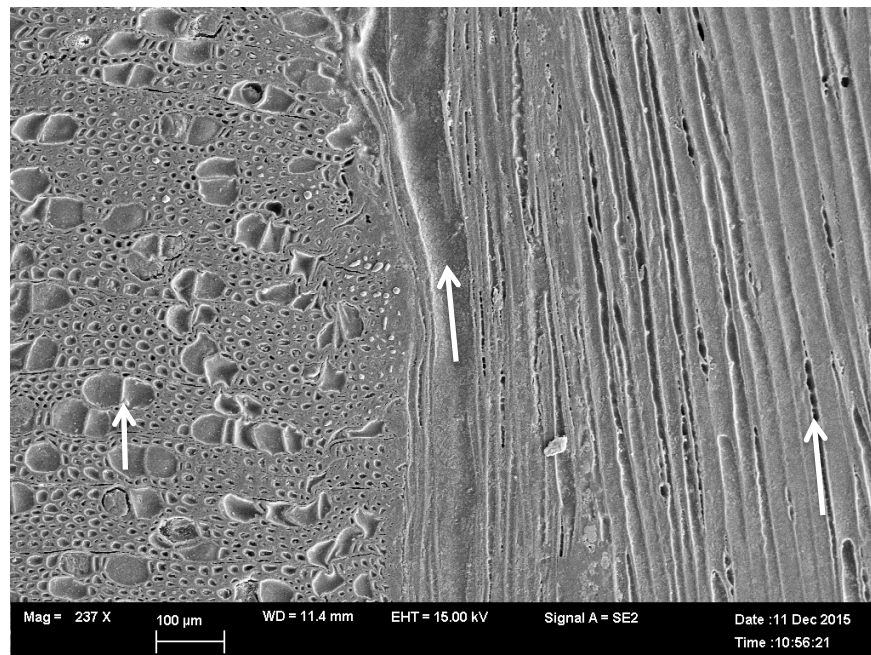


Figure 4.43 - FE-SEM image of an unsoaked OSB specimen that acted as control. Note a long micro-check (arrowed centre) at a radial surface between a pine flake and an adjacent aspen flake (vessel element arrowed left)



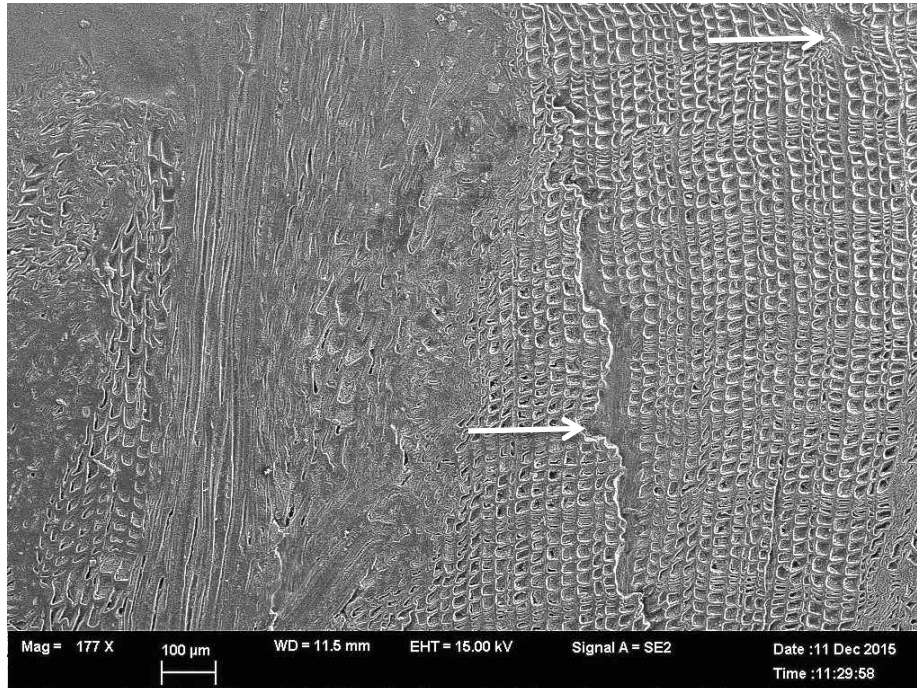


Figure 4.44 - FE-SEM image of an unsoaked OSB specimen that acted as control. Note a long micro-check (arrowed centre) at a cross-section of a pine flake; a resin canal is arrowed right

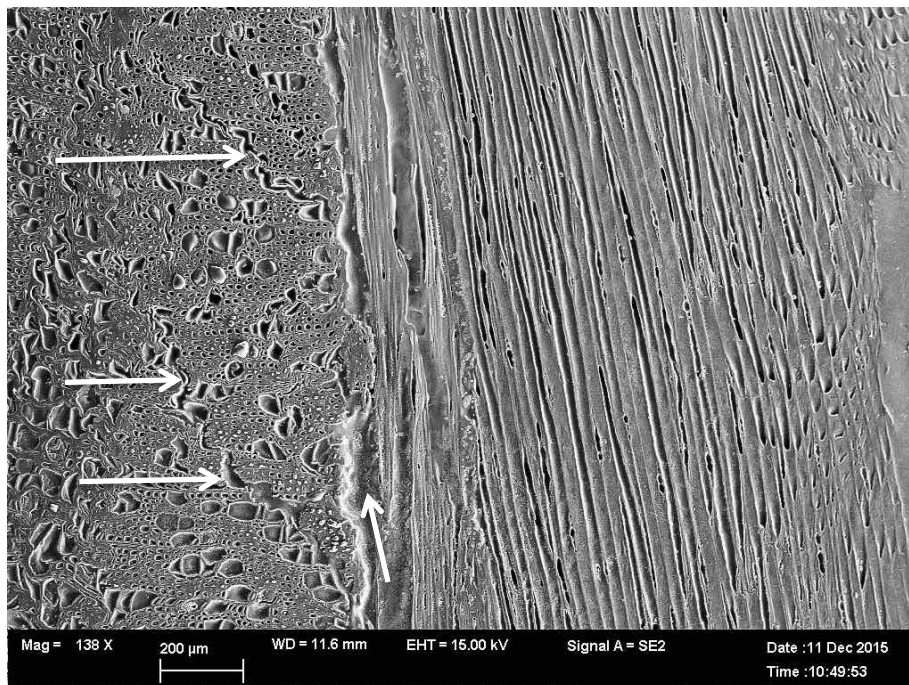


Figure 4.45 - FE-SEM image of an unsoaked OSB specimen that acted as control. Note micro-checks (arrowed left) within a cross-section of an aspen flake; an inter-strand void is arrowed right

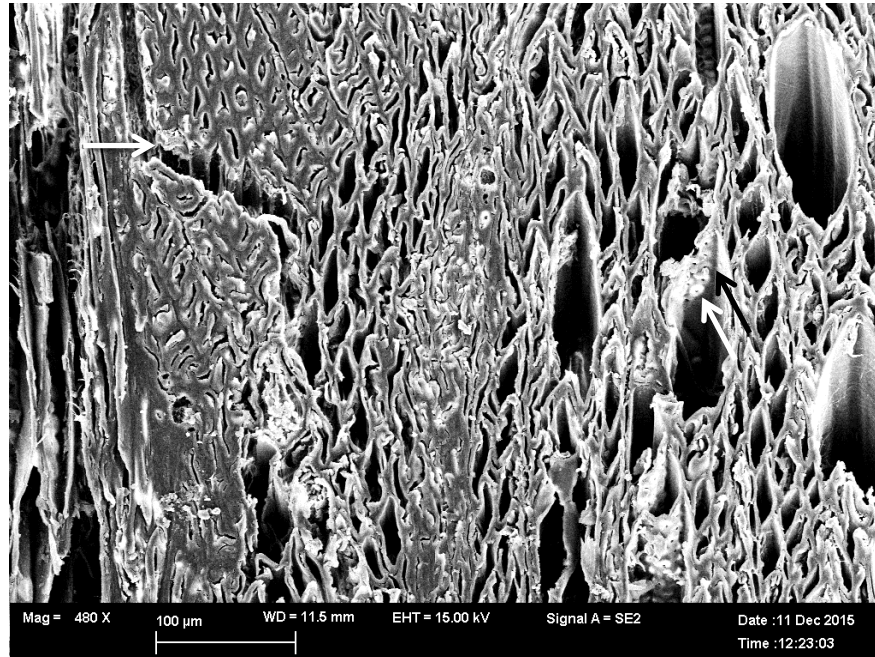


Figure 4.46 - FE-SEM image of an OSB specimen that was not embedded with resin and was exposed to the wetting & drying cycle used in Chapter 3. Note that the surface of the specimen is fuzzy and the interface of the micro-check (arrowed left) in latewood of a softwood flake is not clearly visible. Intervessel pits in part of an aspen flake are arrowed right

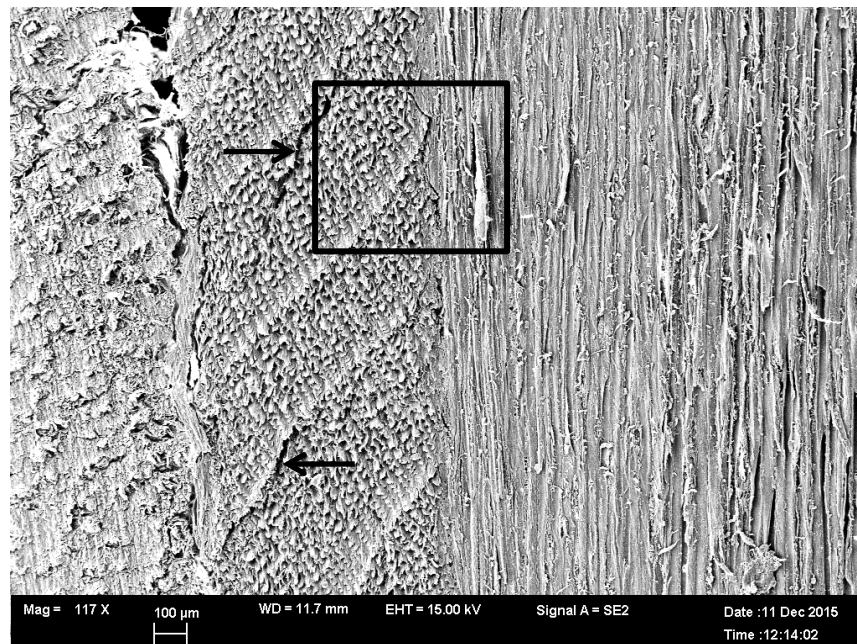


Figure 4.47 - FE-SEM image of an OSB specimen that was not embedded with resin and was exposed to 72 h water soaking and subsequent drying. Note the indistinct checks (arrowed black) in between earlywood and latewood bands of softwood. Higher magnification inset (square box) is shown below in Figure 4.48

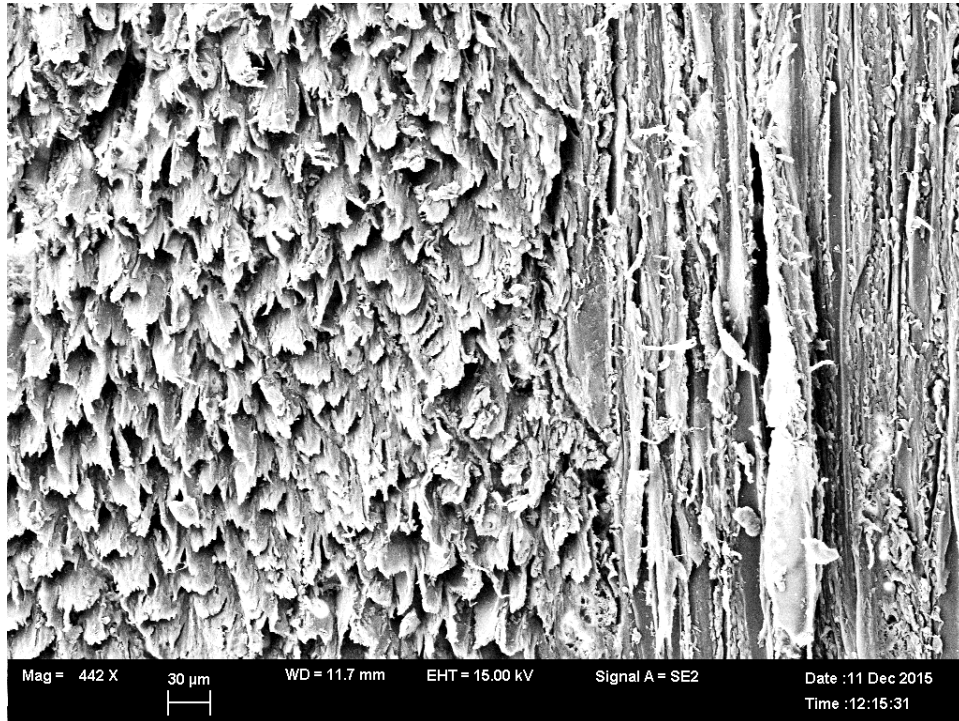


Figure 4.48 - Magnified FE-SEM image of the same OSB specimen shown above in Figure 4.47. Note that the fuzzy torn surface obscures micro-checks

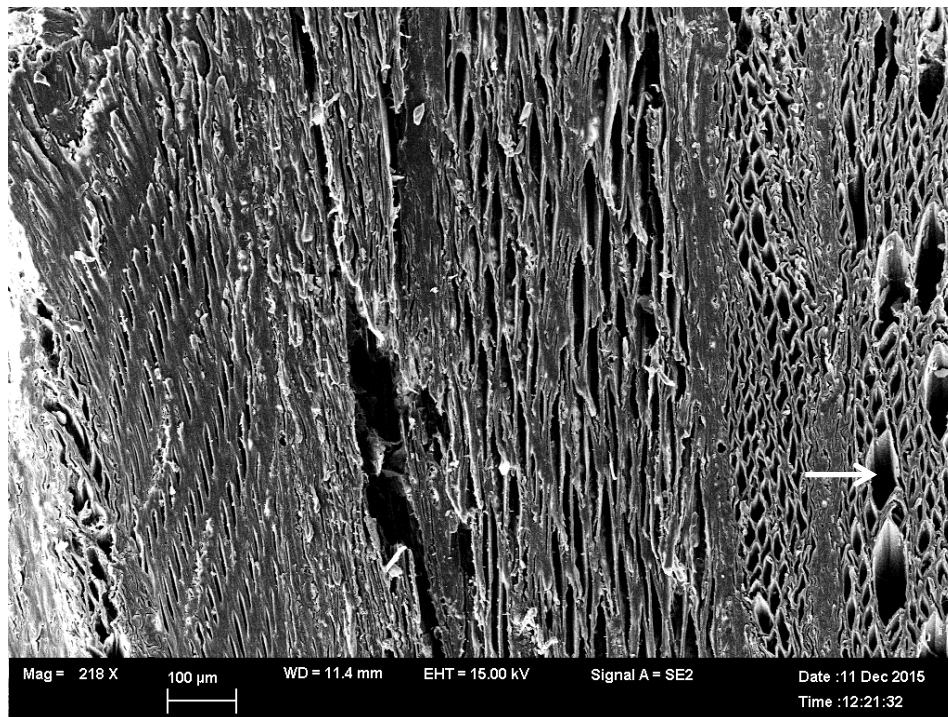


Figure 4.49 - FE-SEM image of an OSB specimen that was not embedded with resin and was exposed to the wetting & drying cycle in Chapter 3. Note aspen vessel element (arrowed)

#### 4.4 Discussion

I suggested in the introduction to this chapter, based on results in Chapter 3, that thickness swelling of OSB might be due in part to internal micro-checking that develops when OSB is exposed to wetting and drying. To test this hypothesis, non-destructive imaging of the internal microstructure of OSB was performed using state-of-the-art X-ray micro-CT. My results in this chapter clearly show that micro-checking develops within the body of OSB exposed to wetting and drying. I observed the enlargement and propagation of new and existing micro-checks, as well as voids internally within OSB samples. Therefore, images of the internal microstructure of OSB before and after moisture-induced swelling support findings from Chapter 3, which showed that voids and checks increased significantly as a result of wetting and drying, and appeared to be associated with the irreversible thickness swelling of OSB. My results accord with some findings of earlier studies that employed other techniques to look at the effects of moisture-induced swelling on the microstructure of OSB. For example, I confirmed the following: (1) the partial recovery of deformed wood flakes (Irle 2001); (2) vessel element or cell wall buckling (Neusser et al. 1965, Halligan 1970, Bucur 2011); (3) enlargement of voids associated with adhesive delamination (Kelly 1977, Hsu et al. 1988, Wu and Piao 1999); and (4) leaching of zinc (Lee and Wu 2007, Evans et al. 2015a). I did not visualize straightening of strands as suggested by Lloyd (1984) and Irle (2001), possibly because the samples I tested in this chapter (and in Chapter 3) were not big enough, but I did notice an increase in the angle of latewood bands in softwood flakes near the surface of samples after wetting and drying which suggests reorientation of flakes.

It was not possible to examine adhesive distribution in OSB using X-ray micro-CT, because the adhesives in the OSB had a similar density to that of the wood flakes. However, zinc accumulated in glue lines and it was possible to map the 3D distribution of zinc in OSB. Hence, zinc acted as a proxy for the location of the adhesives in OSB. My OSB samples contained two different adhesives (PF in

surface layers and pMDI in the core). My X-ray micro-CT results suggest that: (1) both adhesives were mainly oriented in the x-y plane; (2) the adhesives were unevenly distributed across the thickness of the board; (3) they seemed to accumulate (clump) in certain areas. Although it was not my primary aim to look at adhesive distribution, these observations confirm for pMDI and PF some of those made previously for a MUF adhesive in particleboard (Morrison 2004, Evans et al. 2010, Evans et al. 2015a) (listed above). According to Morrison (2004) and Evans et al. (2010), some of the adhesive applied to wood flakes in particleboard does not participate in bonding because it penetrates cracks and the splintered ends of flakes. Hence, it is possible that micro-checking present in flakes before adhesive bonding may diminish adhesive bond strength. Such an effect could result in increased swelling when the composite is exposed to moisture.

Both X-ray micro-CT systems (conventional and helical scanning) had sufficient resolution (10.5 and 4.4  $\mu\text{m}$ , respectively) to visualize and quantify zinc in OSB (leached and unleached). This is noteworthy, because the internal distribution of preservatives and biocides in wood composites influences their effectiveness (Gnatowski et al. 2010). Evans et al. (2015a) used chord length analysis to quantify changes in distribution of zinc in OSB subjected to leaching. They found that leaching caused chord lengths to shift to lower values, indicating that zinc borate deposits became thinner along the thickness direction of OSB, which might be associated with delamination of flakes, as pointed out by Evans et al. (2015a). My results accord with their findings. I also detected a decrease in zinc present in OSB after wetting and drying possibly due to leaching of zinc borate. My observations of an increase in inter-strand voids accord with those of Shaler (1986). He found that an aspen flakeboard with a density of 700  $\text{kg/m}^3$  contained approximately 7.3% of inter-strand voids, which is very similar to my findings.

Zinc particles trapped between well-bonded strands in the OSB plug were very useful for manually matching frames from *dry* and *wet/dry* data sets. This was fortuitous because swelling caused the frames from the *wet/dry* data set to shift

from their original location in the *dry* data set. The benefits of manually segmenting all the phases in the data sets obtained by X-ray micro-CT, was that it allowed precise analysis of the microstructure of OSB, and provided detailed information on what happens to OSB exposed to moisture-induced swelling. However, this approach was very time-consuming. Nevertheless it was the one that gave the most precise information about the microstructure of the entire OSB specimen. As expected, the helical X-ray micro-CT system provided improved resolution and image quality when compared to the conventional CT system. According to Varslot et al. (2011), one of the other benefits of using a helical micro-CT system is the ability to image very long objects. Hence, it could easily accommodate the OSB plug imaged in this chapter.

The embedding of OSB specimens in a low-viscosity epoxy resin medium prior to FE-SEM was useful at preserving the integrity of specimens during surface preparation, and allowed clear images of the microstructure of the fracture of wood cell wall to be taken. However, the labelled epoxy doped with epibromohydrin did not provide the expected contrast between checks and wood when imaging OSB samples in back-scattered electron mode, because the labelled resin penetrated the whole specimen rather than preferentially penetrating micro-checks. On the other hand, specimens that were not embedded with epoxy resin had a fuzzy torn surface as a result of damage that occurred during surface preparation. Such damage prevented micro-checks from being seen with any clarity.

Internal micro-checks and voids imaged in this chapter occupied a larger area compared to surface checking and voids imaged in Chapter 3. For example, the area of surface micro-checks in OSB specimens in Chapter 3 increased more than three times during the wetting and drying cycle, from 0.37 to 1.17%, and the area of voids increased nearly twofold (from 3.05 to 5.98%). In contrast, results in this chapter showed that the area of internal checking increased from 1.91 to 3.60%, and the area of voids increased from 9.66 to 14.21%. The area of checking and voids measured in this chapter might be higher than that measured



in Chapter 3 because of the higher resolution of X-ray micro-CT compared to macro-photography. Alternatively the wet and dry cycle employed in this chapter may have been better at inducing micro-checking than that used in Chapter 3.

#### **4.5 Conclusions**

The helical X-ray micro-CT technique used in this chapter to probe the microstructure of OSB showed that significant internal checking occurs when OSB is exposed to moisture-induced swelling, as I hypothesized. My results suggest that internal micro-checking contributes to irreversible swelling of OSB. I observed where the micro-checks develop in flakes, and I also observed differences between the checking of aspen and pine flakes. My findings have implications for the manufacture of 'superior' OSB that is less susceptible to micro-checking and thickness swelling. I discuss this topic in greater detail in Chapter 5. The helical X-ray micro-CT system used in this chapter had sufficient resolution to provide precise data on the microstructure of an OSB specimen before and after wetting and drying. Because the technique is non-destructive, it could also be used to examine the effects of further moisture cycling on the microstructure of OSB, and also the microstructure of other wood composites. Further research is needed on both of these topics.

## **Chapter 5: General Discussion, Suggestions for Further Research and Conclusions**

### **5.1 General discussion**

In this thesis I hypothesized that micro-checking develops in OSB when it is exposed to wetting and drying. Micro-checks were observed in OSB exposed to wetting and drying in both Chapters 3 & 4, supporting my hypothesis. There were additional similarities in the results from both chapters. For example, results in the chapters indicated that micro-checking was more pronounced in pine than in aspen, and revealed that the microstructure of checks in both species was similar. In Chapter 3, I observed that surface micro-checks and voids are initially present in OSB specimens, and their area increases significantly during wetting and drying. Many of the micro-checks in OSB were oriented parallel to the Z (thickness) direction of specimens, like the voids resulting from delamination, which contribute to the moisture-induced thickness swelling of OSB. Taken together, my observations in Chapters 3 & 4 confirm my general hypothesis, that micro-checking develops when OSB is exposed to wetting and drying. Furthermore, they suggest that micro-checking contributes to the irreversible thickness swelling of OSB.

However, there were some differences in results obtained in Chapters 3 & 4. X-ray micro-CT and FE-SEM, which I used in Chapter 4, had greater resolution and yielded more accurate information on the ultra-structure and areas of checks and voids in specimens than the system used in Chapter 3. These high-resolution imaging techniques provided previously unmatched information on the internal microstructure of OSB exposed to moisture-induced swelling. The limitations of both techniques used in Chapter 4 are: their relatively small field of view, and the fact that they are only capable of analyzing the material statically. On the other hand, the macro-photography system I developed and used in Chapter 3 can observe the swelling and shrinkage of OSB and solid wood specimens dynamically in real-time. The system has several potential applications for the surface analysis of materials. It has sufficient resolution to detect changes at the



cellular level, for example recovery of compressed tracheids during wetting, and also the micro-checking ( $>10\text{ }\mu\text{m}$ ) of solid wood and composites during wetting and drying. In addition, it has a large enough field of view (maximum of  $36 \times 24\text{ mm}$ ) to visualize macroscopic changes in the structure of large samples (for example, gross swelling and shrinkage). The system is inexpensive, reliable, rugged and easier to use than X-ray micro-CT or FE-SEM. It has similar advantages over the microscopy systems that have been used in the past to non-destructively examine the micro-checking of wood during wetting or drying, or exposure to weathering, including confocal laser and environmental SEM (Yamamoto et al. 2013, Hatae et al. 2012).

I also suggested in the introduction to this thesis that surface and internal micro-checking of OSB might contribute to the irreversible thickness swelling of OSB when it is exposed to wetting and drying in addition to the following factors that are known to contribute to irreversible thickness swelling: (1) recovery of deformed wood; (2) enlargement of voids; (3) and straightening of strands. Some of the micro-checks that developed when OSB was exposed to wetting and drying were oriented parallel to voids, and the magnitude of the volume that micro-checks occupied in OSB suggest that they may contribute to permanent increases in thickness of OSB exposed to wetting and drying, albeit probably less than the contribution of the first two factors.

## **5.2 Further research**

The visualization and measurement systems developed and deployed in this thesis show promise as tools for understanding the moisture-induced changes in dimensions of wood and wood composites. Further improvements to the system used in Chapter 3, however, would be desirable. The most pressing requirement is to develop a way of enhancing the contrast between latewood, voids and wood so that measurement of voids and micro-checks in OSB and treated wood can be automated.

According to Lötter (2014), and others, many different approaches can be used to reduce the thickness swelling of OSB (Rowell and Banks 1985, Hsu et al. 1990, Del Menezzi 2004, Paridah et al. 2006, Mantanis and Papadopoulos 2010). These approaches include modification to production processes, such as species selection, stranding, drying, blending and press parameters; or thermal modification of either the strands (pre-treatment) or the consolidated boards (post-treatment); chemical treatments of strands before pressing (pre-treatment); and finally the application of surface coatings and water repellents (post-treatment). Surface coatings and water repellents are common treatments used to reduce water absorption, and improve the dimensional stability and checking resistance of solid wood. Their effectiveness was demonstrated in Chapter 3. Water-repellents can be effectively applied to OSB or incorporated in the furnish of flakes during manufacturing (Preston et al. 2008), making it possible to reduce swelling and micro-checking by preventing water from being absorbed by wood cell walls. On the other hand the irregular surface of OSB makes it difficult to achieve a continuous film with typical surface coatings (Semple et al. 2009), and uncoated voids at panel surfaces may provide pathways for moisture ingress into the composite (Feist 1982, Evans and Cullis 2008). Based on my findings in Chapter 3 with solid wood, which showed that a water repellent reduced the micro-checking of solid pine and aspen wood, and also that micro-checks developed in OSB during wetting, I suggest that treatments of green flakes with water-repellent chemicals will reduce micro-checking of OSB. It might also reduce the irreversible thickness swelling of OSB. My results also suggest that the irreversible thickness swelling of OSB could be reduced by manufacturing boards entirely from aspen rather than a mix of aspen and pine. Further research would be needed to test this hypothesis and also examine whether thickness swelling of OSB could be reduced by manufacturing boards from other wood species that are less susceptible to checking.

In addition, future research should also examine the thickness swelling and micro-checking of OSB and solid wood exposed to multiple wetting and drying

cycles, or cycles with different durations. The system I used in Chapter 3 could be deployed in combination with digital image correlation (DIC) techniques to obtain strain maps of the surface of samples, to better understanding the relationship between surface strains and checking of treated wood and OSB. The imaging system could also be used to analyze the influence of vertical density profile in OSB on thickness swelling.

### **5.3 Conclusions**

Significant micro-checking of flakes in OSB subjected to wetting and drying was visualized for the first time. Checks developed and/or enlarged during wetting as a result of inter and intra cell wall fractures, possibly contributing to irreversible thickness swelling of OSB. Micro-checks show similarities with those that develop in solid wood exposed to wetting and drying suggesting that treatments designed to reduce checking of solid wood i.e. water-repellents, may be useful at reducing micro-checking and possibly thickness swelling of OSB. Tools developed or used in this study to examine microstructure of OSB subjected to wetting and drying have great potential to be used to examine other important aspects of the structure, properties and performance of wood composites.

## Bibliography

- Akrami, A., Barbu, M.C., Frühwald, A. (2014). European hardwoods for reducing dependence on pine for oriented strand board. *International Wood Products Journal*, 5(3), 133-135.
- Alberta Research Council (1990). Mixed species; summary report. Edmonton, AB: Canadian Forest Service and Alberta Forest Service.
- Ambrose, J., Hounsfield, G.N. (1973). Computerized transverse axial tomography. *The British Journal of Radiology*, 46(552), 148-149.
- Amann, F., Ündül, Ö., Kaiser, P.K. (2014). Crack initiation and crack propagation in heterogeneous sulfate-rich clay rocks. *Rock Mechanics and Rock Engineering*, 47(5), 1849-1865.
- APA (2016). Engineered Wood Statistics, First Quarter. Tacoma, WA: APA - The Engineered Wood Association. 9 p. Retrieved May 27, 106 from: <http://www.apawood.org/Data/Sites/1/documents/membersonly/marketstatistics/2016/Qtr1-16.pdf>.
- Aston, R. (1993). Balsam poplar/cottonwood as a furnish material for the manufacture of oriented strand board. *Forintek Canada Corp.*
- Au, K.C., Gertjeansen, R.O., Larntz, K. (1992). Use of response surface methodology to maximize paper birch utilization in a three-layer, two-species oriented strandboard. *Wood and Fiber Science*, 24(4), 432-441.
- Avramidis, S., Smith, L.A. (1989). The effect of resin content and face-to-core ratio on some properties of oriented strand board. *Holzforschung*, 43(2), 131-133.
- Baileys, J.K., Marks, B.M., Ross, A.S., Crawford, D.M. (2003). Providing moisture and fungal protection to wood-based composites. *Forest Products Journal*, 53(1), 76-81.
- Banhart, J. (2008). *Advanced tomographic methods in materials research and engineering* (Vol. 66). New York, Oxford University Press.
- Barbuta, C., Blanchet, P., Cloutier, A., Yadama, V., Lowell, E. (2012). OSB as substrate for engineered wood flooring. *European Journal of Wood and Wood Products*, 70(1-3), 37-43.
- Beer, D.C. (1982). Flaking high density species for structural board. In: *Proceedings of the 16<sup>th</sup> Annual International Particleboard Symposium* (pp. 135-160). Pullman, WA: Washington State University.
- Belford, D.S., Nicholson, J. (1969). Emulsion additives for CCA preservatives to control weathering. In: *Proceedings of the 65<sup>th</sup> Annual Meeting of the American Wood Preservers' Association* (pp. 38-51).
- Biblis, E.J. (1985). Properties of three-layer oriented strandboard from Southern hardwoods. *Forest Products Journal*, 35(2), 28-32.
- Biblis, E.J. (1989). Properties of commercial OSB from three Southern pine mills. *Forest Products Journal*, 39(1), 55-57.
- Biziks, V., Van den Bulcke, J., Grinins, J., Militz, H., Andersons, B., Andersone, I., Dhaene, J., Van Acker, J. (2016). Assessment of wood microstructural changes after one-stage thermo-hydro treatment (THT) by micro X-ray computed tomography. *Holzforschung*, 70(2), 167-177.

- Booker, R.E., Haslett, A., Sole, J. (2000). Acoustic emission study of within-ring internal checking in radiata pine. In: *Proceedings of the 12<sup>th</sup> International Symposium on Nondestructive Testing of Wood* (pp.13-15). Sopron, Hungary: University of Western Hungary.
- Borgin, K. (1961). The effect of water repellents on the dimensional stability of wood. *Norsk Skogind*, 15(11), 507-521.
- Borgin, K. (1971a). The cohesive failure of wood studied with the scanning electron microscope. *Journal of Microscopy*, 94(1), 1-11.
- Borgin, K. (1971b). The mechanism of the breakdown of the structure of wood due to environmental factors. *Journal of the Institute of Wood Science*, 5(4), 26-30.
- Brochmann, J., Edwardson, C., Shmulsky, R. (2004). Influence of resin type and flake thickness on properties of OSB. *Forest Products Journal*, 54(3), 51-55.
- Brunette, G. (1991). Properties of waferboard/OSB manufactured from alternate and/or mixed species; a literature review. Ottawa, ON: Canadian Forest Service and Forintek Canada Corp.
- Brunette, G. (1993). Strandboard from mixed species. Ottawa, ON: Canadian Forest Service and Forintek Canada Corp.
- Buades, A., Coll, B., Morel, J.M. (2005). A non-local algorithm for image denoising. In: *IEEE Computer Society Conference on Computer Vision and Pattern Recognition (CVPR'05)* (Vol. 2, pp. 60-65).
- Bucur, V. (ed) (2011). *Delamination in wood, wood products and wood-based composites*. Springer, Berlin.
- Canadido, L.S., Saito, F., Suzuki, S. (1990). Influence of strand thickness and board density on the orthotropic properties of oriented strandboard. *Mokuzai Gakkaish*, 36(8), 632-636.
- Carl Zeiss International (n.d.). Field emission scanning electron microscopy. Retrieved June 18, 2016 from: [http://www.zeiss.com/microscopy/en\\_us/products/scanning-electron-microscopes.html](http://www.zeiss.com/microscopy/en_us/products/scanning-electron-microscopes.html).
- Carll, C., Wiedenhoef, A.C. (2009). Moisture-related properties of wood and the effects of moisture on wood and wood products. In: H.R. Trechsel, M.T. Bomberg (Eds.), *Moisture control in buildings: the key factor in mold preventions* (2<sup>nd</sup>ed., pp. 54-79). West Conshohocken, PA: American Society for Testing and Materials.
- Chen, P.Y.S., Workman Jr, E.C. (1980). Effect of steaming on some physical and chemical properties of black walnut heartwood. Part 1: Steam pretreatment. *Wood and Fiber Science*, 11(4), 218-227.
- Cheng, K.J. (2015). *Reducing the surface checking of deck-boards exposed to natural weathering: effects of wood species and surface profiling*. (Master of Science Honours Thesis). University of British Columbia, Vancouver, B.C., Canada. Retrieved May 13, 2016 from: <http://hdl.handle.net/2429/52828/>.
- Christy, A.G., Senden, T.J., Evans, P.D. (2005). Automated measurement of checks at wood surfaces. *Measurement*, 37(2), 109-118.
- Cloutier, A. (1998). Oriented strandboard (OSB): raw material, manufacturing process, properties of wood-based fiber and particle materials. In: *Proceedings of the 1<sup>st</sup> International Seminar on High Technology Solid Wood Products* (pp. 173-185). Belo Horizonte, Brazil: Universidade Federal de Viçosa.

- Cnudde, V., Boone, M.N. (2013). High-resolution X-ray computed tomography in geosciences: A review of the current technology and applications. *Earth-Science Reviews*, 123(2013), 1-17.
- Côté, W.A., Hanna, R.B. (1983). Ultrasound characteristics of wood fracture surfaces. *Wood and Fiber Science*, 15:135-163.
- Coupe, C., Watson, R.W. (1967). Fundamental aspects of weathering. In: *Record of the 17<sup>th</sup> Annual Convention of the British Wood Preservers' Association* (pp. 37-49).
- Cox, S.F., Etheridge, M.A. (1989). Coupled grain-scale dilatancy and mass transfer during deformation at high fluid pressures: examples from Mount Lyell, Tasmania. *Journal of Structural Geology*, 11(1/2), 147-162.
- Davis, J., Wells, P. (1992). Computed tomography measurements on wood. *Industrial Metrology*, 2(3-4), 195-218.
- Del Menezzi, C.H.S. (2004). *Estabilização dimensional por meio do tratamento térmico e seus efeitos sobre as propriedades de painéis de partículas orientadas (OSB)*. (Doctor of Philosophy in Forest Sciences Dissertation). Federal University of Paraná, Curitiba, Brazil.
- Deskey, D., inventor, United States Plywood Corporation, assignee. (1942). Plywood panel. *United States Patent US 2,286,068*.
- Donaldson, L.A. (1995). Cell wall fracture properties in relation to lignin distribution and cell dimensions among three genetic groups of radiata pine. *Wood Science and Technology*, 29(1), 51-63.
- Donaldson, L.A. (1997). Ultrastructure of transwall fracture surfaces in radiata pine wood using transmission electron microscopy and digital image processing. *Holzforschung*, 51(4), 303-308.
- Donaldson, L. (2010). Delamination of wood at the microscopic scale: current knowledge and methods. In: *Delamination in wood, wood products and wood-based composites* (pp. 123-144). Springer Netherlands.
- Donaldson, L., Bardage, S., Daniel, G. (2007). Three-dimensional imaging of a sawn surface: a comparison of confocal microscopy, scanning electron microscopy, and light microscopy combined with serial sectioning. *Wood Science and Technology*, 41(7), 551-564.
- Donaldson, L., Frankland, A. (2004). Ultrastructure of iodine treated wood. *Holzforschung*, 58(3), 219-225.
- Eckert, J.R., Edwardson, C.F. (1998). The development of an optimal wax emulsion for oriented strandboard. In: *Proceedings of the 32<sup>nd</sup> International Particleboard/Composite Materials Symposium* (pp. 135-142). Pullman, WA: Washington State University.
- Einspahr, D.W., Wyckoff, G.W. (1990). North American aspen: Timber supply, utilization, and research. *Northern Journal of Applied Forestry*, 7(4), 168-171.
- Elmendorf, A. (1950). Plywood panel. *United States Patent US 2,514,318*.
- EN (2006). BS EN 300:2006. Oriented strand board (OSB): Definitions, classification and specifications. Brussels, Belgium: European Committee of Standardization.
- Evans, P.D., Cullis, I. (2008). Effect of sanding and coating with UV-cured finishes on the surface roughness, dimensional stability and fire resistance of oriented strandboard. *Holz als Roh-und Werkstoff*, 66(3), 191-199.

- Evans, P.D., Urban, K., Chowdhury, M.J.A. (2008). Surface checking of wood is increased by photodegradation caused by ultraviolet and visible light. *Wood Science and Technology*, 42(3), 251-265.
- Evans, P.D., Morrison, O., Senden, T.J., Vollmer, S., Roberts, R., Limaye, A., Arns, C.H., Averdunk, H., Lowe, A., Knackstedt, M.A. (2010). Visualization & numerical analysis of adhesive distribution in particleboard using X-ray micro-computed tomography Elsevier International. *Journal of Adhesion and Adhesives* 30(8), 754-762.
- Evans, P.D., Lube, V., Averdunk, H., Limaye, A., Turner, M., Kingston, A., Senden, T.J. (2015a). Visualizing the micro-distribution of zinc borate in oriented strand board using X-ray micro-computed tomography and SEM-EDX. *Journal of Composites*, ID 630905, doi:10.1155/2015/630905.
- Evans P.D., Morrison, O., Averdunk, H., Turner, M., Limaye, A., Arns, C.H., Lube, V., Vollmer, S., Roberts, R., Kingston, A., Knackstedt, M.A., Senden, T.J. (2015b). Probing the structure of particulate wood composites using x-ray microcomputed tomography. In: *Proceedings of the International Panel Products Symposium* (pp. 3-16), Llundudno, Wales.
- Febrianto, F., Hidayat, W., Samosir, T.P., Lin, H.C., Soong, H.D. (2010). Effect of strand combination on dimensional stability and mechanical properties of oriented strand board made from tropical fast growing tree species. *Journal of Biological Sciences*, 10(3), 267-272.
- Feldkamp, L.A., Davis, L.C., Kress, J.W. (1984). Practical cone-beam algorithm. *Journal of the Optical Society of America A: Optics, Image Science, and Vision*. 1(6), 612-619.
- Feng, M.W., Knudson, R.M. (2007). Effect of log rehydration on quality of OSB strands manufactured from beetle-killed lodgepole pine. *Forest Products Journal*, 57(1/2), 35-42.
- Fischer, K. (1972). Modern flaking and particle reductionizing. In: *Proceedings of the 6<sup>th</sup> International Particleboard Symposium* (pp. 195-213). Pullman, WA: Washington State University.
- Flæte, P.O., Høibø, O.A., Fjærtoft, F., Nilsen, T.N. (2000). Crack formation in unfinished siding of aspen (*Populus tremula* L.) and Norway spruce (*Picea abies* (L.) Karst.) during accelerated weathering. *Holz als Roh-und Werkstoff*, 58(3), 135-139.
- Forintek Canada Corp. (1998). Wood-based panel products: special report. Sainte-Foy, QC: Industry Canada.
- Fowlie, D.A., Preston, A.F., Zahora, A.R. (1990). Additives: an example of their influences on the performance and properties of CCA-treated southern pine. *Proceedings of the 86<sup>th</sup> Annual Meeting of the American Wood-Preservers' Association* (pp. 11-21).
- Fromm, J.H., Sautter, I., Matthies, D., Kremer, J., Schumacher, P., Ganter, C. (2001). Xylem water content and wood density in spruce and oak trees detected by high-resolution computed tomography. *Plant Physiology*, 127(2), 416-425.
- Frühmann, K., Burgert, I., Stanzl-Tschegg, S.E., Tschegg, E.K. (2003). Mode I fracture behaviour on the growth ring scale and cellular level of spruce (*Picea abies* [L.] Karst.) and beech (*Fagus sylvatica* L.) loaded in the TR crack propagation system. *Holzforschung*, 57(6), 653-660.
- Funt, B.V., Bryant, E.C. (1987). Detection of internal log defects by automatic interpretation of computer tomography images. *Forest Products Journal*, 37(1), 56-62.
- Galbraith, C.J., Cohen, S.C., Ball, G.W. (1983). Self-releasing emulsifiable MDI isocyanate: An easy approach for all-isocyanate bonded boards. In: *Proceedings of the 17<sup>th</sup> International Particleboard/Composite Symposium* (pp. 263-282). Pullman, WA: Washington State University.



- Gargiulo, L., Mele, G., Terribile, F. (2015). The role of rock fragments in crack and soil structure development: a laboratory experiment with a Vertisol. *European Journal of Soil Science*, 66(4), 757-766.
- Geimer, R.L. (1976). Flake alignment in particleboard as affected by machine variables and particle geometry. *Research Paper FPL 275. USDA Forest Service, Forest Products Laboratory, Madison, Wisconsin*.
- Geimer, R.L. (1982). Dimensional stability of flakeboards as affected by board specific gravity and flake alignment. *Forest Products Journal*, 32(8), 44-52.
- Geimer, R.L., Mahoney, R.J., Loehnertz, S.P., Meyer, R.W. (1985). Influence of processing-induced damage on strength of flakes and flakeboards. *Research Paper FPL 463. USDA Forest Service, Forest Products Laboratory, Madison, Wisconsin*.
- Generalla, N.C., Biblis, E.J., Carino, H.F. (1989). Effect of two resin levels on the properties of commercial Southern OSB. *Forest Products Journal*, 39(6), 64-68.
- Glass, S.V., Zelinka, S.L. (2010). Chapter 4: Moisture relations and physical properties of wood. In: *Wood Handbook, Wood as an Engineering Material: USDA General Technical Report FPL-GTR-190* (Centennial ed., pp. 1-19). Madison, WI: Forest Service, Forest Products Laboratory.
- Gnatowski, M.J., Mah, C.L., Merrick, G.P. (2010). Methods for determining organic biocide concentration in a composite wood product. *United States Patent US 7,785,896*.
- Gomez-Bueso, J., Haupt, R. (2010). Wood composite adhesives. In: L. Pilato (Ed.), *Phenolic resins: A century of progress* (pp. 155-187). Heidelberg, Germany: Springer.
- Goroyias, G.J., Hale, M.D. (2002). Heat treatment of wood strands for OSB production: effect on the mechanical properties, water absorption and dimensional stability. *The International Research Group on Wood Preservation, IRG/WP/02-4023*.
- Grant, D.R. (1995). A literature review of alternate species in oriented strand board and waferboard. Edmonton, AB: Canadian Forest Service, Land and Forest Service. Retrieved May 16, 2016 from: [http://www.cfs.nrcan.gc.ca/bookstore\\_pdfs/21260.pdf](http://www.cfs.nrcan.gc.ca/bookstore_pdfs/21260.pdf).
- Grigoriou, A.H., Biblis, E.I. (1995). Performance of two overlays and two coating materials for oriented strand board substrates after 21 days continuous water spraying. *Holzforschung und Holzverwertung*, 47(4), 72-73.
- Grossman, L.M. (1992). Expanding your OSB market with protective coatings. In: *Proceedings of the 26<sup>th</sup> International Particleboard/Composite Materials Symposium* (pp. 227-235). Pullman, WA: Washington State University.
- Halligan, A.F. (1970). A review of thickness swelling in particleboard. *Wood Science and Technology*, 4(4), 301-312.
- Han, G., Cheng, W., Manning, M., Eloy, P. (2012). Performance of zinc borate-treated oriented structural straw board against mold fungi, decay fungi and termites-a preliminary trial. *BioResources*, 7(3), 2986-2995.
- Hanhijärvi, A., Wahl, P., Räsänen, J., Silvennoinen, R. (2003). Observation of development of microcracks on wood surface caused by drying stresses. *Holzforschung*, 57(5), 561-565.
- Hatae, F., Kataoka, Y., Kiguchi, M., Matsunaga, H., Matsumura, J. (2012). Use of variable pressure scanning electron microscopy for in situ observation of degradation of wood surfaces during artificial weathering. *International Research Group on Wood Protection, IRG/WP/12-20489*.

- Haygreen, J.G., Bowyer, J.L. (1996). *Forest products and wood science: an introduction*, 3<sup>rd</sup> Ed. The IOWA State University Press. Ames, IA.
- Haygreen, J.G., Gertjeansen, R.O. (1971). Improving the properties of particleboard by treating the particles with phenolic impregnating resin. *Wood and Fiber Science*, 3(2), 95-105.
- He, W., Xiaoxiang, L., Yukun, H. (2000). Study on waterproof performance of paint coated OSB. *China-Wood-Industry*, 14(6), 28-29.
- Hill, C.A.S., Mallon, S. (1998). The chemical modification of Scots pine with succinic anhydride or octenyl succinic anhydride. I. Dimensional stabilisation. *Holzforschung*, 52(4), 427-433.
- Hounsfield, G.N. (1973). Computerized transverse axial scanning (tomography): Part 1. Description of system. *The British Journal of Radiology*, 46(552), 1016-1022.
- Hsu, O.H., Bender, H.S. (1988). Water repellent efficacy of wax used in hardboard. *Industrial and Engineering Chemistry Research*, 27(7), 1296-1300.
- Hsu, W.E., Melanson, R.J., Kozak, P.J., Maloney, T.M. (1990). The effect of wax type and content on waferboard properties. In: *Proceedings of the 24<sup>th</sup> International Particleboard/Composite Materials Symposium* (pp. 85-93). Pullman, WA: Washington State University.
- Hsu, W.E., Schwald, W., Schwald, J., Shields, J. A. (1988). Chemical and physical changes required for producing dimensionally stable wood-based composites, Part 1: Steam pretreatment. *Wood Science and Technology*, 22(3), 281-289.
- Hsu, W.E., Schwald, W., Shields, J.A. (1989). Chemical and physical changes required for producing dimensionally stable wood-based composites, Part 2: Heat post-treatment. *Wood Science and Technology*, 23(3), 281-288.
- Irlle, M., Barbu., M.C. (2010). Wood-based panel technology. In: T. Thoemen, M. Irlle, M. Sernek (Eds.), *Wood-Based Panels: An Introduction for Specialists* (pp. 1-94). London, UK: Brunel University Press.
- Irlle, M.A. (2001). Technical Terms: Compaction Ratio. *Wood Based Panels International*, 21(3), 52.
- Iwakiri, S., Mendes, L.M., Saldanha, L.K. (2002). Production of oriented strand board (OSB) from *Eucalyptus grandis* with different resin content, wax sizing and face to core layer ratios. *Ciência Florestal*, 13(1), 89-94.
- Janssens, D.P. (1998). The increasing recognition of oriented strandboard (OSB) as preferred structural panel. In: *Proceedings of the 1<sup>st</sup> International Seminar on High Technology Solid Wood Products* (pp. 169-172). Belo Horizonte, Brazil: Universidade Federal de Viçosa.
- Kain, G., Lienbacher, B., Barbu, M. C., Plank, B., Richter, K., Petutschnigg, A. (2016). Evaluation of relationships between particle orientation and thermal conductivity in bark insulation board by means of CT and discrete modeling. *Case Studies in Nondestructive Testing and Evaluation*. Retrieved October 25, 2016 from: <http://dx.doi.org/10.1016/j.csndt.2016.03.002>.
- Kamke, F.A., Lee, J.N. (2007). Adhesive penetration in wood-a review. *Wood and Fiber Science*, 39(2), 205-220.
- Kelly, M.W. (1977). Critical literature review of relationships between processing parameters and physical properties of particleboard. *USDA General Technical Report FPL-10*. Madison, WI: Forest Service, Forest Products Laboratory.

- Kirkpatrick, J.W., Barnes, H.M. (2006). Biocide treatments for wood composites-a review. *The International Research Group on Wood Protection, IRG/WP/06-40323*.
- Kline, D.E. (2005). Gate-to-gate life-cycle inventory of oriented strandboard production. *Wood and Fiber Science* 37 (CORRIM Special Issue), 74-84.
- Koch, P. (1976). Prototype flaking head smooths surfaces left by headrig or edger chipping heads. *Forest Products Journal*, 26(12), 22-27.
- Konnerth, J., Gindl, W. (2006). Mechanical characterisation of wood-adhesive interphase cell walls by nanoindentation. *Holzforschung*, 60(4), 429-433.
- Kretschmann K.E. (2010). Chapter 5: Mechanical properties of wood. In: *Wood Handbook, Wood as an Engineering Material: USDA General Technical Report FPL-GTR-190* (Centennial ed., pp. 1-46). Madison, WI: Forest Service, Forest Products Laboratory.
- Kučera, L.J., Bariska, M. (1982). On the fracture morphology in wood. *Wood Science and Technology*, 16(4), 241-259.
- Lau, K., Kagan, A., McDonald, R., Macey, T., Gendi, R., Lam, F. (2006). Innovative methods for moisture conditioning mountain pine beetle logs for OSB production. Forestry Innovation Investment Ltd. Retrieved September 13, 2016 from: <https://www.for.gov.bc.ca/hfd/library/documents/bib106708Report.pdf>.
- Lee, S.Y., Wu, Q. (2007). Leachability of zinc borate-modified oriented strandboard (OSB). *Mokchae Konghak*, 35(5), 46-57.
- Lehmann, W.F. (1972). Moisture-stability relationships in wood-base composition boards. *Forest Products Journal*, 22(7), 53-59.
- Lenth, C.A., Kamke, F.A. (1996). Investigations of flakeboard mat consolidation. Part I. Characterizing the cellular structure. *Wood and Fiber Science*, 28(2), 153-167.
- Levi, M.P., Coupe, C., Nicholson, J. (1970). Distribution and effectiveness in *Pinus* sp. of a water repellent additive for water-borne wood preservatives. *Forest Products Journal*, 20(11), 32-37.
- Li, P., Tao, Y., Wang, F. (2010). Research on macrovoids of bio-based strand composites using image processing technology. *Journal of Information and Computational Science*, 7(4), 1007-1012.
- Limaye, A. (2012). Drishti: a volume exploration and presentation tool. Proc. SPIE 8506, Developments in X-Ray Tomography VIII, 85060X.
- Lloyd, R.H. (1984). *Investigations of thickness swelling in cement particleboards* (Bachelor of Science Thesis). University of Wales, Bangor, UK.
- Lötter, B.T. (2014). *Molten wax spray treatment makes oriented strandboard (OSB) more water repellent and reduces thickness swelling*. (Master of Science Honours Thesis). University of British Columbia, Vancouver, B.C., Canada. Retrieved October 10, 2016 from: <http://hdl.handle.net/2429/46523/>.
- Mackes, K.H., Lynch, D.L. (2001). The effect of aspen wood characteristics and properties on utilization. *USDA Forest Service Proceedings RMRS-P-18* (pp. 429-440).
- Maire, E. (2012). X-ray tomography applied to the characterization of highly porous materials. *Annual Review of Materials Research*, 42(7.1), 163-178.

- Maire, E., Withers, P.J. (2014). Quantitative X-ray tomography. *International Materials Reviews*, 59(1), 1-43.
- Maloney, T.M. (1977). *Modern particleboard and dry-process fiberboard manufacturing*. USA: Miller Freeman Publication (pp. 95-105).
- Maloney, T.M. (1993). *Modern particleboard and dry-process fiberboard manufacturing*. San Francisco, CA: Miller Freeman.
- Mantanis, G.I., Papadopoulos, A.N. (2010). Reducing the thickness swelling of wood based panels by applying a nanotechnology compound. *European Journal of Wood and Wood Products*, 68(2), 237-239.
- Marra, A.A. (1992). *Technology of wood bonding: Principles in practice*. New York: Van Nostrand Reinhold (pp. 76-80).
- McIntyre, C.R., Fox, R.F. (1990). Update on Wolman ET™. A new CCA/oil treating system. In: *Proceedings Eighty-Sixth Annual Meeting of the American Wood-Preservers' Association* (pp. 63-77).
- McKay, T.J. (2015). *Tomography, scanning electron microscopy techniques and image analysis of coal for natural gas recovery*. (Master of Engineering Thesis). The Australian National University, Canberra, Australia.
- McNatt, J.D., Bach, L., Wellwood, R.W. (1992). Contribution of flake alignment to performance of strandboard. *Forest Products Journal*, 42(3), 45-50.
- Morén, T.J. (1994). Heating and conditioning by steaming during low temperature drying. In: *Proceedings of the 4<sup>th</sup> International IUFRO Wood Drying Conference* (pp. 341-348), Rotorua, New Zealand.
- Morrison, O. (2004). *Resin distribution in particleboard*. (Bachelor of Engineering Honours Thesis). The Australian National University, Canberra, Australia.
- Morrison-Knudsen Forest Products. (1987). *Ring flaked maxi-chips: the manufacture, testing and evaluation of composite board made from Alberta woods*. Edmonton, AL: Canadian Forest Service and Alberta Forest Service.
- Moslemi, A.A., (1974a). Particleboard vol. I. *Materials*. Southern Illinois University Press, London-Amsterdam. 244p.
- Moslemi, A.A., (1974b). Particleboard vol. II. *Technology*. Southern Illinois University Press, London-Amsterdam. 245p.
- Moya, L., Winandy, J.E., Tze, W.T., Ramaswamy, S. (2008). Use of fire-impacted trees for oriented strandboards. *Forest Products Journal*, 58(6), 45-52.
- Muszyński, L., Launey, M.E. (2010). Advanced imaging techniques in wood-based panels research. In: *Wood-Based Panels - An Introduction for Specialists. State-of-the-Art in Wood-Based Panels Research*. COST Action E, 49,177-201.
- Neusser, H., Krames, U., Haidinger, K. (1965). Das verhalten von spanplatten gegenüber feuchtigkeit unter besonderer berücksichtigung der quellung. *Holzforschung und Holzverwertung*, 17(3), 43-69.
- Niemz, P. (2002). Thermisch vergütetes Fichtenholz. *Holzforschung Schweiz*, 1, (pp. 28-29).

- NIST (2004). Voluntary product standard PS 2-04: Performance standard for wood-based structural-use panels. Gaithersburg, MD: U.S. Department of Commerce, National Institute of Standards and Technology.
- Ondro, W.J. (1989). *Utilization and Market Potential of Poplar in Alberta*; Northern Forestry Centre, Forestry Canada: Edmonton, Canada, (pp. 271-274).
- Panshin, A.J., De Zeeuw, C. (1980). Textbook of Wood Technology: Structure, Identification, Properties, and Uses of the Commercial Woods of the United States and Canada. 4<sup>th</sup> Ed., New York: McGraw-Hill.
- Panshin, A.J., De Zeeuw, C., Brown, H.P. (1964). Textbook of Wood Technology. Vol. I - Structure, Identification, Uses, and Properties of the Commercial Woods of the United States, Vol. I, 2<sup>nd</sup> Ed., New York: McGraw-Hill.
- Paridah, M.T., Ong, L.L., Zaidon, A., Rahim, S., Anwar, U.M.K. (2006). Improving the dimensional stability of multilayered strand board through resin impregnation. *Journal of Tropical Forest Science*, 18(3), 166-172.
- Pecho, R., Ananias, R.A., Ballerini, A., Cloutier, A. (2005). Influencia de la madera juvenil de pino radiata sobre las propiedades físicas y mecánicas de tableros OSB. *Bosque (Valdivia)*, 26(1), 123-132.
- Plinke, B., Aderhold, J., Berthold, D. (2010). Increase of material yield in Plywood Production with new Veneer Processing Technologies. In: *1<sup>st</sup> International Conference on Processing Technologies for the Forest and Biobased Products Industries* (pp. 21-27). Kuchl, Austria: Salzburg University of Applied Sciences.
- Preston, A.F., Fowlie, D.A., Archer, K. J. (2008). Methods of incorporating treatment agents into wood based composite products. *United States Patent US 7,371,787*.
- Pugel, A.D., Price, E.W., Hse, C.Y. (1990). Composites from southern pine juvenile wood. Part 2. Durability and dimensional stability. *Forest Products Journal*. 4(3), 57-61.
- Putoczki, T.L., Nair, H., Butterfield, B., Jackson, S.L. (2007). Intra-ring checking in *Pinus radiata* D. Don: the occurrence of cell wall fracture, cell collapse, and lignin distribution. *Trees*, 21(2), 221-229.
- Ratu, R.N. (2009). *Development and testing of a weathermometer to accelerate the checking of wood*. (Master of Science Thesis). University of British Columbia, Vancouver, B.C., Canada. Retrieved July 20, 2016 from: <http://hdl.handle.net/2429/7213>.
- Reed, S. (2005). *Electron microprobe analysis and scanning electron microscopy in geology*, 2<sup>nd</sup> Ed., New York, Cambridge University Press.
- Roffael, E., Rauch, W. (1973). Einfluß von Temperatur und thermischer Nachbehandlung auf einige physikalische Eigenschaften von diisocyanat-gebundenen spanplatten. *Holz als Roh-und Werkstoff*, 31(10), 402-405.
- Rowell, R.M., Banks, W.B. (1985). Water repellency and dimensional stability of wood. *USDA Research Note FPL-50*. Madison, WI: Forest Service, Forest Products Laboratory.
- Rowell, R.M., Tillman, A.M., Simonson, R. (1986). A simplified procedure for the acetylation of hardwood and softwood flaxes for flakeboard production. *Journal of Wood Chemistry and Technology*, 6(3), 427-448.
- Rowell, R.M., Youngs, R.L. (1981). Dimensional stabilization of wood in use. *USDA Research Note FPL-0243*. Madison, WI: Forest Service, Forest Products Laboratory.

- Ruddick, J.N.R., Ross, N.A. (1979) Effect of kerfing on checking of untreated Douglas-fir pole sections. *Forest Products Journal*, 29(9), 27-30.
- Sakagami, H., Hatae, F., Yamamoto, H., Kijidani, Y., Matsumura, J. (2013). Microcrack propagation in red and black heartwoods of *Cryptomeria japonica* during drying. *BioResources*, 8(4), 5983-5994.
- Sakagami, H., Matsumura, J., Oda, K. (2009). In situ visualization of hardwood microcracks occurring during drying. *Journal of Wood Science*, 55(5), 323-328.
- Sakellariou, A., Sawkins, T.J., Senden, T.J., Limaye, A. (2004). X-ray tomography for mesoscale physics applications. *Physica A: Statistical Mechanics and its Applications*, 339(1-2), 145-151.
- Sasaki, H., Kawai, S., Pulido, O.R., Pengprecha, N. (1989). Production of oriented board with an electrostatic field III. Semi-strand board having better orientation toward both surfaces. *Mokuzai Gakkaishi*, 35(8), 725-730.
- Schniewind, A.P. (1963). Mechanism of check formation. *Forest Products Journal*, 13(11), 475-480.
- Shaler, S., Landis, E., Muszynski, L., Vasic, S., Cheng, Q. (2003). Damage assessment in wood-plastic composites by means of material level microstructural characterization. In: *Proceedings of the 7<sup>th</sup> International Conference on Wood Fiber-Plastic Composites* (pp. 151-156).
- Shaler, S.M. (1986). *The usefulness of selected polymer composite theories to predict the elastic moduli of oriented flakeboard*. (Doctor of Philosophy Dissertation). University Park, PA: Pennsylvania State University.
- Shen, K.C. (1974). Improving the surface quality of particleboard by high-temperature pressing. *Forest Products Journal*. 24(10), 36-39.
- Shmulsky, R., Jones, P.D. (2011). *Forest Products and Wood Science*. 6<sup>th</sup> Edition. Malaysia: Wiley-Blackwell.
- Shuler, C.E., Kelly, R.A. (1976). Effect of flake geometry on mechanical properties of eastern spruce flake-type particleboard. *Forest Products Journal*, 26(6), 24-28.
- Singh, A.P., Ratz, A., Dawson, B.S. (2007). A novel method for high-resolution imaging of coating distribution within a rough-textured plywood surface. *Journal of Coatings Technology and Research*, 4(2), 207-210.
- Smook, P. (2011). *Costing the production of OSB using fibre impacted by mountain pine beetle*. (Master of Science Thesis). University of Northern British Columbia, Prince George, B.C., Canada.
- Sobral Filho, M. (1981). Influence of wood furnish type on properties of oriented strand panels. *Forest Products Journal*, 31(9), 43-52.
- Song, D., Ellis, S. (1997). Localized properties in flakeboard: A simulation using stacked flakes. *Wood and Fiber Science*, 29(4), 353-363.
- Spurr, A.R. (1969). A low-viscosity epoxy resin embedding medium for electron microscopy. *Journal of Ultrastructure Research*, 26(1-2), 31-43.
- Standfest, G., Salaberger, D., Plank, B., Petutschnigg, A., Dunky, M. (2010). Sub-micron-CT for the characterization of wood based panels. *Journal Holztechnologie*, 51(4), 44-49.



- Stark, N.M., Cai, Z., Carll, C. (2010). Chapter 11: Wood-based composite materials panel products, glued-laminated timber, structural composite lumber, and wood-nonwood composite materials. In: *Wood Handbook, Wood as an Engineering Material: USDA General Technical Report FPL-GTR-190* (Centennial ed., pp. 1-28). Madison, WI: Forest Service, Forest Products Laboratory.
- Structural Board Association (2005). Binders and waxes in OSB. Technical Bulletin No. TB114. Retrieved July 10, 2016 from: <http://osbguide.tecotested.com/pdfs/en/tb114.pdf>.
- Suchsland, O. (1959). An analysis of the particleboard process. *Quarterly Bulletin. Michigan State University Agricultural Experiment Station*, 42(2), 350-372.
- Suchsland, O. (1962). The density distributions in strand boards. *Quarterly Bulletin. Michigan State University Agricultural Experiment Station*, 45(1), 104-121.
- Suchsland, O. (1973). Hygroscopic thickness swelling and related properties of selected commercial particleboards. *Forest Products Journal*, 23(7), 26-30.
- Suchsland, O., Xu, H. (1991). Model analysis of flakeboard variables. *Forest Products Journal*, 41(11-12), 55-60.
- Sugimori, M., Lam, F. (1999). Macro-void distribution analysis in strand-based wood composites using an X-ray computer tomography technique. *Journal of Wood Science*, 45(3), 254-257.
- Summitt, R., Sliker, A. (1980). CRC handbook of materials science. Vol. 4. Boca Raton, FL: CRC Press, Inc.
- Taylor, A., Wang, S., Freitag, C., Morrell, J.J. (2008). Properties of “enhanced” OSB subfloor panels. *Forest Products Journal*, 58(5), 77-79.
- Taylor, F.W., Wagner, F.G., McMillin, C.W., Morgan, I.L., Hopkins, F.F. (1980a). Locating knots by industrial tomography-A feasibility study. *Forest Products Journal*, 34(5), 42-46.
- Taylor, J.A., Morgan, I.L., Ellinger, H. (1980b). Examination of power poles by computerized tomography. *The International Research Group on Wood Preservation, IRG/WP/2142*.
- Thoemen, H., Irle, M., Šernek, M. (2010). Wood-based panels - an introduction for specialists. *Brunel University Press*, London.
- Thuvander, F., Berglund, L.A. (2000). In situ observations of fracture mechanisms for radial cracks in wood. *Journal of Materials Science*, 35(24), 6277-6283.
- Thuvander, F., Jernkvist, L.O., Gunnars, J. (2000). Influence of repetitive stiffness variation on crack growth behaviour in wood. *Journal of Materials Science*, 35(24), 6259-6266.
- Torgovnikov, G., Vinden, P. (2009). High-intensity microwave wood modification for increasing permeability. *Forest Products Journal*, 59(3), 1-9.
- Tsoumis, G. (1991). Science and technology of wood: structure, properties, utilization (Vol. 115). New York: Van Nostrand Reinhold.
- Turner, H.D. (1954). Effect of particle size and shape on strength and dimensional stability of resin bonded wood-particle panels. *Forest Products Journal*, 4(5), 210-222.

UNECE/FAO (2015). Forest Products Annual Market Review 2014 - 2015. Geneva, Switzerland: United Nations Publications. Retrieved July 20, 2016 from: <http://www.unece.org/fileadmin/DAM/timber/publications/2015-FPAMR-E.pdf>.

Varslot, T., Kingston, A., Myers, G., Sheppard, A. (2011). High-resolution helical cone-beam micro-CT with theoretically-exact reconstruction from experimental data. *Medical Physics*, 38(10), 5459-5476.

Vital, B.R., Wilson, J.B., Kanarek, P.H. (1980). Parameters affecting dimensional stability of flakeboard and particleboard. *Forest Products Journal*, 30(12), 23-29.

Wang, S., Winistorfer, P.M. (2000). The effect of species and species distribution on the layer characteristics of OSB. *Forest Products Journal*, 50(4), 37-44.

Wardrop, A.B. (1951). Cell wall organization and the properties of the xylem. I. Cell wall organization and the variation of breaking load in tension of the xylem in conifer stems. *Australian Journal of Scientific Research*, B-4, 391-414.

Wiemann, M.C. (2010). Chapter 2: Characteristics and availability of commercially important woods. In: *Wood Handbook, Wood as an Engineering Material: USDA General Technical Report FPL-GTR-190* (Centennial ed., pp. 1-45). Madison, WI: Forest Service, Forest Products Laboratory.

Williams, R.S., Swan, L., Sotos, P., Knaebe, M., Feist, W.C. (2005). Performance of finishes on western juniper lumber and particleboard during outdoor exposure. *Forest Products Journal*, 55(11), 65-72.

Winandy, J.E., Kamke, F.A. (2003). Fundamentals of composite processing. In: *Proceedings of a Workshop*. Madison, WI: U.S. Department of Agriculture, Forest Service, Forest Products Laboratory. 118 p.

Winistorfer, P.M., McFarland, D.L., Slover, R.C. (1992). Evaluating the performance of ten wax formulations and three application rates on properties of oriented strand board. In: *Proceedings of the 26<sup>th</sup> International Particleboard/Composite Materials Symposium* (pp. 236-250). Pullman, WA: Washington State University.

Winterowd, J.G., Lewis, C.E., Izan, J.D. Shantz, R.M. (2003). Weyerhaeuser Company. *Edge sealant formulation for wood-based panels*. U.S. Patent 6,608,131.

Witowski, P., Krajewski, A., Narojek, T. (2010). Measurements of wood density using X-ray computer tomography. *Annals of Warsaw Agricultural University*, (72), 485-489.

Wolcott, M.P., Tichy, R.J., Yukun, H., Guo, Z.D. (1997). The development of OSB in the People's Republic of China. *Forest Products Journal*, 47(1), 19-25.

Wu, Q. (1999). In-plane dimensional stability of oriented strand panel: effect of processing variables. *Wood and Fiber Science*, 31(1), 28-40.

Wu, Q., Piao, C. (1999). Thickness swelling and its relationship to internal bond strength loss of commercial oriented strandboard. *Forest Products Journal*, 49(7/8), 50-55.

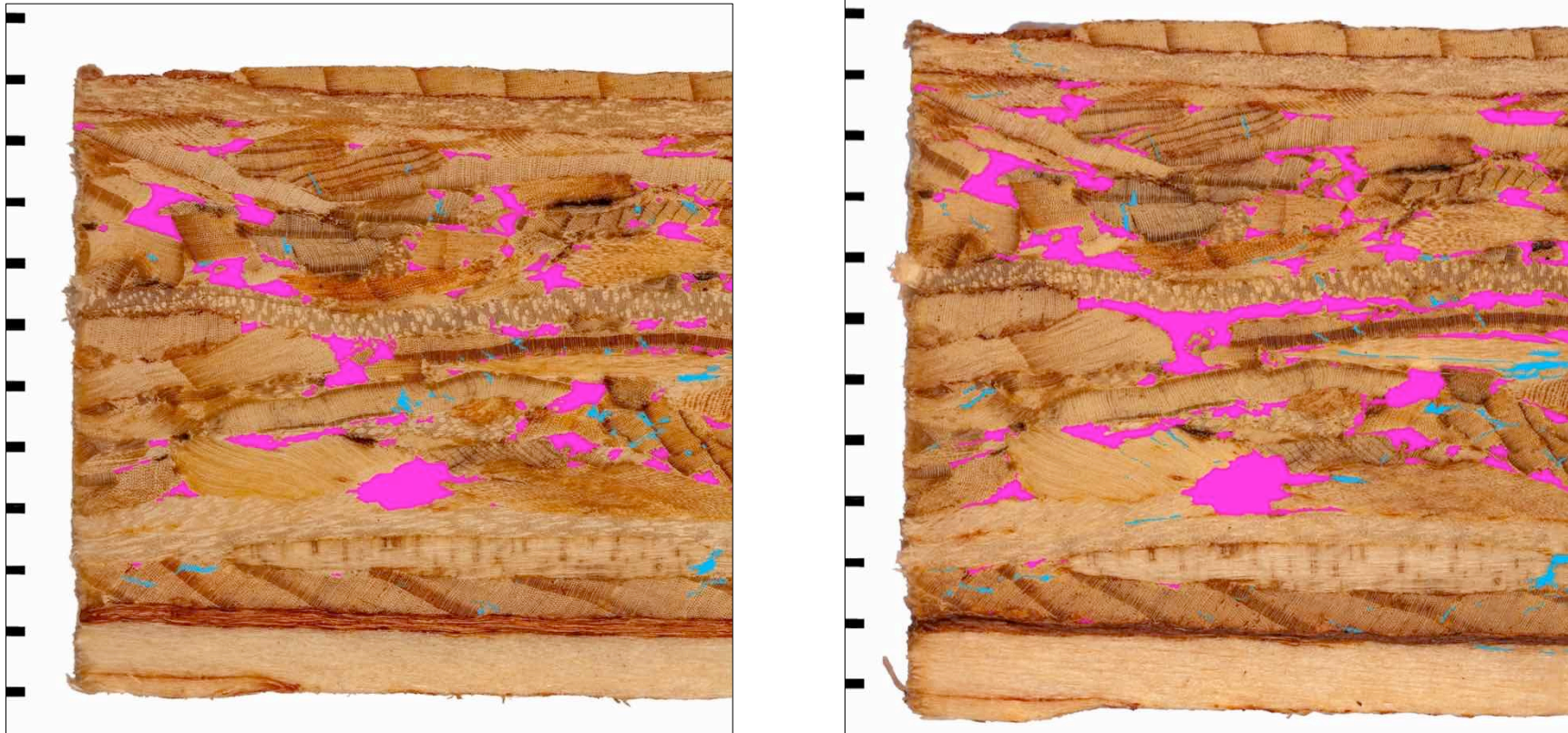
Wu, Q., Suchsland, O. (1997). Effect of moisture on the flexural properties of commercial oriented strandboards. *Wood and Fiber Science*, 29(1), 47-57.

Wu, Q., Zhang, B., Wang, L., Han, G. (2006). The application of 3-D X-ray tomography with finite element analysis for engineering properties of strand based composites. In: *Proceedings of the 8<sup>th</sup> Pacific Rim Bio-based Composites Symposium* (pp. 200-209). Kuala Lumpur, Malaysia.

- Xu, W., Suchsland, O. (2007). Modulus of elasticity of wood composite panels with a uniform vertical density profile: A model. *Wood and Fiber Science*, 30(3), 293-300.
- Yamamoto, H., Sakagami, H., Kijidani, Y., Matsumura, J. (2013). Dependence of microcrack behavior in wood on moisture content during drying. *Advances in Materials Science and Engineering*. ID 802639, doi:10.1155/2013/802639.
- Yusoff, M.N.M., Horie, H. (1997). The manufacture of oriented strand boards from rubberwood. *Journal of Tropical Forest Products*. 3(1), 43-50.
- Zahora, A.R. (2000). Long-term performance of a wax type additive for use with water-borne pressure preservative treatments. *The International Research Group on Wood Preservation, IRG/WP/40159*.
- Zhang, B. (2007). *Digital test of composite material using X-ray tomography and finite element simulation*. (Doctor of Philosophy Dissertation). Blacksburg: Virginia Polytechnic Institute and State University.
- Zhang, B., Wu, Q., Wang, L., Han, G. (2005). Characterization of internal void structure of strand-based wood composites using X-ray tomography and digital tools. In: *Proceedings of the McMat2005: 2005 Joint ASME/ASCE/SES Conference on Mechanics and Materials*, June 1-3, 2005. Eds. Voyiadjis, G.Z. and Dorgan, R.J. American Society of Civil Engineers, Baton Rouge, LA, USA. Paper 257
- Zhang, C., Fujita, M., Takabe, K. (2003). Contact and non-contact proportions between axial elements and rays. *IAWA Journal*, 24(3), 247-255.
- Zhang, M., Wong, E.D., Kawai, S., Kwon, J.H. (1998). Manufacture and properties of high-performance oriented strand board composite using thin strands. *Journal of Wood Science*, 44(3), 191-197.
- Zhou, D. (1989). A study of oriented structural board made from hybrid poplar. Effects of some factors of mechanical forming installation for orientation effectiveness. *Holz als Roh-und Werkstoff*, 47(10), 405-407.
- Zhou, D. (1990). A study of oriented structural board made from hybrid poplar-physical and mechanical properties of OSB.. *Holz als Roh-und Werkstoff*, 48(7-8), 293-296.
- Zsuffa, L.E., Giordano, L.D., Stettler, R.F. (1996). Trends in poplar culture: Some global and regional perspectives. In: *Biology of Populus and Its Implications for Management and Conservation* (pp. 515-539); Stettler, R.F., Bradshaw, H.D., Heilman, P.E., Hinckley, T.M., Eds.; NRC Research.

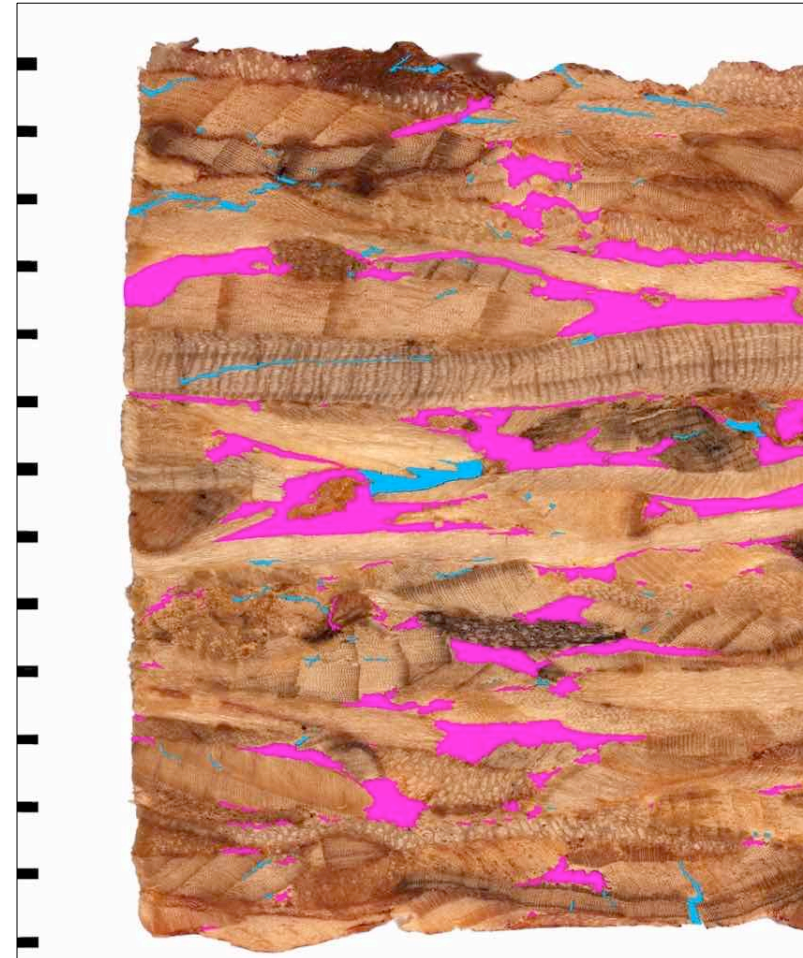
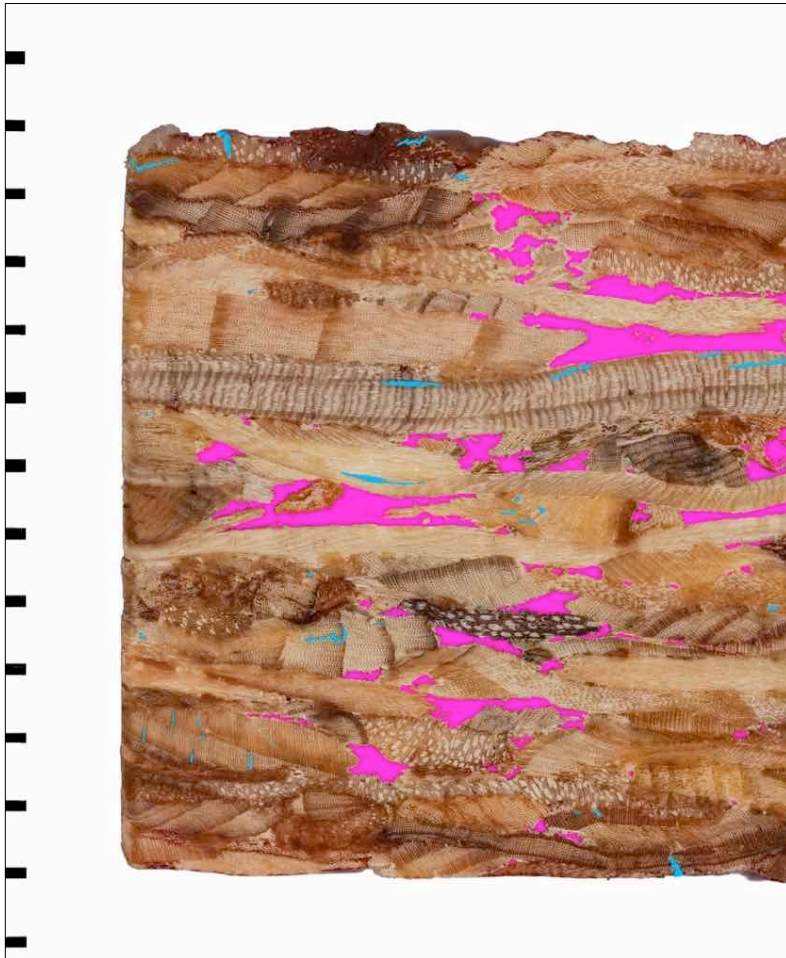
## Appendices

### Appendix 1 - Surface checking and voids of OSB specimens before and after the wetting and drying cycle used in Chapter 3

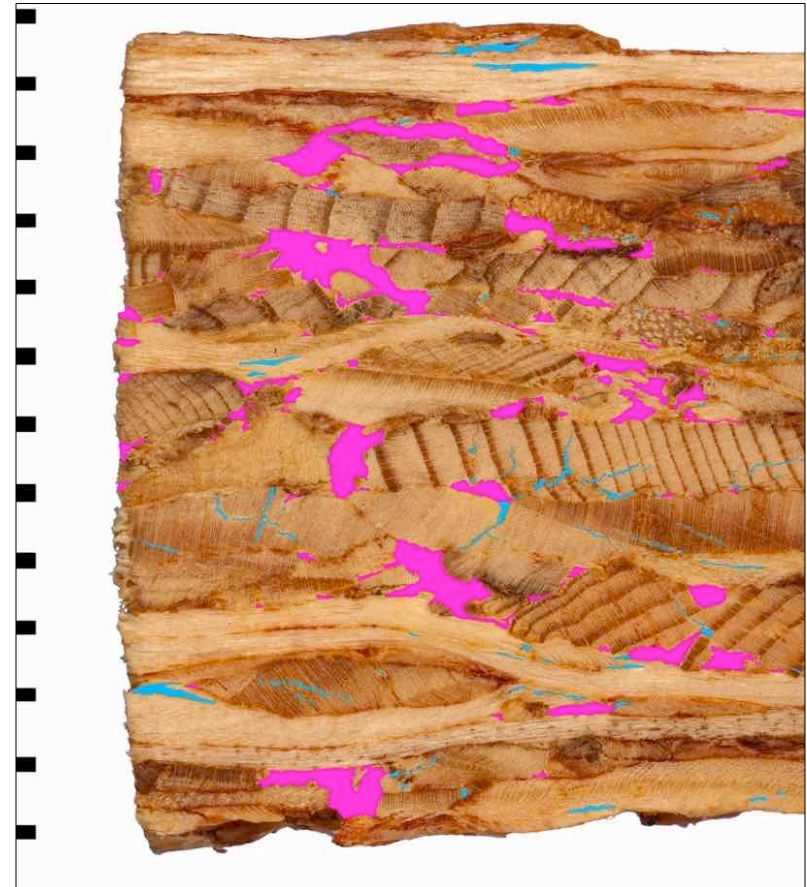
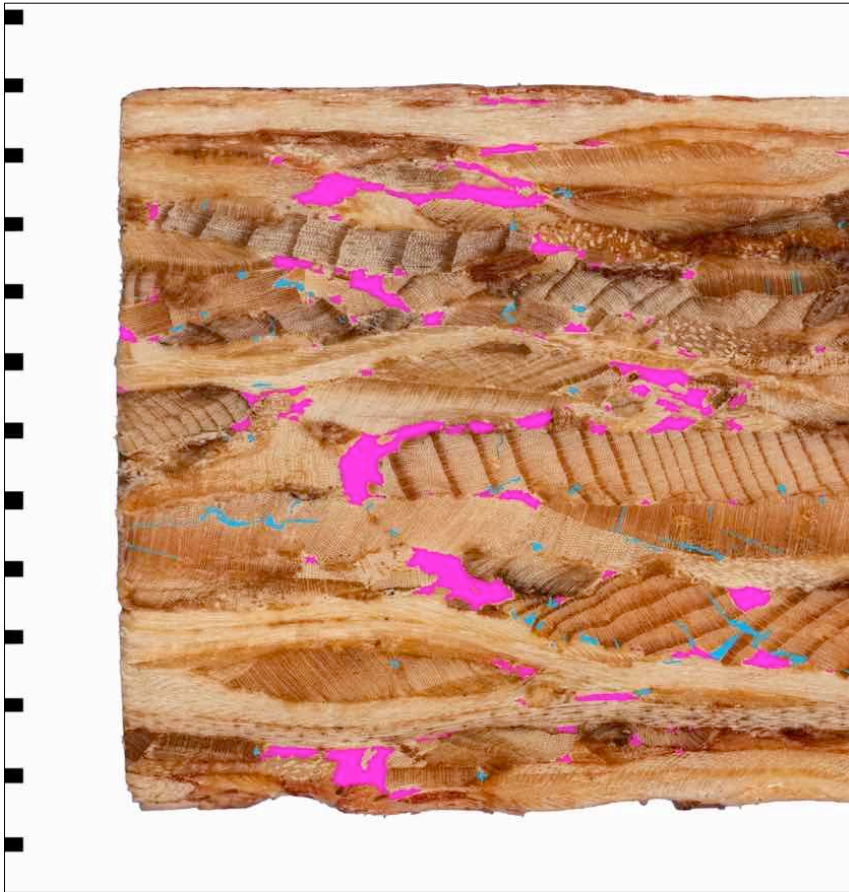


Appendix Figure 1.1 - Surface checking (blue) and voids (magenta) in part of an OSB (brown) specimen before (left) and after (right) wetting and drying. The area occupied by checks is 0.476 and 0.721% of the specimen's area before and after swelling, respectively. The area occupied by voids is 4.738 and 7.31% of the specimen's area before and after swelling respectively. The irreversible swelling of the specimen was 11.85%. Vertical scale in mm



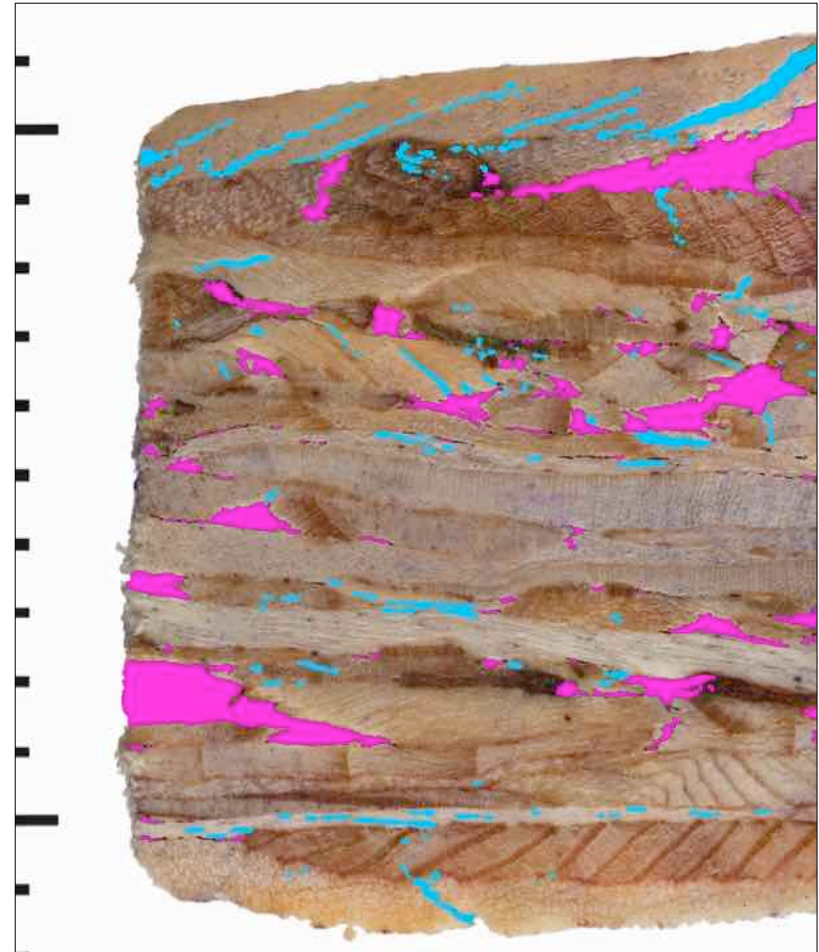
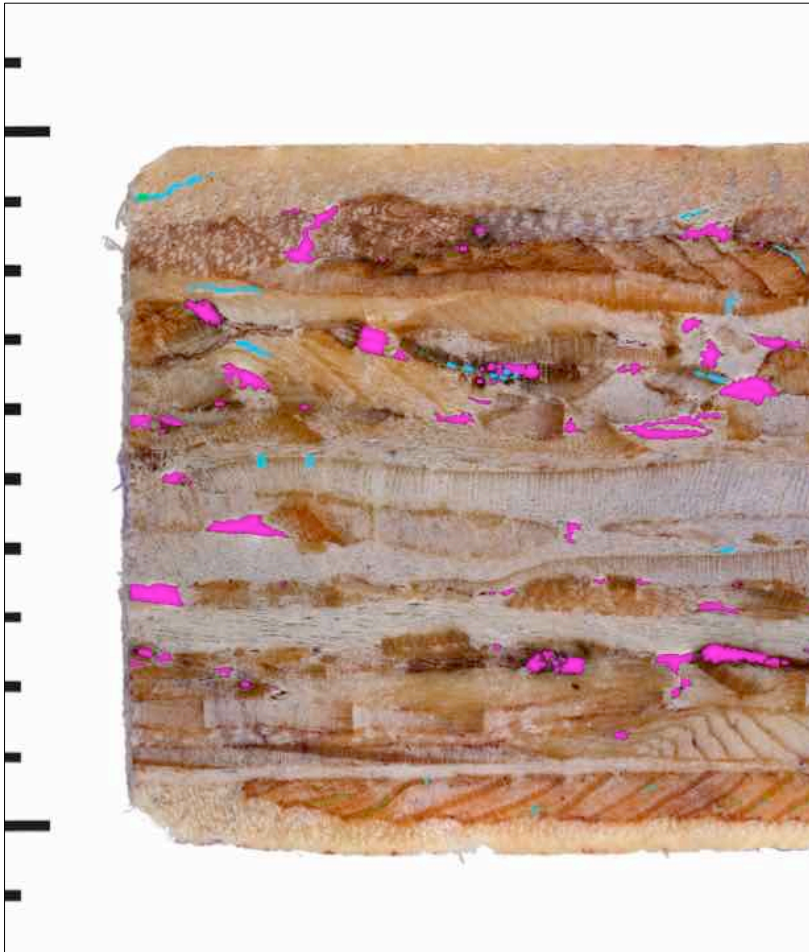


Appendix Figure 1.2 - Surface checking (blue) and voids (magenta) in part of an OSB (brown) specimen before (left) and after (right) wetting and drying. The area occupied by checks is 0.384 and 1.097% of the specimen's area before and after swelling, respectively. The area occupied by voids is 5.613 and 9.271% of the specimen's area before and after swelling respectively. The irreversible swelling of the specimen was 19.1%. Vertical scale in mm

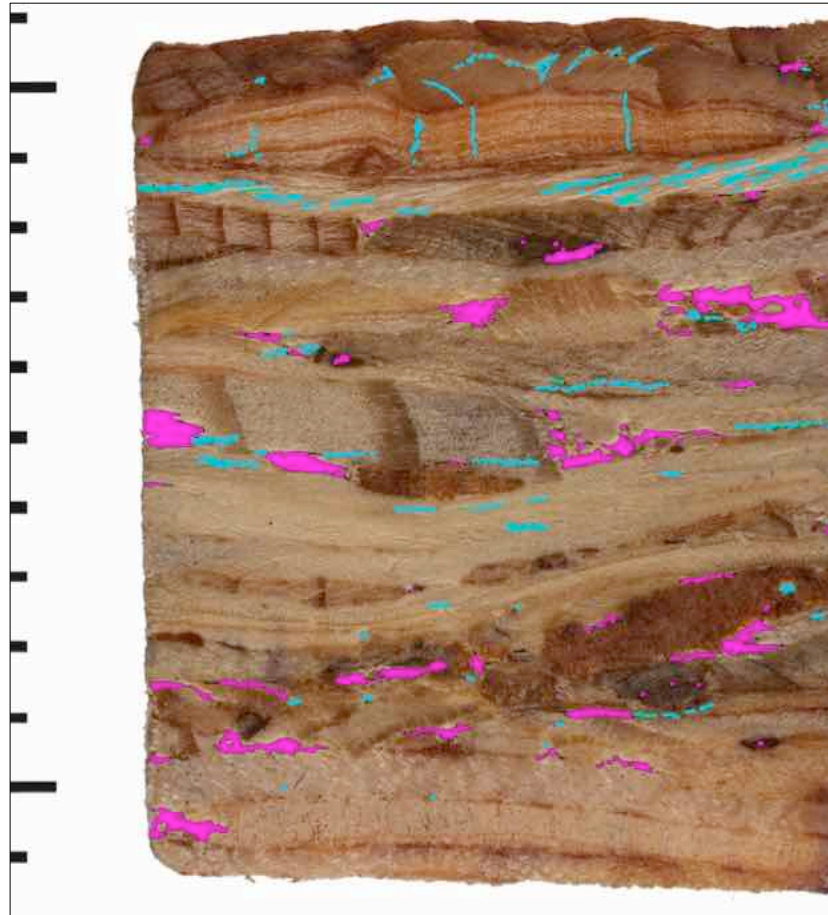
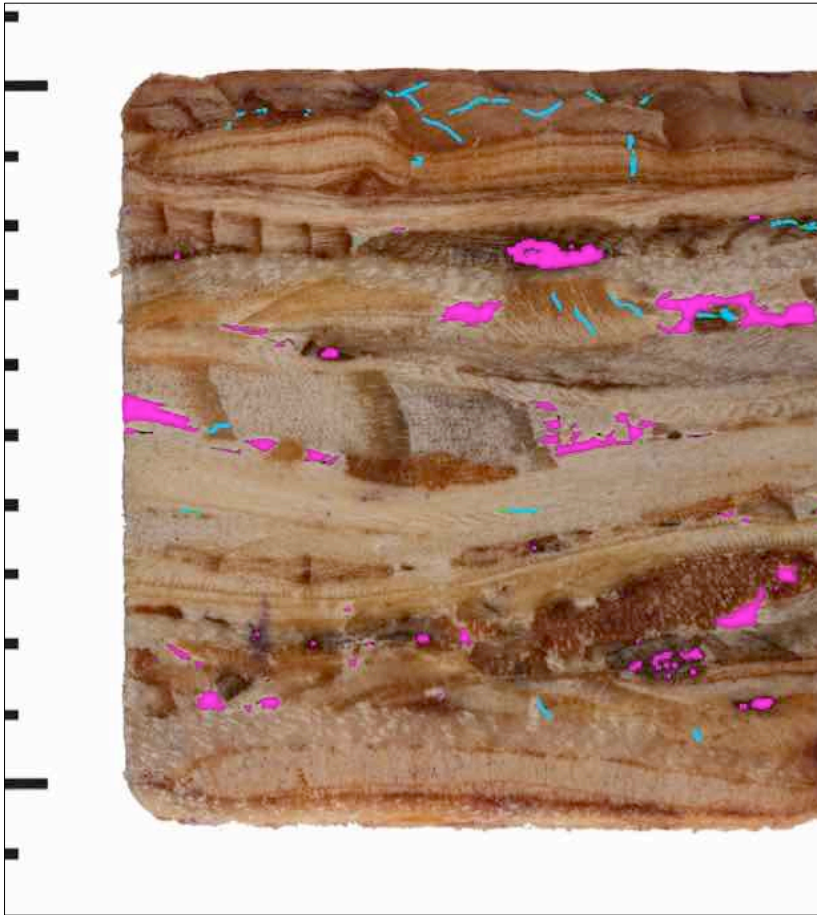


Appendix Figure 1.3 - Surface checking (blue) and voids (magenta) in part of an OSB (brown) specimen before (left) and after (right) wetting and drying. The area occupied by checks is 0.541 and 0.989% of the specimen's area before and after swelling, respectively. The area occupied by voids is 4.027 and 7.029% of the specimen's area before and after swelling respectively. The irreversible swelling of the specimen was 12.88%. Vertical scale in mm





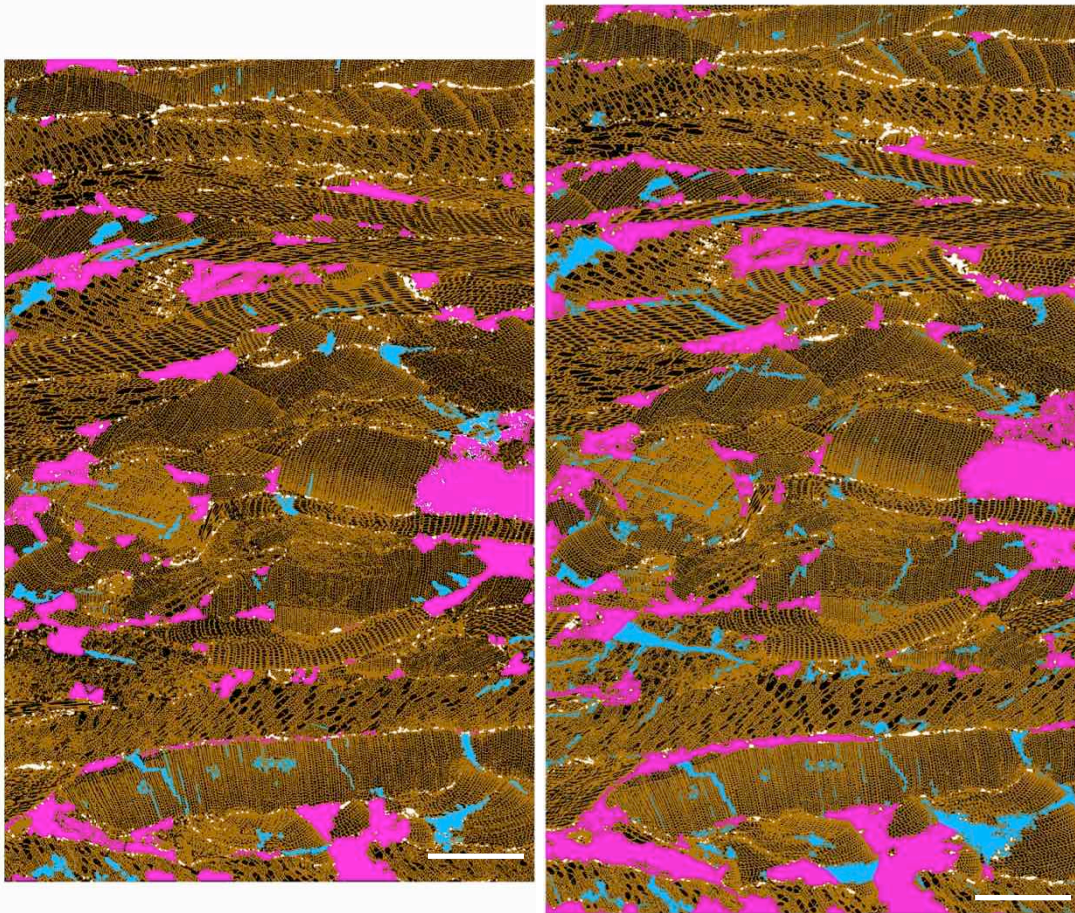
Appendix Figure 1.4 - Surface checking (blue) and voids (magenta) in part of an OSB (brown) specimen before (left) and after (right) wetting and drying. The area occupied by checks is 0.109 and 1.338% of the specimen's area before and after swelling, respectively. The area occupied by voids is 1.612 and 6.449% of the specimen's area before and after swelling respectively. The irreversible swelling of the specimen was 21.07%. Vertical scale in mm



Appendix Figure 1.5 - Surface checking (blue) and voids (magenta) in part of an OSB (brown) specimen before (left) and after (right) wetting and drying. The area occupied by checks is 0.167 and 0.832% of the specimen's area before and after swelling, respectively. The area occupied by voids is 1.515 and 2.239% of the specimen's area before and after swelling respectively. The irreversible swelling of the specimen was 11.58%. Vertical scale in mm

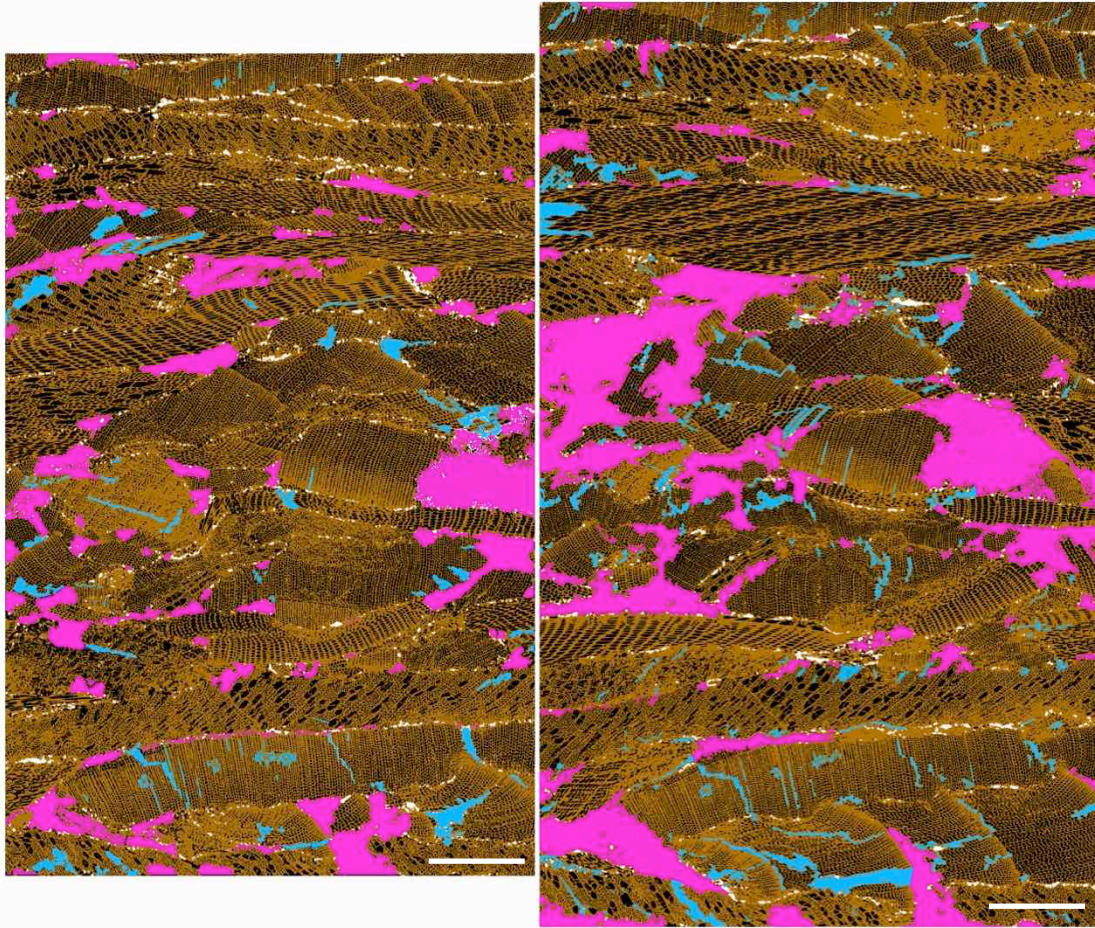


**Appendix 2 - Internal microstructure of OSB data sets. Helical X-ray micro-CT images of all 2D frames that were subject to image analysis**



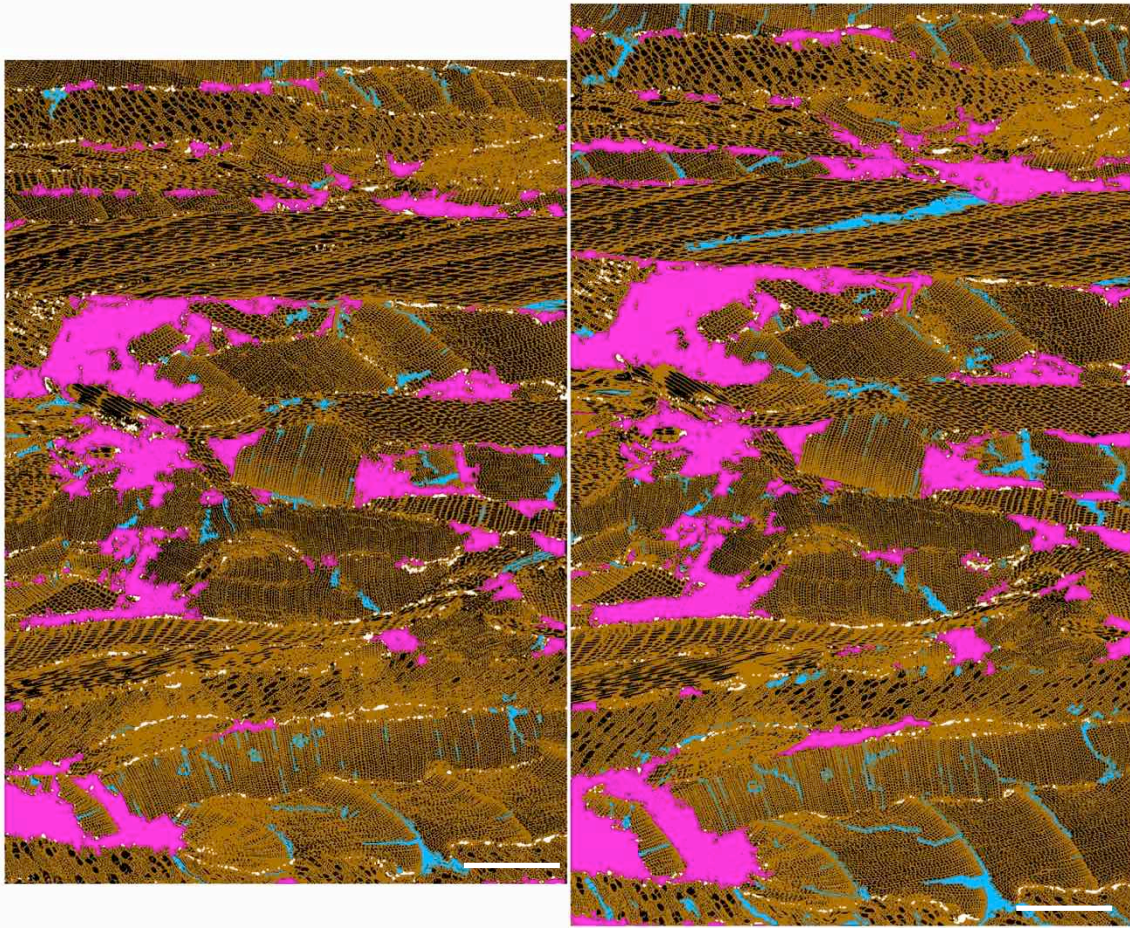
Appendix Figure 2.1 - In-plane rendered helical X-ray micro-CT image of the 0% slice of part of a *dry* (left) and *wet/dry* (right) OSB data set. Wood is rendered brown; lumens are black; voids magenta; cracks blue; and zinc is white. The areas within the cross-section (width x thickness) occupied by the different segmented phases before (left) and after (right) wetting and drying are: 52.48 and 50.53% wood, 34.93 and 32.96% cell-lumen, 9.17 and 11.42% voids, 2.15 and 4.1% cracks, 1.26 and 1.0% zinc, respectively. Scale bars are 1 mm





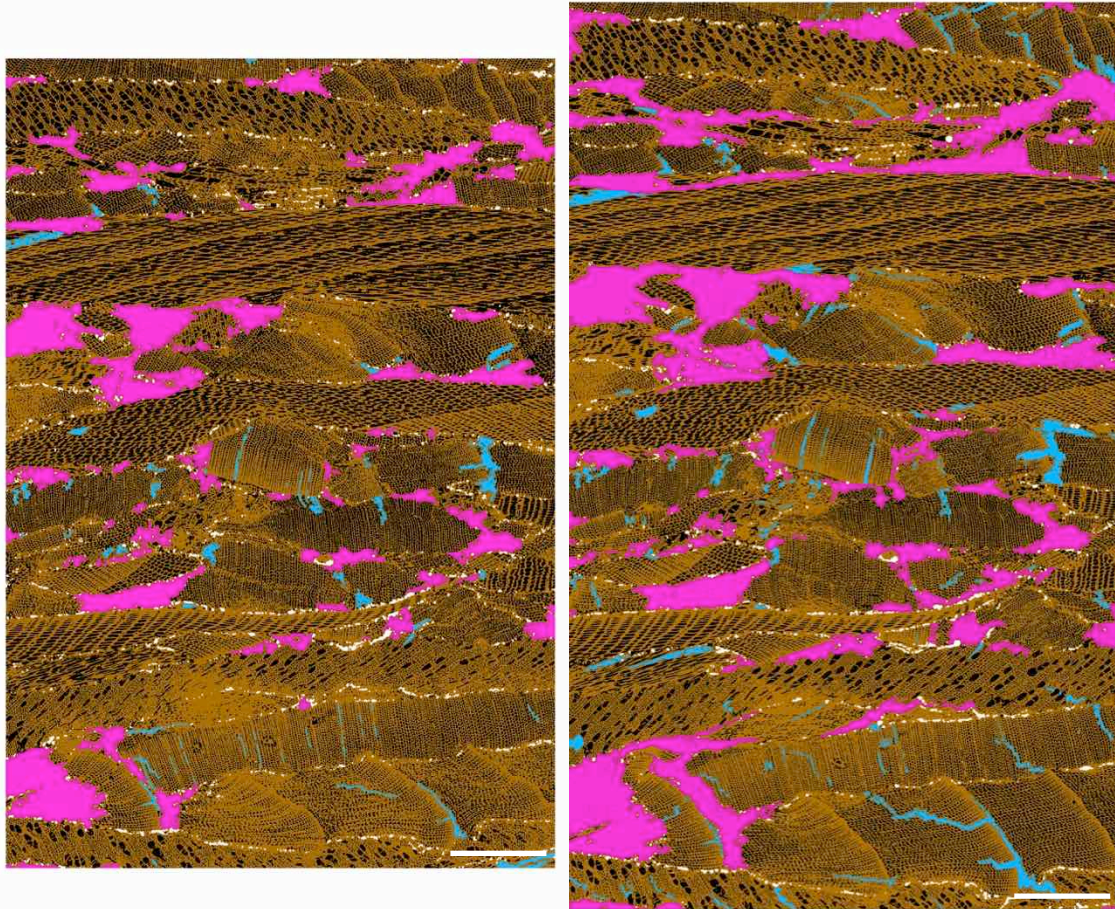
Appendix Figure 2.2 - In-plane rendered helical X-ray micro-CT image of the 10% slice of part of a *dry* (left) and *wet/dry* (right) OSB data set. Wood is rendered brown; lumens are black; voids magenta; cracks blue; and zinc is white. The areas within the cross-section (width x thickness) occupied by the different segmented phases before (left) and after (right) wetting and drying are: 53.59 and 51.64% wood, 33.16 and 30.89% cell-lumen, 10.48 and 13.1% voids, 1.39 and 3.4% cracks, 1.38 and 0.97% zinc, respectively. Scale bars are 1 mm





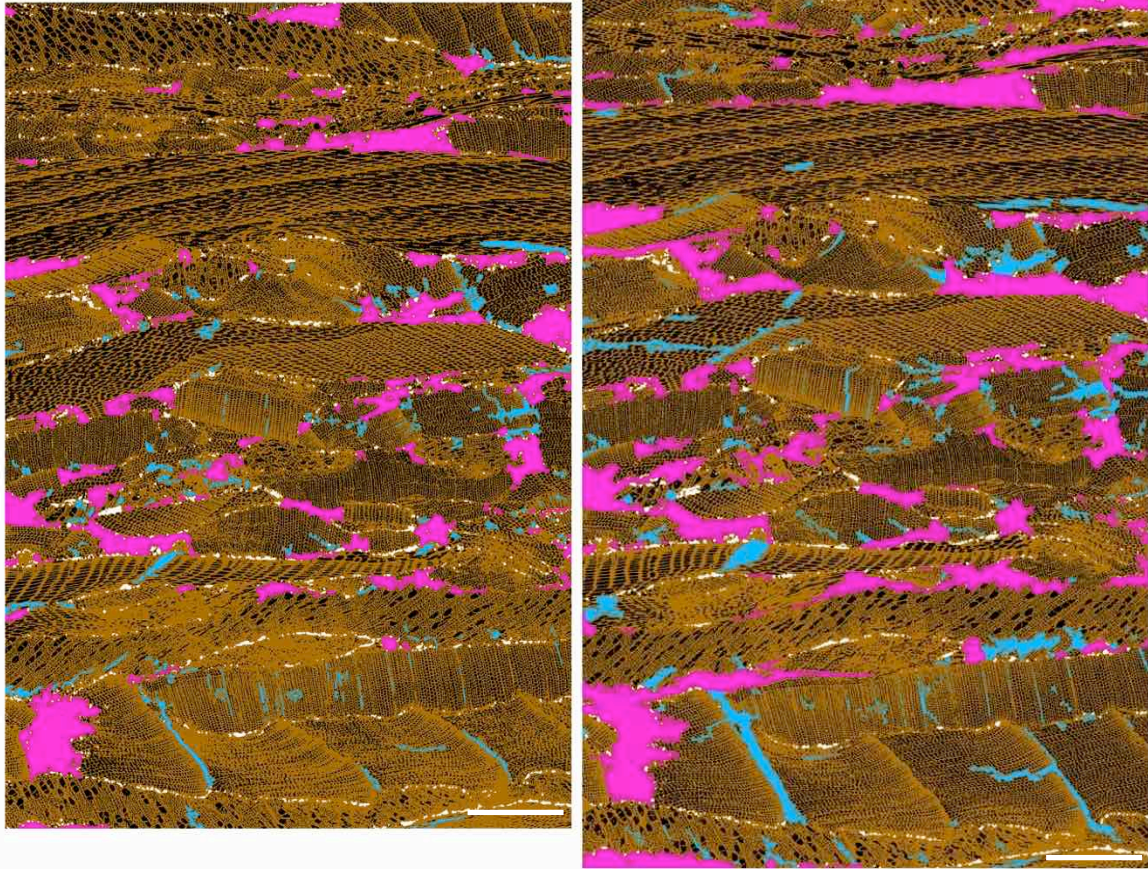
Appendix Figure 2.3 - In-plane rendered helical X-ray micro-CT image of the 20% slice of part of a *dry* (left) and *wet/dry* (right) OSB data set. Wood is rendered brown; lumens are black; voids magenta; cracks blue; and zinc is white. The areas within the cross-section (width x thickness) occupied by the different segmented phases before (left) and after (right) wetting and drying are: 55.92 and 49.61% wood, 30.25 and 31.21% cell-lumen, 10.83 and 14.66% voids, 1.75 and 3.65% cracks, 1.25 and 0.88% zinc, respectively. Scale bars are 1 mm





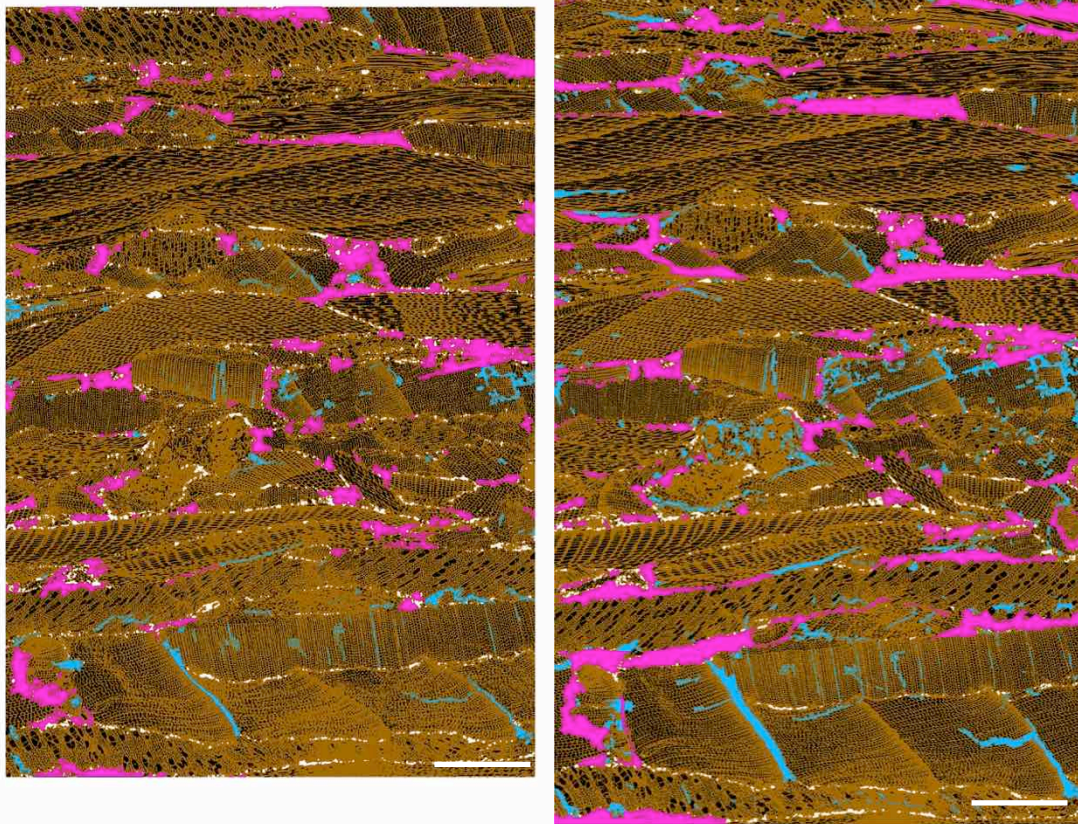
Appendix Figure 2.4 - In-plane rendered helical X-ray micro-CT image of the 30% slice of part of a *dry* (left) and *wet/dry* (right) OSB data set. Wood is rendered brown; lumens are black; voids magenta; cracks blue; and zinc is white. The areas within the cross-section (width x thickness) occupied by the different segmented phases before (left) and after (right) wetting and drying are: 53.85 and 49.82% wood, 35.56 and 33.78% cell-lumen, 8.34 and 13.22% voids, 0.99 and 2.28% cracks, 1.25 and 0.89% zinc, respectively. Scale bars are 1 mm





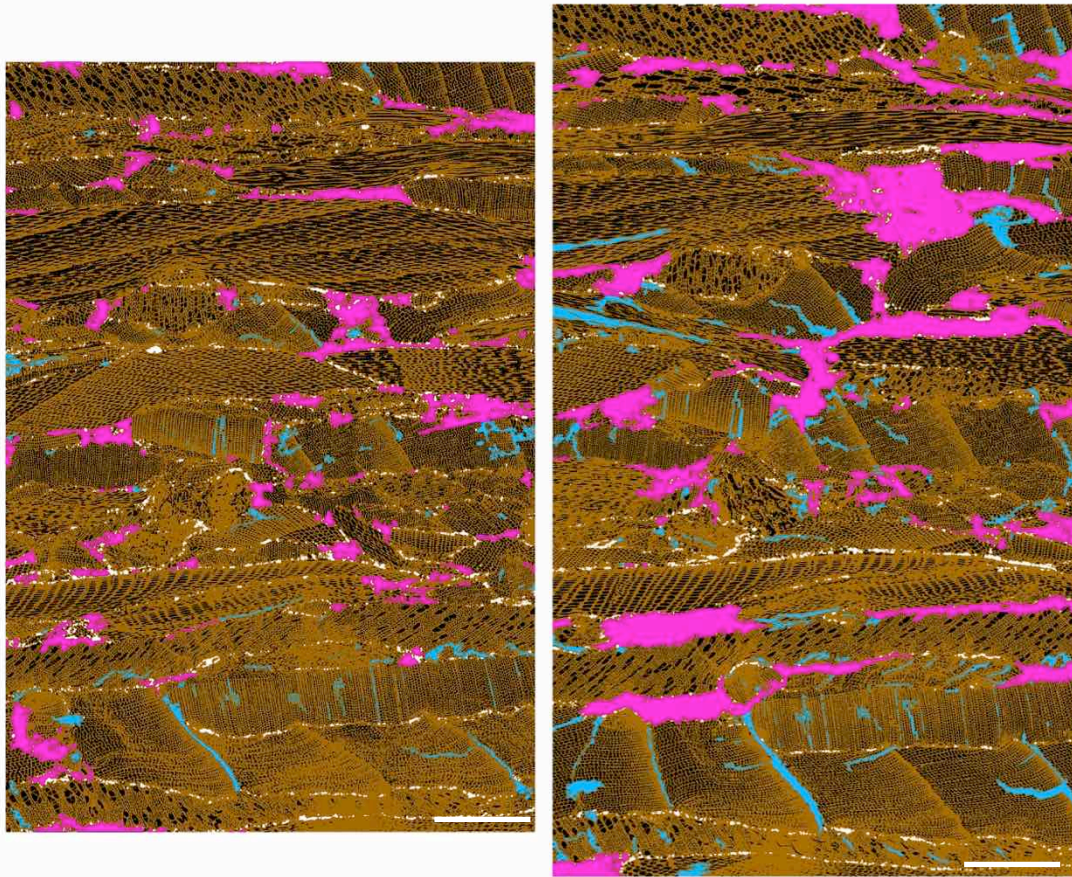
Appendix Figure 2.5 - In-plane rendered helical X-ray micro-CT image of the 40% slice of part of a *dry* (left) and *wet/dry* (right) OSB data set. Wood is rendered brown; lumens are black; voids magenta; cracks blue; and zinc is white. The areas within the cross-section (width x thickness) occupied by the different segmented phases before (left) and after (right) wetting and drying are: 57.38 and 52.24% wood, 32.98 and 33.09% cell-lumen, 5.62 and 9.28% voids, 2.63 and 4.45% cracks, 1.38 and 0.94% zinc, respectively. Scale bars are 1 mm





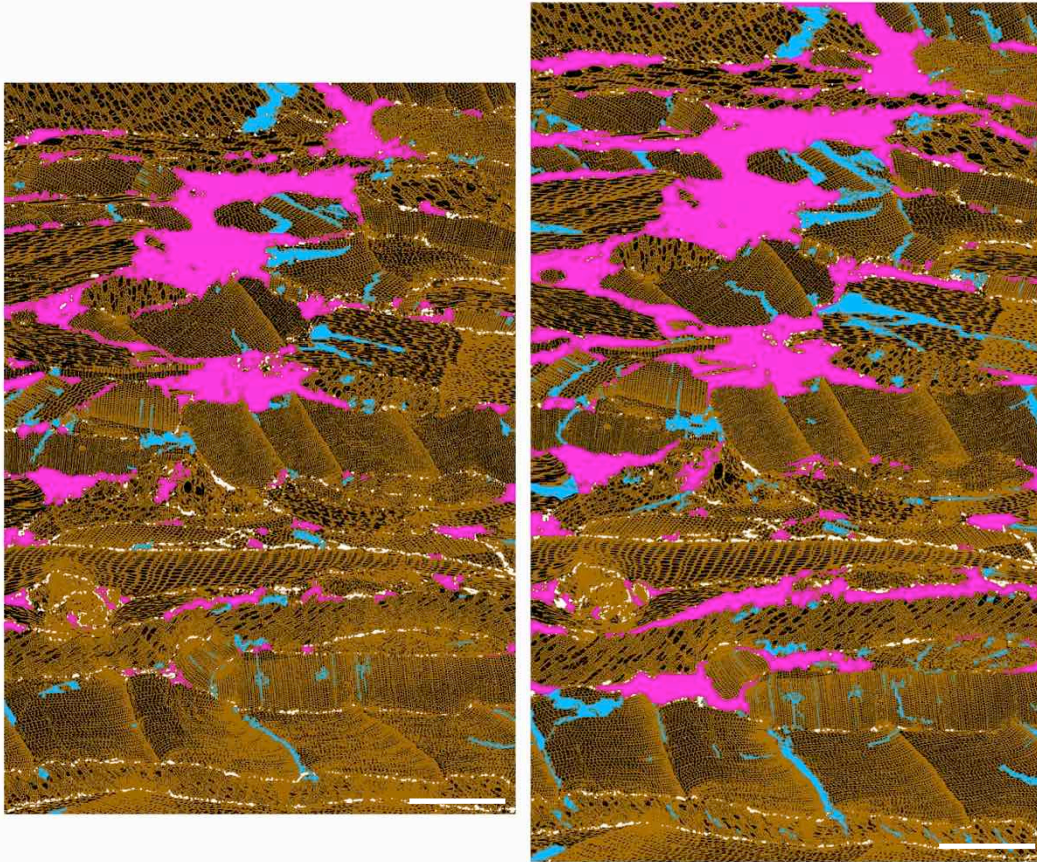
Appendix Figure 2.6 - In-plane rendered helical X-ray micro-CT image of the 50% slice of part of a *dry* (left) and *wet/dry* (right) OSB data set. Wood is rendered brown; lumens are black; voids magenta; cracks blue; and zinc is white. The areas within the cross-section (width x thickness) occupied by the different segmented phases before (left) and after (right) wetting and drying are: 60.42 and 55.13% wood, 31.09 and 32.20% cell-lumen, 5.57 and 8.40% voids, 1.40 and 3.32% cracks, 1.52 and 0.95% zinc, respectively. Scale bars are 1 mm



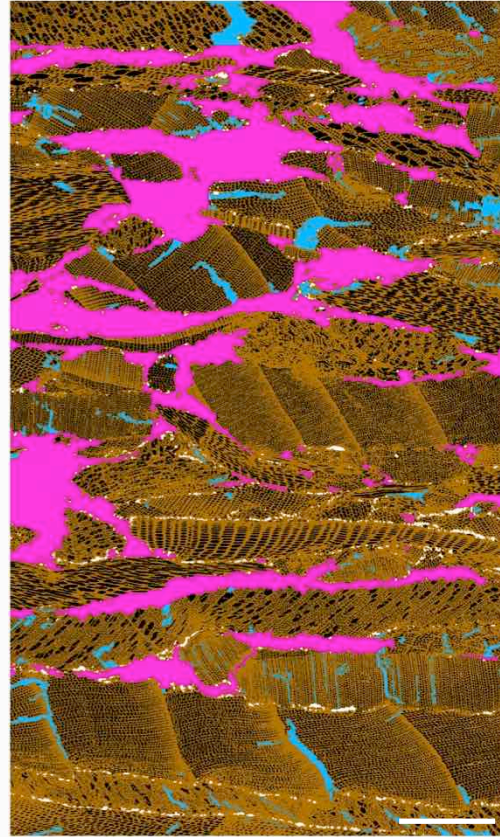
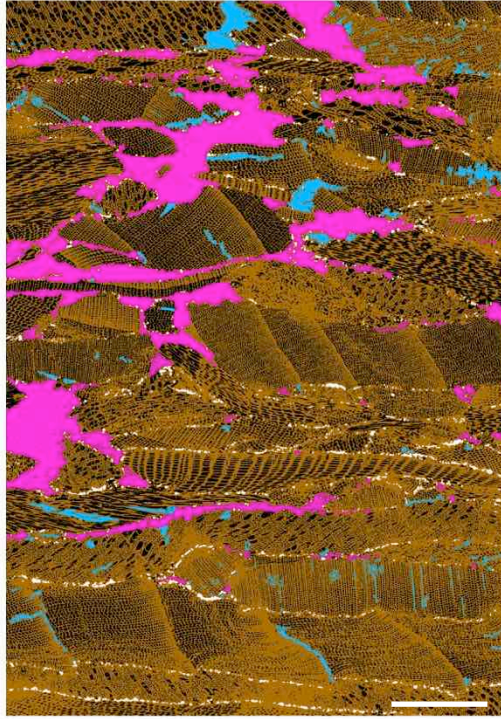


Appendix Figure 2.7 - In-plane rendered helical X-ray micro-CT image of the 60% slice of part of a *dry* (left) and *wet/dry* (right) OSB data set. Wood is rendered brown; lumens are black; voids magenta; cracks blue; and zinc is white. The areas within the cross-section (width x thickness) occupied by the different segmented phases before (left) and after (right) wetting and drying are: 59.93 and 54.61% wood, 31.19 and 30.38% cell-lumen, 6.28 and 10.91% voids, 1.03 and 3.08% cracks, 1.57 and 1.03% zinc, respectively. Scale bars are 1 mm



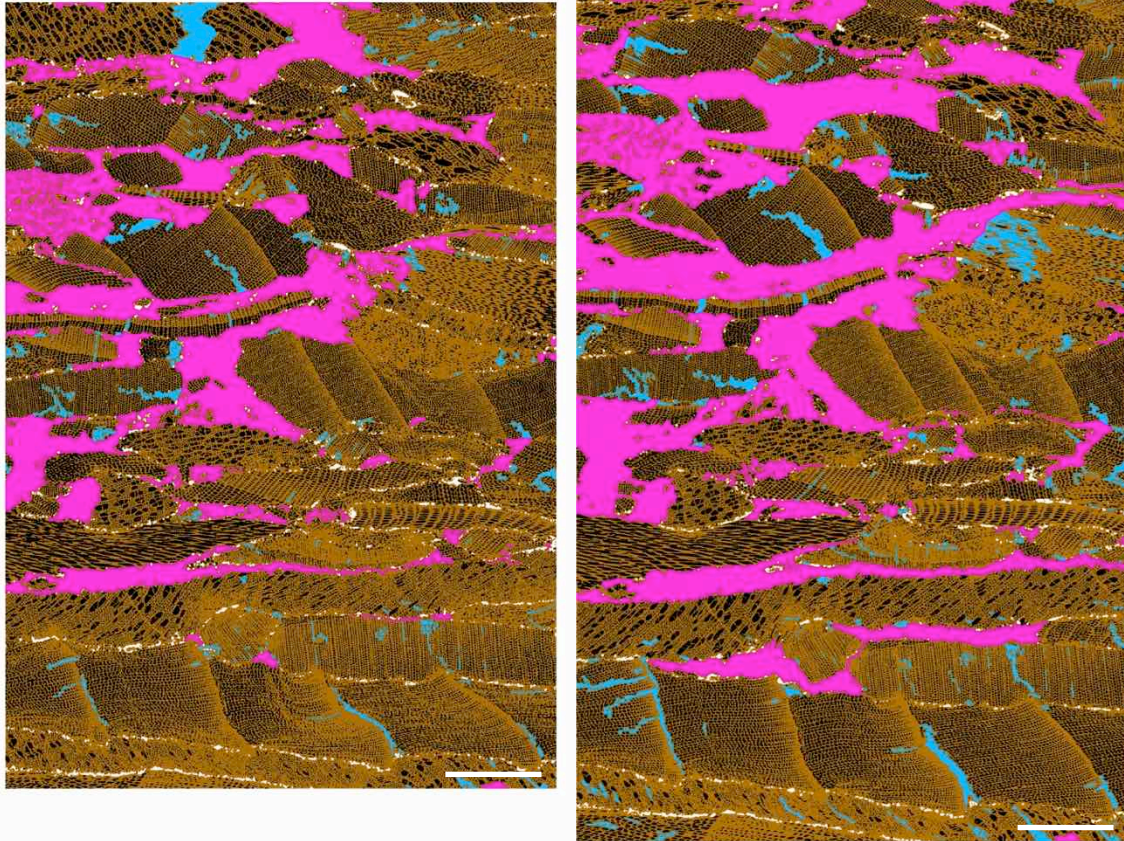


Appendix Figure 2.8 - In-plane rendered helical X-ray micro-CT image of the 70% slice of part of a *dry* (left) and *wet/dry* (right) OSB data set. Wood is rendered brown; lumens are black; voids magenta; cracks blue; and zinc is white. The areas within the cross-section (width x thickness) occupied by the different segmented phases before (left) and after (right) wetting and drying are: 57.60 and 51.27% wood, 29.26 and 28.65% cell-lumen, 9.10 and 14.86% voids, 2.32 and 4.15% cracks, 1.72 and 1.08% zinc, respectively. Scale bars are 1 mm



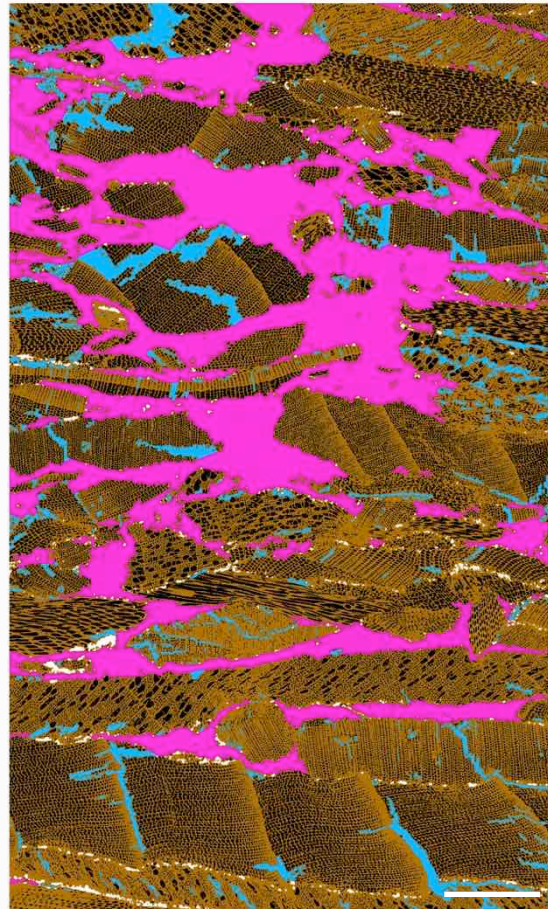
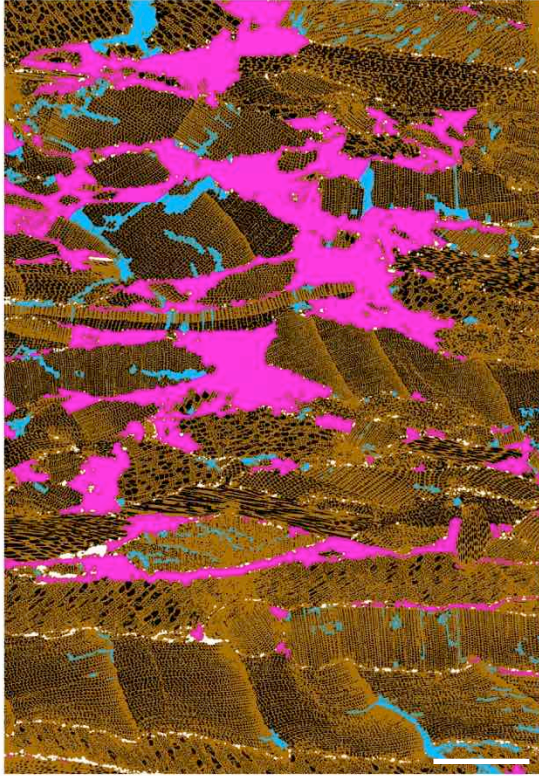
Appendix Figure 2.9 - In-plane rendered helical X-ray micro-CT image of the 80% slice of part of a *dry* (left) and *wet/dry* (right) OSB data set. Wood is rendered brown; lumens are black; voids magenta; cracks blue; and zinc is white. The areas within the cross-section (width x thickness) occupied by the different segmented phases before (left) and after (right) wetting and drying are: 54.39 and 50.30% wood, 31.98 and 28.98% cell-lumen, 10.32 and 16.95% voids, 2.11 and 2.87% cracks, 1.21 and 0.89% zinc, respectively. Scale bars are 1 mm





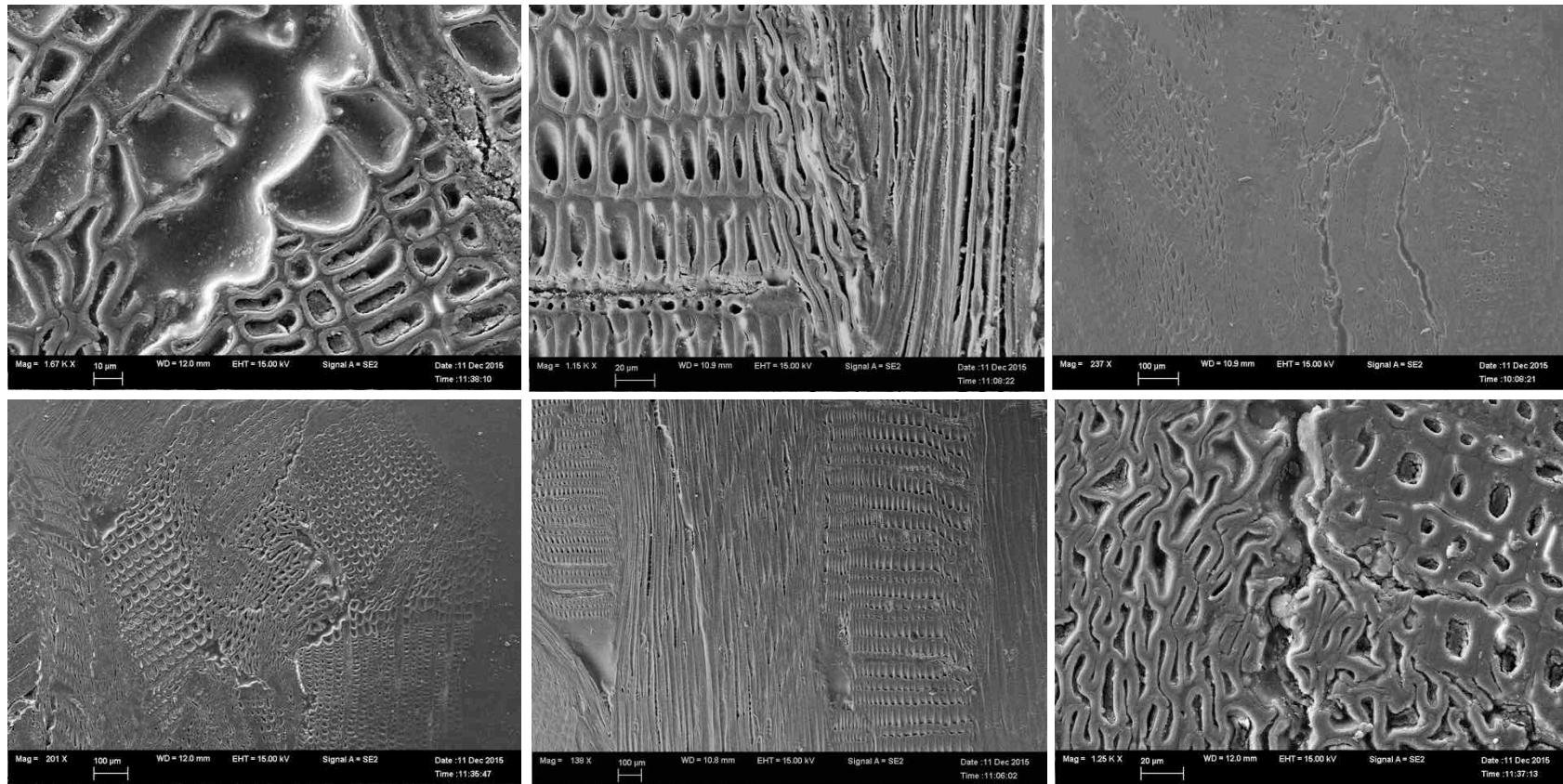
Appendix Figure 2.10 - In-plane rendered helical X-ray micro-CT image of the 90° slice of part of a *dry* (left) and *wet/dry* (right) OSB data set. Wood is rendered brown; lumens are black; voids magenta; cracks blue; and zinc is white. The areas within the cross-section (width x thickness) occupied by the different segmented phases before (left) and after (right) wetting and drying are: 49.28 and 45.47% wood, 32.74 and 29.11% cell-lumen, 14.84 and 21.34% voids, 2.06 and 3.31% cracks, 1.08 and 0.77% zinc, respectively. Scale bars are 1 mm



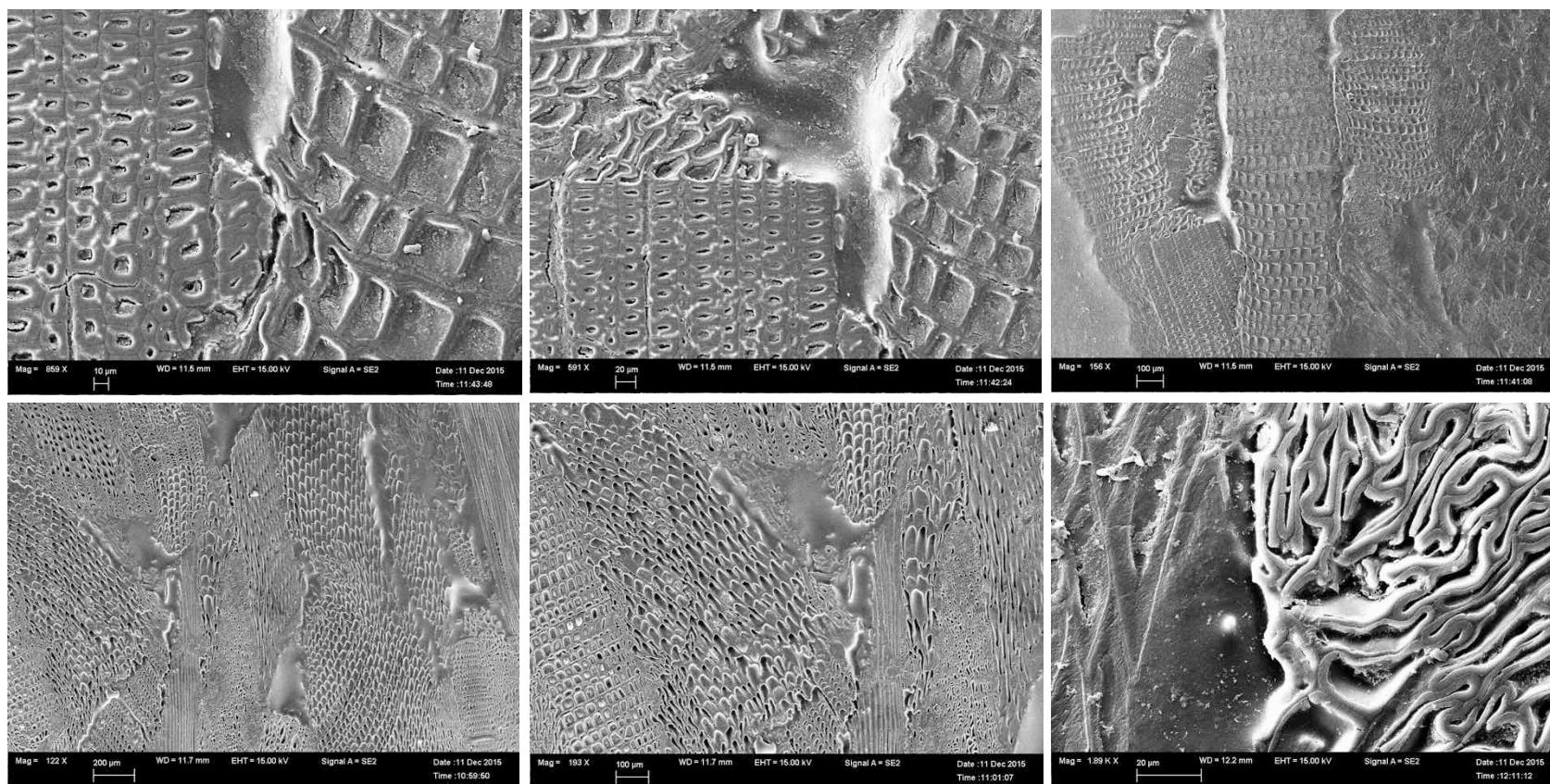


Appendix Figure 2.11 - In-plane rendered helical X-ray micro-CT image of the 100% slice of part of a *dry* (left) and *wet/dry* (right) OSB data set. Wood is rendered brown; lumens are black; voids magenta; cracks blue; and zinc is white. The areas within the cross-section (width x thickness) occupied by the different segmented phases before (left) and after (right) wetting and drying are: 52.82 and 42.93% wood, 27.09 and 29.22% cell-lumen, 15.68 and 22.14% voids, 3.22 and 4.97% cracks, 1.19 and 0.75% zinc, respectively. Scale bars are 1 mm

### Appendix 3 - FE-SEM images of OSB samples embedded with a low-viscosity epoxy resin

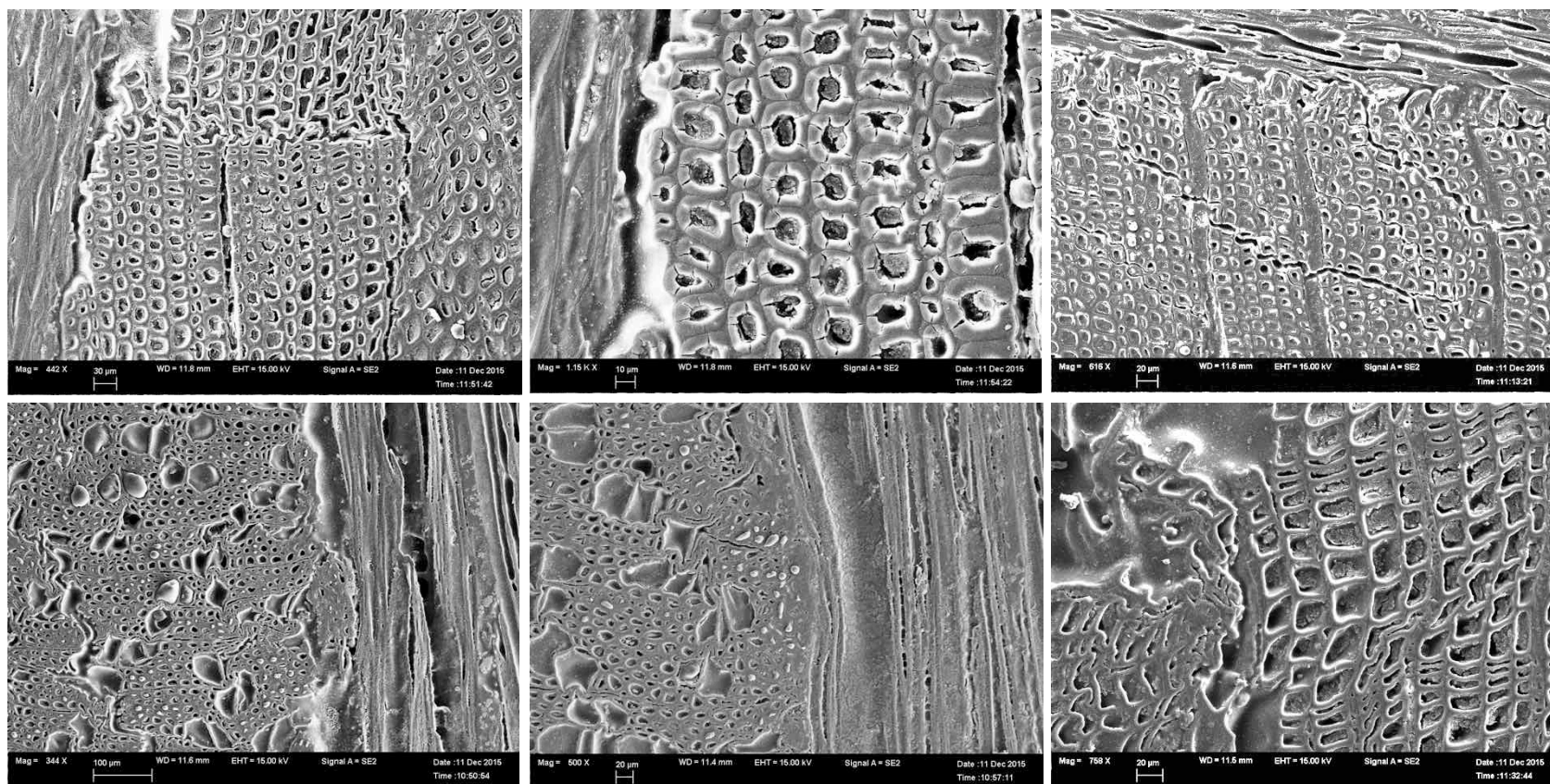


Appendix Figure 3.1 - FE-SEM images obtained from OSB specimens exposed to the wetting & drying cycle used in Chapter 3



Appendix Figure 3.2 - FE-SEM images from OSB specimens exposed to 72 h of water soaking and subsequent drying





Appendix Figure 3.3 - FE-SEM images of OSB specimens that acted as control